



저작자표시-비영리-변경금지 2.0 대한민국

이용자는 아래의 조건을 따르는 경우에 한하여 자유롭게

- 이 저작물을 복제, 배포, 전송, 전시, 공연 및 방송할 수 있습니다.

다음과 같은 조건을 따라야 합니다:



저작자표시. 귀하는 원저작자를 표시하여야 합니다.



비영리. 귀하는 이 저작물을 영리 목적으로 이용할 수 없습니다.



변경금지. 귀하는 이 저작물을 개작, 변형 또는 가공할 수 없습니다.

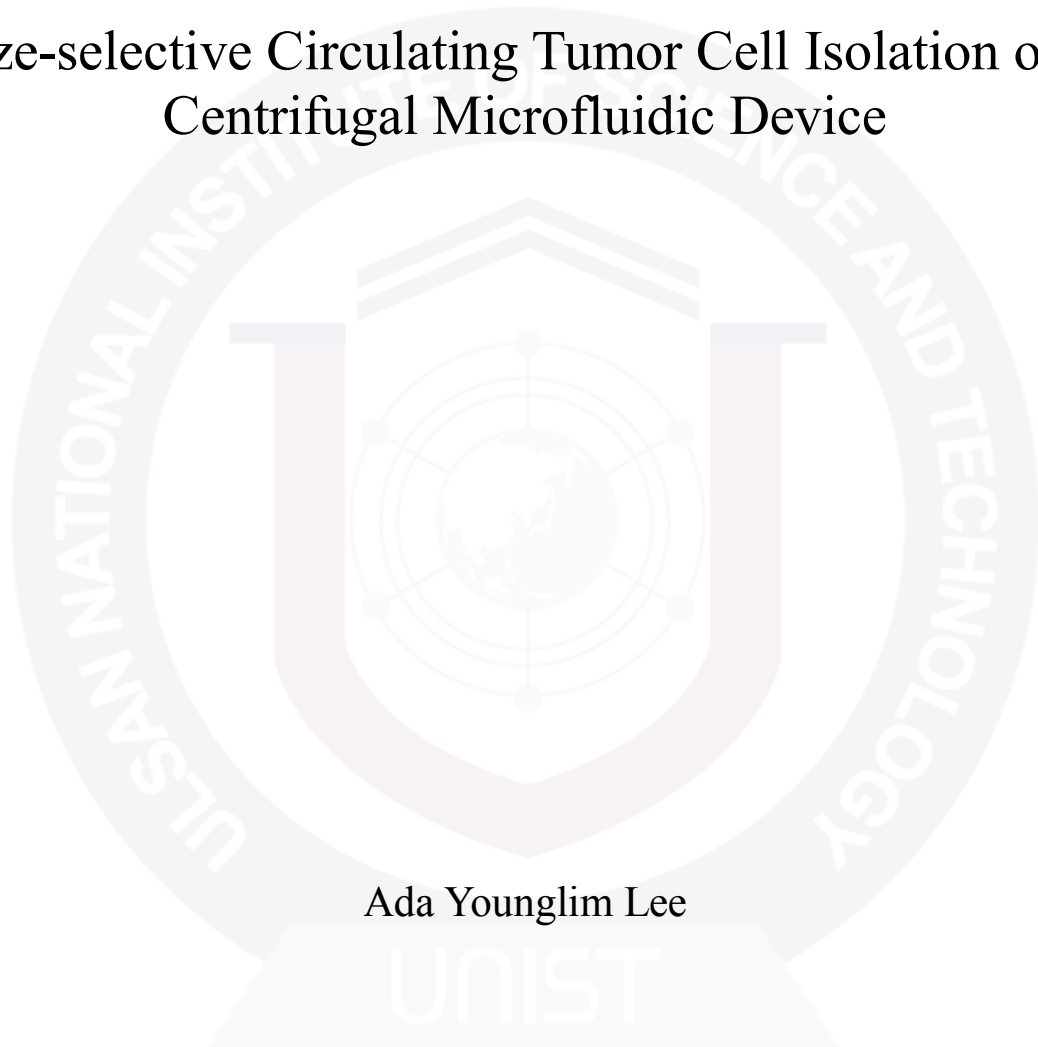
- 귀하는, 이 저작물의 재이용이나 배포의 경우, 이 저작물에 적용된 이용허락조건을 명확하게 나타내어야 합니다.
- 저작권자로부터 별도의 허가를 받으면 이러한 조건들은 적용되지 않습니다.

저작권법에 따른 이용자의 권리는 위의 내용에 의하여 영향을 받지 않습니다.

이것은 [이용허락규약\(Legal Code\)](#)을 이해하기 쉽게 요약한 것입니다.

[Disclaimer](#)

Size-selective Circulating Tumor Cell Isolation on a Centrifugal Microfluidic Device



Ada Younglim Lee

Department of Biomedical Engineering

Graduate School of UNIST

2014

Size-selective Circulating Tumor Cell Isolation on a Centrifugal Microfluidic Device

Ada Younglim Lee

Department of Biomedical Engineering

Graduate School of UNIST

Size-selective Circulating Tumor Cell Isolation on a Centrifugal Microfluidic Device

A thesis
submitted to the Graduate School of UNIST
in partial fulfillment of the
requirements for the degree of
Master of Science

Ada Younglim Lee

02. 04. 2014

Approved by

Advisor

Yoon-Kyoung Cho

Size-selective Circulating Tumor Cell Isolation on a Centrifugal Microfluidic Device

Ada Younglim Lee

This certifies that the thesis of Ada Y. Lee is approved.

02. 04. 2014

Advisor: Yoon-Kyoung Cho

Yoon-Kyoung Cho

Sebyung Kang

Steven A. Soper

Abstract

Detection of circulating tumor cells (CTCs) has gained increasing attention as scientists and physicians learn more about the roles these malignant cells play in metastatic cancer and disease progression. Quantification and molecular analysis of CTCs are considered very important because they can function as potential indicators of early diagnosis and prognosis of cancer metastasis. Therefore, many efforts have been made to develop a reliable method to detect the CTCs. However, one major drawback of CTC detection using a conventional microfluidic approach is that it generally requires a long and complicated processing time due to its small scale and slow fluid velocity. In addition, commonly used immunoaffinity-based positive selection method has a limitation that its recovery rate heavily relies on EpCAM expression of target CTCs, which is known to be heterogeneous among different cell types. In this thesis, a size-selective lab-on-a-disc platform is introduced for a rapid and label-free isolation of CTCs from whole blood. The polycarbonate track-etch (PCTE) membrane was utilized to isolate CTCs based on the size difference between the target cell and other blood cells. Validation of the device was performed using the MCF7 breast cancer cell line spiked into PBS buffer solution as well as healthy donor blood. The capture efficiency of approximately 50~65 % was achieved with the devised CTC isolation system. The purity of the captured cells varied, ranging from 15 % to 30 %. For the clinical studies, patient blood samples from gastric cancer and breast cancer patients were tested and analyzed. The number of CTCs ranging from 5 to 29 CTCs was captured. Overall, the CTC detection rate for the lung cancer patient was 50 %, and the detection rate for the gastric cancer patients was 38.4 %.

Table of Contents

CHAPTER 1 Introduction	13
1.1 Circulating Tumor Cell.....	13
1.1.1 Circulating Tumor Cell: Indicator of Cancer Metastasis	13
1.1.2 CTC Detection in Microfluidic System	16
1.1.3 Commercial Technologies for CTC Detection	21
1.1.4 Challenges for CTC Studies	24
1.2 Centrifugal Microfluidics	25
1.2.1 Theory	25
1.2.2 Diagnostics in Centrifugal Microfluidics System.....	25
1.3 Literature Survey: Size-Selective CTC Separation	27
1.3.1 Hydrodynamic Force-driven Separation	27
1.3.2 Direct Filtration	28
1.3.3 Size Amplification	31
1.4 Research Outline.....	32
1.4.1 Objectives of the Thesis	32
1.4.2 Outline of the Thesis.....	33
CHAPTER 2 Experimental Methods & Materials.....	34
2.1 Sample Preparation	34
2.1.1 Chemicals and Reagents	34
2.1.2 Blood Specimen Collection and Processing.....	34
2.1.3 Cancer Cell Lines	35
2.2 Device Fabrication	37
2.2.1 Fabrication of the CTC-capture Disc.....	37
2.2.2 Surface Passivation.....	37

2.3 System Settings.....	38
2.3.1 Disc-based Microfluidic System	38
2.3.2 ScreenCell™ System	40
2.4 Imaging	40
2.5 Fabrication of the PDMS Through-hole Membrane	41
CHAPTER 3 CTC Isolation on a Centrifugal Microfluidic Device	43
3.1 Performance Metrics	43
3.2 Preliminary Studies	44
3.2.1 Size Distribution of Different Cancer Cell Lines	44
3.2.2 Optimization of the Staining Protocol	45
3.3 Optimization of Device Fabrications	46
3.3.1 Disc Design	46
3.3.2 Membrane Installation	48
3.3.3 Surface Passivation.....	49
3.4 Cell-line Experiments.....	51
3.4.1 Determination of the Spin Condition.....	51
3.4.2 Capture Efficiencies at Various Flow Conditions.....	53
3.4.3 Capture Efficiencies at Different Cell Concentrations.....	55
3.4.4 Dilution Factor	57
3.5 CTC Isolation from Patient Blood	58
3.5.1 Clinical Test.....	58
3.6 Conclusion.....	64
CHAPTER 4 Future Directions	65
4.1 Negative Depletion	65
4.2 PDMS Through-hole Membrane Fabrication	65
4.1.1 Mask Design.....	65
4.1.2 SU-8 Master Fabrication	66

4.1.3	PDMS Master Fabrication.....	69
4.1.4	Surface Passivation and Demolding of PDMS Membrane	71
4.1.5	Back-side Etching.....	73
4.1.6	Performance Evaluation	75
CHAPTER 5 Concluding Remarks		76
5.1	Summary of the Work	76
5.2	Strength and Limitation.....	76
5.3	Future Prospect	77
References		78
Acknowledgements.....		85
Curriculum Vitae.....		86

List of Figures

Figure 1 Diagrammed illustration of cancer metastasis.....	14
Figure 2 Clinical relevance of CTC abundance in patient samples.....	15
Figure 3 Schematic illustration of current CTC isolation approaches in a blood sample.....	16
Figure 4 Examples of CTC separation technologies.....	20
Figure 5 Examples of commercialized CTC detection system.....	23
Figure 6 Schematic illustration of the centrifugal microfluidics.....	26
Figure 7 Examples of centrifugal microfluidic platforms used in biomedical applications.....	26
Figure 8 Examples of size-based CTC isolation using the hydrodynamic properties of the fluids.....	27
Figure 9 Examples of size-based CTC isolation using the direct filtration method.....	29
Figure 10 Schematic illustration of size amplification method using multi-obstacle architecture filtration device.....	31
Figure 11 Schematic illustration of a rare cell counting process.....	36
Figure 12 The system settings for the disc-based microfluidic system and the ScreenCell™ filtration system.....	40
Figure 13 Schematic illustration of PDMS through-hole membrane fabrication process.....	42
Figure 14 The cell size analysis of cancer cell lines.....	44
Figure 15 Fluorescence images of fluorescently labeled MCF7 breast cancer cells.....	45
Figure 16 Illustration of the centrifugal microfluidic device for CTC isolation.....	47
Figure 17 Result of the leakages test on a CTC-capture disc.....	48
Figure 18 The result showing the effectiveness of the different types of passivation methods.....	50
Figure 19 Variation of pressure drop across the membrane at different filtration settings.....	50
Figure 20 The effect of the angular velocity of a rotating disc on the cancer cell capture efficiency and purity.....	54
Figure 21 Comparison between different filter devices.....	54
Figure 22 The capture efficiency of MCF7 cells spiked into PBS buffer solution and whole blood at	

various cell concentrations.	56
Figure 23 The effect of the dilution factors on the cancer cell capture efficiency and purity.	57
Figure 24 Results showing the performance of CTC-capture disc in clinical samples.....	59
Figure 25 Gallery of CTCs and leukocytes captured using the size selective CTC-capture disc from cancer patients.	61
Figure 26 Histogram plots showing the size distribution of the CTCs isolated from gastric patient blood samples and cancer cells from AGS gastric cancer cell line.....	62
Figure 27 Example of the mask design used for through-hole membrane fabrication	66
Figure 28 Microstructures with undercuts	68
Figure 29 Results of SU-8 master fabrication	68
Figure 30 Results of PDMS master fabrication.....	70
Figure 31 Results of PDMS through-hole membrane fabrication	73
Figure 32 Results of PDMS through-hole membrane fabrication after the completion of back-side etching.....	74

List of Tables

Table 1 Recent research in size selective filtration based CTC separation methods.....	30
Table 2 Comparison of different types of CTC isolation system.	302
Table 3 The operation program for the disc-based CTC isolation.....	329
Table 4 Summary of the contact angle analysis of six different surfaces using various surface passivation methods.....	39
Table 5 List of lung cancer patient samples and gastric cancer patient samples showing the number of captured CTCs with the stage information.....	60
Table 6 Summary of the clinical evaluation results using different types of CTC isolation systems. ...	63
Table 7 The surface passivation results for the PDMS mold with different conditions.....	60
Table 8 The surface passivation results for the slide glass with different conditions..	72

CHAPTER 1 Introduction

1.1 Circulating Tumor Cell

1.1.1 Circulating Tumor Cell: Indicator of Cancer Metastasis

Cancer is one of the leading causes of death worldwide, contributing nearly twenty percent of the total disease-related mortality.²⁸ In point of fact, however, primary tumor is not the main factor that leads to lethal consequences for patients with cancer; instead, it is the metastasis, i.e. the spread of cancer, which accounts for the vast majority of cancer-associated deaths.² For this reason, it is critical for clinicians to have reliable diagnostic tools to detect cells that disseminate from primary tumors to other parts of the body. Effective isolation and identification of these cells, referred to as circulating tumor cells (CTCs), will serve as a better guide for medical diagnosis and treatment as well as an excellent prognostic marker for many cancer patients.

As stated above, CTCs are the cancerous cells that reside in the circulatory system, and they are known to be the essential components in the process of cancer metastasis. During metastasis, primary tumor cells or existing metastatic cancer cells undergo a series of successive steps in order to spread the disease to distant organs of a human body (Figure 1). In the initial step of the metastatic cascade, tumor cells are detached from the primary tumor site by undergoing a process known as epithelial-mesenchymal transition (EMT).^{8, 29} During this process, the cells lose their polarity as well as their adhesive capability, permitting them to easily disassociate from their neighboring cells. The cells then invade into the surrounding stroma and intravasate into blood vessels nearby the tumor. Once they enter the vascular system, the circulating tumor cells, or CTCs, survive in the blood stream until they reach a secondary site. Eventually, extravasated CTCs survive and proliferate in a newfound microenvironment where pre-metastatic niche is created. CTC dissemination can also occur through the lymphatic system. In most cases, however, the cells choose to escape from this route and eventually reenter the blood circulation, simply due to the lack of the direct fluid flow from the lymphatic system to other organs.^{8, 30} The investigation of each of the individual step of the metastatic cascade is critical for understanding the invasive and migratory properties of CTCs in the patient's body.

Isolation and enumeration of CTCs can certainly play a significant role as a diagnostic tool and potential therapeutic target.^{7, 10} A recent study has discovered that the presence of CTCs in the

blood from cancer patients can be associated with both decrease in progression-free survival rate and overall survival rate.¹⁵ Specifically, for the patients with more than 5 CTCs per 7.5 mL of whole blood, the overall survival rate dropped down to approximately 20 % after 17.5 months of the treatment, whereas, for the patients with less than 5 CTCs per 7.5 mL of whole blood, the overall survival rate was close to 80 % at the same time point (Figure 2b). Additionally, CTC assay was utilized to study the effectiveness of clinical therapies. In this study, tumor progression of cancer patients was monitored during the course of therapy. It was discovered that, throughout the course of therapy, the size of the tumor and the CTC counts have a strong correlation in most cases (Figure 2c).¹⁰ From the clinical point of view, it is important to be able to sample tumors at particular time points during the course of cancer therapy. In this aspect, CTC detection is a suitable tool since the method provides a “less invasive alternative” to tissue biopsy which involves highly invasive procedures. Moreover, as it can be implied from above clinical studies, CTC assay offers the potential for patient monitoring over a period time to help improve selection of individualized therapy.

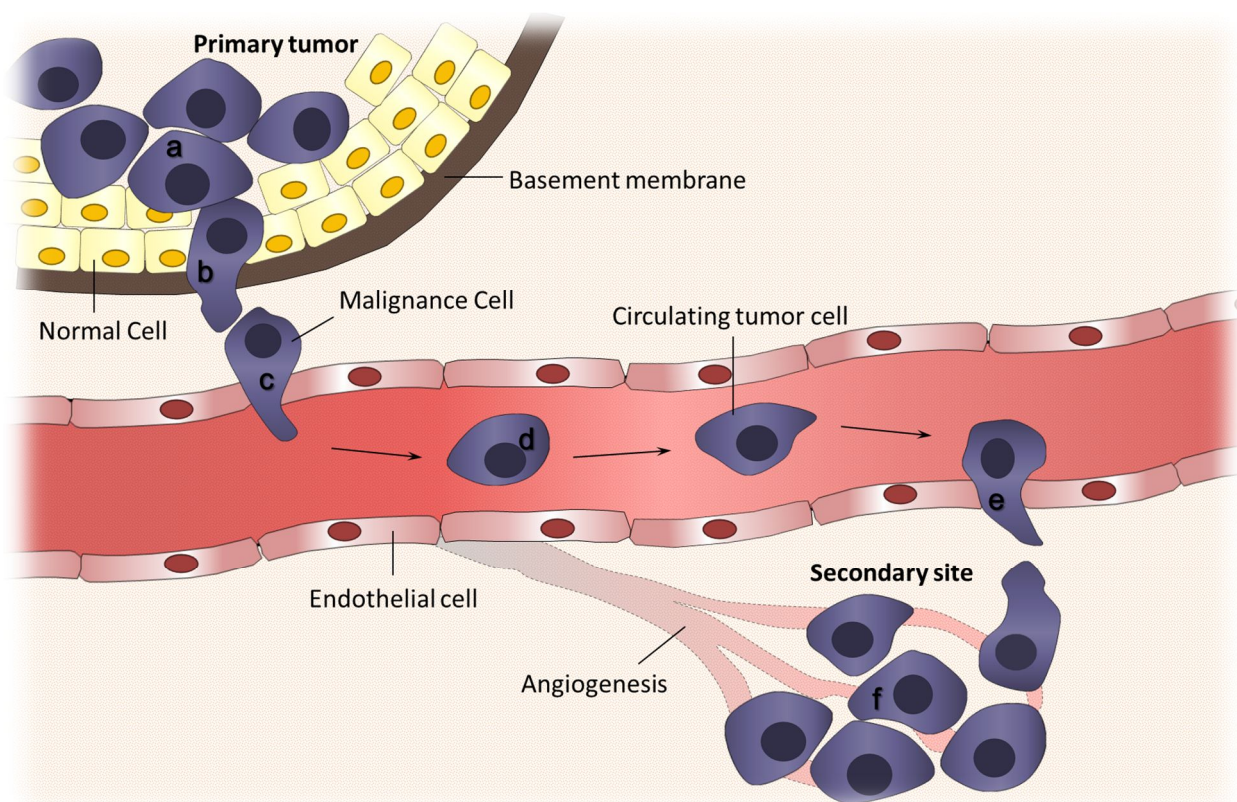


Figure 1 Diagrammed illustration of cancer metastasis. The sequential steps of metastatic cascade is comprised of (a) epithelial-mesenchymal transition (EMT) of tumor cells , (b) degradation of basement membrane, (c) intravasation of tumor cells into a blood vessel, (d) dissemination of circulating tumor cells in the blood stream, (e) extravasation of tumor cells out of a blood vessel, and (f) proliferation at a secondary site.⁸

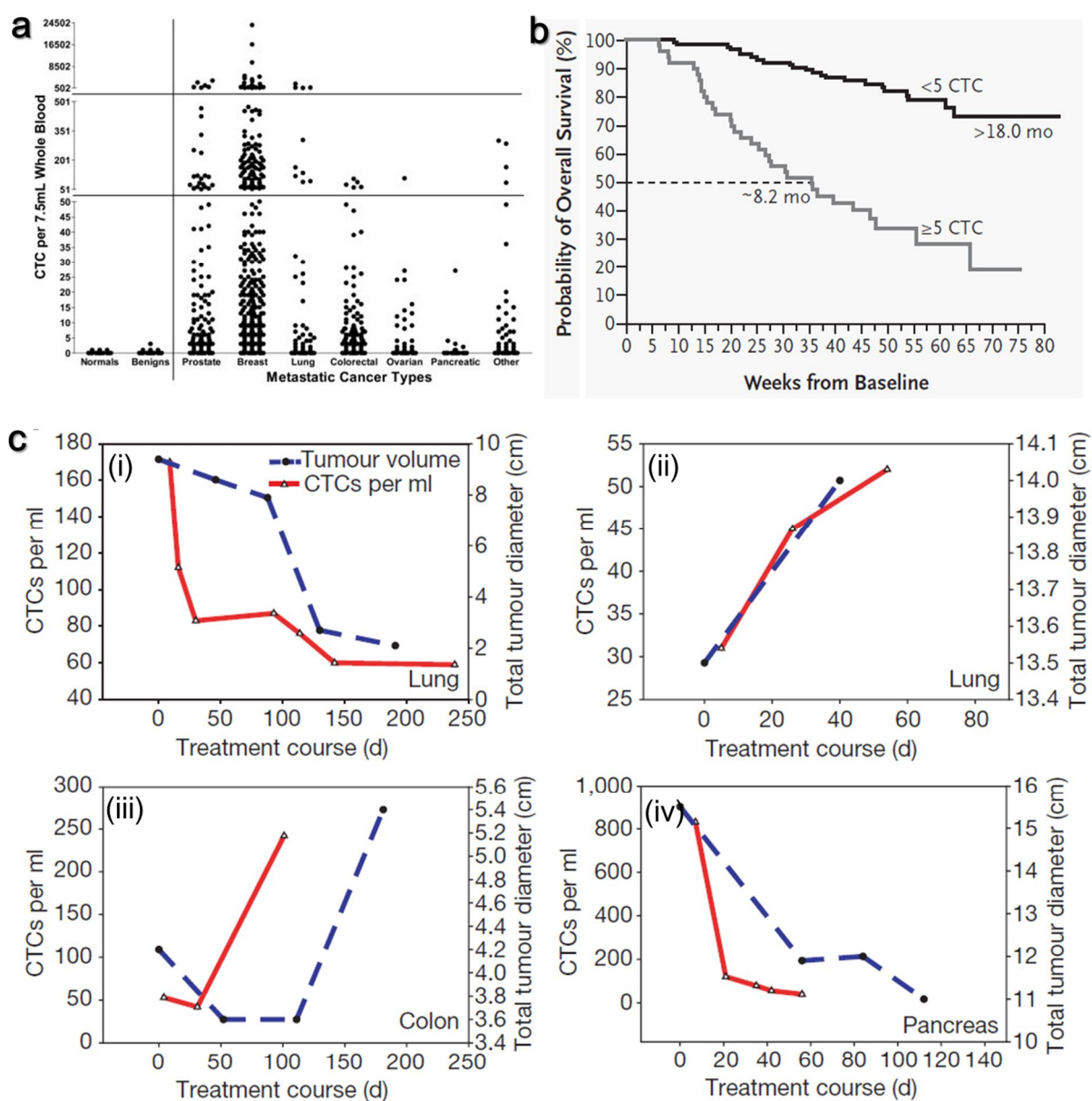


Figure 2 Clinical relevance of CTC abundance in patient samples. (a) CTC enumeration results from healthy donors, patients with nonmalignant disease, and patients with various types of metastatic cancers.⁷ (b) Comparison of probabilities of overall survival percentage between patients with metastatic breast cancer for those with < 5 CTCs per 7.5 mL of whole blood and those with CTCs per 7.5 mL for whole blood.¹⁵ (c) The correlation between the change in the number of CTCs (red) and the size of the tumor (blue) for four individual patients with (i), (ii) lung, (iii) colon, and (iv) pancreatic cancers during the course of therapy.¹⁰

1.1.2 CTC Detection in Microfluidic System

Throughout the decades, worldwide efforts have been continuously made to develop efficient and reliable CTC isolation, enumeration, and characterization methods. As a result, a variety of CTC detection methods are now accessible in bench-top research environment. For example, scientists now study CTCs by exploiting a variety of technologies including quantitative RT-PCR technique³¹⁻³², imaging-based approaches³³⁻³⁶, flow cytometry³⁶⁻³⁸, and microfluidic chip-based techniques^{10, 39-40}. Among these techniques, microfluidic chip-based CTC detection has been a fast-emerging research area because the device can provide biocompatible environment and its microfabricated structures allows precise fluid control. A wide variety of microfluidic chip-based isolation techniques have been proposed and some popular separation methods include immunoaffinity-based separation, immunomagnetic separation, dielectrophoretic-force based separation, density based separation, and size-based separation (Figure 3). In this section, CTC separation technique based first four methods will be discussed. Size-based CTC separation method will be discussed separately in chapter 3.

Immunoaffinity-based CTC Isolation

Immunoaffinity based CTC capture is a method that selectively captures tumor cells from normal blood cells by binding with substrate-immobilized antibodies. **Toner's group** in Massachusetts Institute of Technology (MIT) developed a microfluidic chip which contains freestanding microposts functionalized with EpCAM antibodies (Figure 3, Figure 4a).¹⁰ Advantage of this system is that a whole blood sample can flow directly through the device. The structure is optimized to maintain the minimum amount of shear stress; the shear of blood going through the device is calculated to be less than blood going through the heart valves during the normal circulations.¹⁰ The same group later developed a second generation chip named “herringbone-chip,” in order to improve the performance

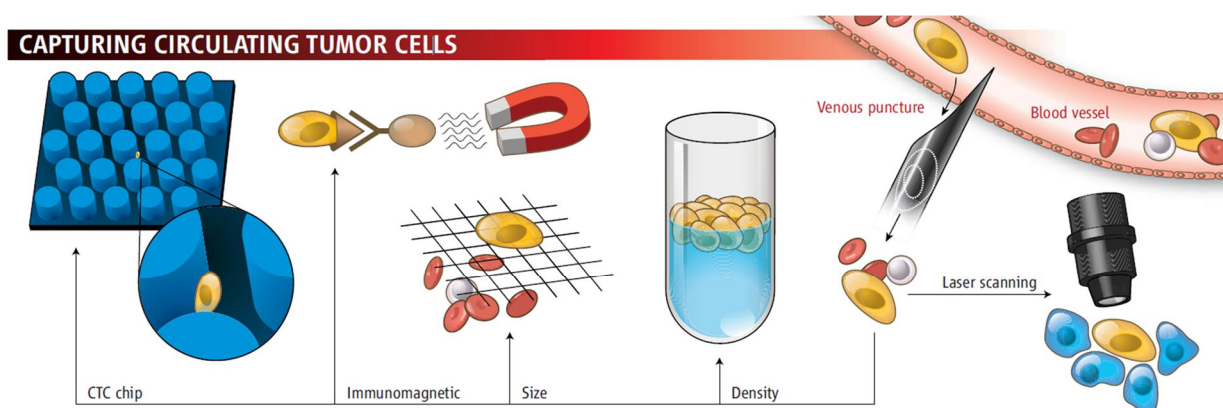


Figure 3 Schematic illustration of current CTC isolation approaches in a blood sample.²

of the CTC capture. Newly devised platform further enhances the mixing of the fluids in the channels. Specifically, herringbone patterns in the channel ceiling produces vortices within the flow and maximize collision between CTCs and the surface of the channel, further increasing the possibility of cell-to-surface interactions, thereby a yielding high cell recovery rate.¹⁶ Scientists in Toner's group further developed a more advanced version of CTC capture device, referred to as "CTC-iChip." The CTC-iChip consists of three functional modules including hydrodynamics-based cell sorting module, inertial focusing module, and magnetophoresis-based enrichment module.¹² The advantage of this system is that it can be operated in both positive isolation mode and negative depletion mode.

Soper's group in University of North Carolina, developed a polymer-based microfluidic device which contains a series of unique sinusoidal cell capture channels immobilized with anti-EpCAM (Figure 4b).²⁰ The device is capable of capturing CTCs directly from whole blood, with high efficiency and specificity. Furthermore, in order to perform automatic enumeration of captured target cells, the isolated CTCs were released by trypsin and counted using a single-cell conductivity sensor. The same group later enhanced the performance of the sinusoidal channel-based CTC isolation system by applying additional microfluidic components including the imaging module in addition to isolation and enumeration modules.²¹

Tseng's group in University of California Los Angeles (UCLA) developed a Velcro-like microchip device where they employed electrospun TiO₂ nanofibers as a substrate for the anti-EpCAM immobilization (Figure 4c). Densely packed TiO₂ nanofibers provided more surface area than the flat surface for the antibody immobilization, consequently, improving the cell capture performances. This group also developed a striking technology that releases captured cells, retaining close to 90 % of the viability, by adding temperature-sensitive polymers to the nanofibers.²³

Immunomagnetic isolation of CTCs

Immunomagnetic isolation method is a type of immunoaffinity-based separation where antibody-antigen interaction is used in conjunction with the external magnetic force. Similarly, EpCAM antibodies are tagged with the magnetic nanoparticles, and the magnetic field is applied such that the rare CTCs are driven in a magnetic field to be able to allow their isolation. The main factor that influences the separation efficiency in this approach is the balance between hydrodynamic force and external magnetic force.⁴⁰ In other words, it is possible to adjust the net force acting on the magnetized cells by manipulating the dynamics of the fluid flow in the microchannel, thereby collecting the target cells at the specific location inside the channel where the magnetic field strength becomes the maximum.⁴⁰ An example of such type of an approach can be found in the work

performed by **Zhang's group** in the University of Texas at Austin. They developed a microfluidic system that employed a magnetic field gradient as an external force (Figure 4d). The microchip consisted of a simple rectangular micro channel in which a stack of neodymium magnets are secured underneath²⁵. In this system, the magnetic field gradient was generated between the adjoining magnets, efficiently attracting magnetic particle labeled tumor cells at the floor of the channel.

Alternatively, **Ingber's group** at Wyss Institute, Harvard focused more on the architecture of their magnetic-based separation device. They invented a unique PDMS-based microfluidic chip with the magnets placed underneath the collection chambers (Figure 4e). Specifically, the device is comprised of a slanted inlet channel that connects to a main collection channel which is then extended in the opposite direction to form a “redundant double collection channel.”²⁷ Additionally, multiple rows of perpendicularly oriented side chambers are protruded from the main channel and a double collection channel. As the fluid passes through the channel, magnetic bead-bound tumor cells are sequentially collected in these dead-end side chambers.

Immunoaffinity-based CTC detection methods discussed above heavily depend on the use of the EpCAM biomarker to identify the presence of the target CTCs. The EpCAM-dependent CTC detection technology is based upon the assumption that the target cancer cells have a sufficient EpCAM expression level to readily interact with corresponding antibodies. In reality, however, EpCAM expression is highly heterogeneous in different types of tumor cells, and even absent in some tumor types which are of nonepithelial origin.⁴¹ Moreover, circulating tumor cells are very susceptible to degradation, apoptosis, and other real-life phenomena that really cannot be easily recapitulated with cancer cell lines.⁴¹ Therefore, new enrichment process might be necessary to overcome the pitfall of this technology.

Density-based separation

Density gradient centrifugation is a leukocyte separation technique which can also be applied in CTC separation (Figure 3). Using the commercially available **Ficoll-Paque PLUS®** (Pharmacia-Fine Chemicals, Uppsala, Sweden) medium, a solution with a density of 1.077 g/mL, it is possible to generate a layered separation of cell types based on cellular density.⁴² Mononuclear leukocytes and circulating tumor cells have similar densities of lower than 1.077 g/mL, whereas densities of other cells in blood are higher than 1.077 g/ml.⁴³ As a result of 20 minutes of centrifugation, the bottom layer will contain aggregated red blood cells (RBCs), and the layer which is located immediately above the erythrocyte layer will mostly consist of granulocytes, having a density high enough to migrate through the Ficoll-Paque PLUS layer. Lastly, the leukocytes and CTCs will be located at the

interface between the Ficoll-Paque PLUS and plasma layers. The disadvantage of this technique is that it provides poor separation efficiency, mainly because of the loss of target tumor cells that might be either migrated to the plasma layer or trapped in the aggregates of the RBCs. Furthermore, the system is not designed to separate CTCs from leukocytes; therefore, additional steps are necessary to increase the purity of the final product.

Electrokinetic Isolation of CTCs

Electric dipoles can be induced when a non-uniform electric field is applied on the cells; hence, cells are considered as a “dielectric bioparticles”.⁴⁴ Dielectrophoretic (DEP) force-based CTC isolation approach takes advantage of the dielectric phenotype of tumor cells. Different types of cells will experience different DEP forces because the magnitude and the direction of the force applied on the cells partially depend on intrinsic properties of the cells such as membrane capacitance and cytoplasmic conductivity.³⁹ **Jung’s group** in Yonsei University demonstrated the separation of breast cancer cells from whole blood exploiting dielectrophoretic separation method together with hydrodynamic approach in order to enhance the separation efficiency (Figure 4f).¹⁹ DEP-based CTC separation method is known as one of the efficient label-free CTC detection methods. However, this approach may affect the physiology of the target cells due to the use of a low conductivity medium during the separation process.

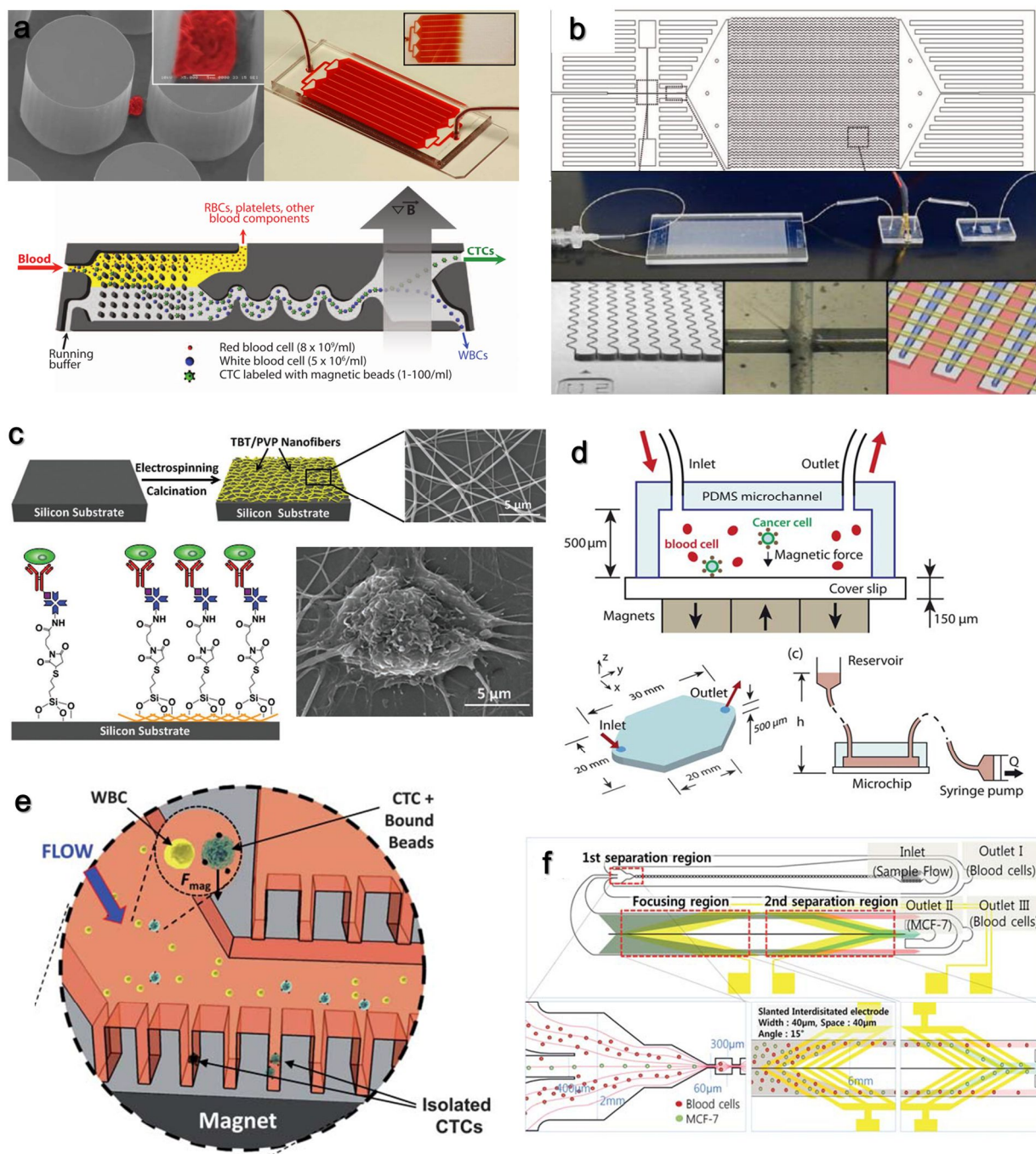


Figure 4 Examples of CTC separation technologies. (a) CTC capture method using anti-EpCAM coated silicon microposts¹⁰, herringbone structure¹⁶, and inertial focusing method¹². (b) CTC separation method using anti-EpCAM sinusoidally shaped channels.²⁰⁻²¹ (c) CTC separation method using immobilized TiO₂ nanofibers.²³ (d) Immunomagnetic-based CTC separation by employing a magnetic field gradient across the microchannels.²⁵ (e) Immunomagnetic-based CTC isolation using dead-end side channels for a sequential collection of magnetized tumor cells.²⁷ (f) CTC separation using dielectrophoresis (DEP) and multi-orifice force fractionation (MOFF).¹⁹

1.1.3 Commercial Technologies for CTC Detection

CellSearch

The enrichment process of CellSearch™ (Janssen Diagnostics, South Raritan, NJ), the only FDA-approved CTC detection instrument on the market, involves the use of immunomagnetic-based separation technique (Figure 5a,b).¹ The system can be used to aid in the monitoring of patients with prostate, breast, and colorectal metastatic cancer and predict progression free survival and overall survival.^{1, 15} CellSearch™ utilizes EpCAM antibodies conjugated to ferromagnetic fluid particles as a mean of attracting the EpCAM expressed tumor cells. Afterwards, immunostaining procedure is performed for the characterization of captured tumor cells using the predefined criteria- DAPI positive, CD45 negative, and cytokeratin and 8 and 18 positive. A large number of clinical investigations were demonstrated with this system.^{10, 15, 42} As a semi-automated platform, however, CellSearch™ system yield a relatively lower capture efficiency and purity compared to more recently developed technologies.⁴²

Isoflux

Isoflux™ System (Fluxion Bioscience, San Francisco, CA) is another type immunomagnetic-based isolation approach which takes advantage of magnetic beads and proprietary microfluidic flow focusing technology to achieve high cell enrichment (Figure 5c,d).⁴ The recovered cells can move immediately to downstream molecular analysis including mutation detection, next-generation sequencing, and gene expression.⁴ Limitation of this system is that it requires a long sample preparation step, which may adversely affect the enrichment results.

ScreenCell

ScreenCell™ (ScreenCell, Sarcelles, France) is a simple and robust size-selective CTC enrichment device which allows phenotypical, genotypical, and functional downstream characterization of captured CTCs (Figure 5e,f).^{11, 26} Prior to the separation process, the blood sample is treated with a proprietary dilution buffer in order to cell fix mononucleated cells and lyse the RBCs. ScreenCell™ system can also be applied in separating isolating circulating fetal cells (CFCs), which are known to be found in maternal peripheral blood.

Cytotrack

The basic mechanism of Cytotrack CT4 (Cytotrack ApS, Lyngby, Denmark) scanning system is derived from a conventional CD/DVD technology (Figure 5g,h).¹³ In this system, RBC lysed-blood sample including all the leukocytes are immobilized onto a Cytotrack glass disc, which is then coated

with a proprietary reagent that binds the cells to the surface of the glass disc. Then, the entire surface of the glass disc is scanned within a few minutes. During the scanning, all data are processed in real time by the control system. The scanner automatically identifies a number of locations on the disc where candidates are positioned.

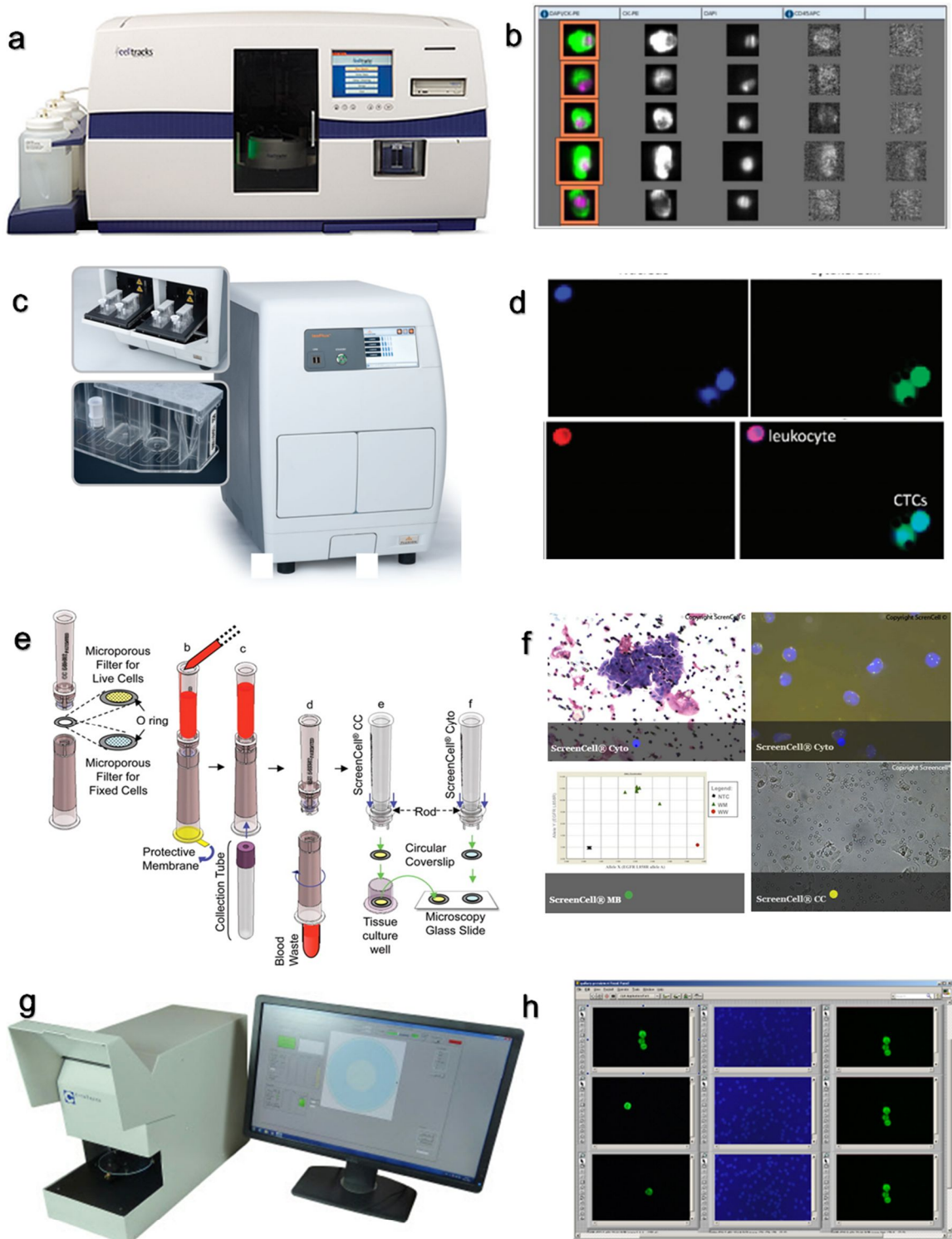


Figure 5 Examples of commercialized CTC detection system. (a,b) CellSearch™ system of Janssen Diagnostics LCC, Johnson & Johnson Corp.¹ (c,d) IsoFLux System™ of Fluxion Biosciences.⁴ (e,f) ScreenCell™ size-selective isolation device from ScreenCell™.¹¹ (g,h) Cytotrack CT4 scanning system from Cytotrack ApS.¹³

1.1.4 Challenges for CTC Studies

A major challenge that still remains in CTC studies is that the low-abundant target cells must be detected in a limited amount of sample. CTCs are extremely rare in whole blood, occurring at a frequency as low as 1~10 cells per $10^6\sim 10^7$ of other blood cells.⁴⁵ In this regard, the simplest way of improving the detection efficiency would be to increase the input volume of the sample. A recent study by Lalmahomed *et al.* used the CellSearch™ system to test the detection rate at different sample volume for a group of 15 patients with colorectal cancer.⁴⁶ They compared the numbers of detected CTC in 7.5 mL and 30 mL of whole blood from the same patient. As a result, the median CTC count was 1 with a range of 0 to 4 in 7.5 mL of blood, whereas in 30 mL of blood, the median CTC count was 2 with a range of 0 to 9. Also, CTCs were found in 13 % of the entire patient samples for 7.5 mL assay, and 47 % of the entire patient samples for 30 mL assay. The results indicate that the larger sample size might be required for a CTC assay in order to generate a meaningful enumeration statistics. However, it is still challenging in microfluidic system to handle a large volume of the sample because it requires a long time for a micro-scale chip to process milliliters of blood.

In addition to low population, the heterogeneity of CTCs is another factor that poses a challenge for efficient detection of target cancer cells. For example, even though EpCAM is prominently selected as a biomarker for CTCs of epithelial origin, the EpCAM expression level is highly heterogeneous among different types of tumor cells. In a nutshell, in order to overcome some intrinsic challenges of CTC detection technologies, it is essential to develop a high-throughput CTC detection platform which is capable of processing samples with high sensitivity, within a short period of time.

1.2 Centrifugal Microfluidics

1.2.1 Theory

Centrifugal microfluidics, also known as lab-on-a-disc, is a branch of microfluidics that exploits the spinning of a disc to induce fluid transfer. As the disc rotates, centrifugal force is exerted on the fluids, driving them radially outwards from the center of the disc. For the fluid propulsion, the flow rate depends on the rotational speed, radial location of the fluid reservoirs/channels, channel geometry, and fluidic properties (e.g. viscosity, density, etc.) of the sample (Figure 6).⁴⁷ The average velocity, U , of the liquid in a microchannel can be derived from centrifugal theory as the following³:

$$U = \frac{D_h^2 \rho \omega^2 \bar{r} \Delta r}{32 \mu L} \quad \text{Eq. 1}$$

where D_h is the hydraulic diameter of the channel (defined as $4A/P$, where A is the cross-sectional area and P is the wetted perimeter of the channel), ρ is the density of the liquid, ω is the angular velocity of the disc, \bar{r} is the average distance of the liquid in the channels to the center of the disc, Δr is the radial extent of the fluid, μ is the viscosity of the fluid, and L is the length of the liquid in the microchannel.³

1.2.2 Diagnostics in Centrifugal Microfluidics System

The centrifugal microfluidic platform offers many advantages over other microfluidic systems. Only a simple rotary motor is necessary to generate forces needed for fluid actuation, while laminar flow-based microfluidic systems require a complex setup for external apparatus.³ In addition, centrifugal microfluidic devices have capabilities of valving, mixing, and metering which induces an effective fluid control and an efficient mixing of solutions. For these reasons, lab-on-a-disc platforms have been utilized in a variety of biomedical applications. One of the examples is the performance of immunoassays on a disc. Lee *et al.* has developed bead-based immunoassay on a lab-on-a-disc for the detection of hepatitis B virus (Figure 7b).¹⁸ The device offers a full integration, performing steps including plasma separation from whole blood, binding of a target sample on the surface of antibody conjugated microbeads, washing, reactions with enzymes, and finally, the detection. Furthermore, by taking advantage of the fact the disc-based microfluidics is capable of manipulating a complex fluid flow by applying active valves in the system, Park *et al.* devised a fully automated lab-on-a-disc for simultaneous detection of multiple protein biomarkers, i.e., fully-integrated multiplex immunoassays.⁴⁸ Sample preparation^{17, 49}, nucleic acid amplification⁵⁰, DNA microarray hybridization^{22, 51}, and cell assays²⁴ are some of other applications that have been performed in a centrifugal microfluidic system (Figure 7).

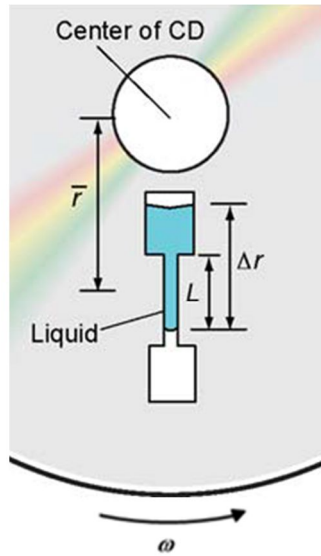


Figure 6 Schematic illustration of the centrifugal microfluidics.³ \bar{r} is the average distance of the liquid in the channels to the center of the disc, Δr is the radial extent of the fluid, and L is the length of the liquid in the microchannel.³

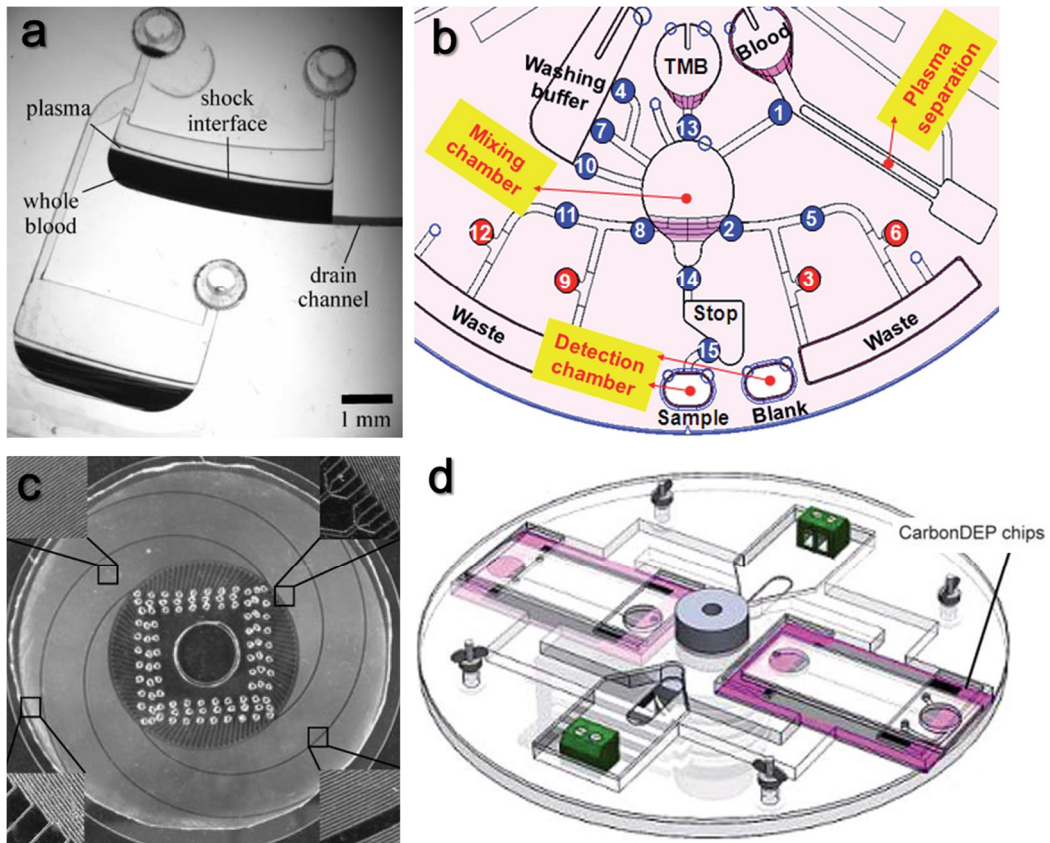


Figure 7 Examples of centrifugal microfluidic platforms used in biomedical applications. (a) Plasma separation on a disc.¹⁷ (b) Fully integrated immunoassay on a disc.¹⁸ (c) DNA microarray on a disc.²² (d) DEP trapping of yeast cells on a disc.²⁴

1.3 Literature Survey: Size-Selective CTC Separation

In this chapter, we will primarily focus on CTC detection platforms which does not take advantage of any external forces (e.g. electric field or magnetic field) or target specific antibodies (e.g. EpCAM antibody), but rely exclusively on hydrodynamic characteristics of microfluidic system and the size of target cells for separation.

1.3.1 Hydrodynamic Force-driven Separation

The primary assumption underlying hydrodynamic force-driven filtration is that, the fluidic system with low Reynolds number where the laminar flow predominates, the particles in the center of the defined channel will always follow fluid streamlines. Hydrodynamic cell sorting method separates cells based on differences in size of the cells by using specialized microstructures to transport cells to desired streamlines through a flow manipulation. Specifically, the flow manipulation can be achieved through contracting and expanding the flow by varying the widths of the microchannel. A popular hydrodynamic method is “pinched flow fractionation”⁵. In the work done by Yamada *et al.*, a pinch channel was used for guiding the particles of specific sizes to the desired streamline, where they can be collected at the end of the extended channel (figure 8a). Once the fluid reaches the end of the

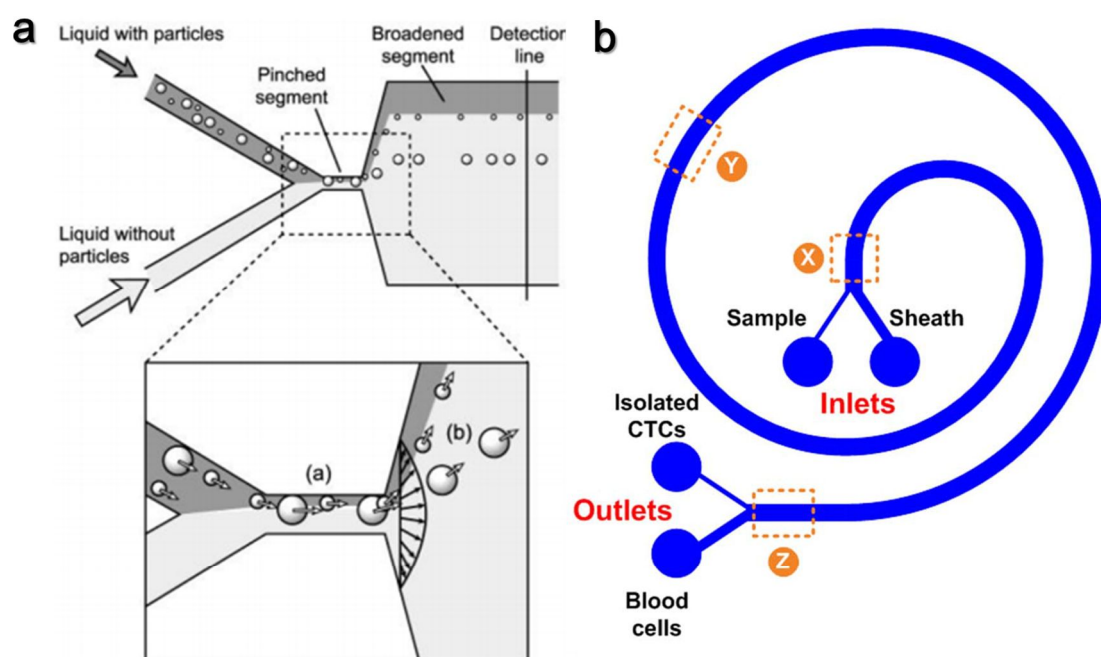


Figure 8 Examples of size-based CTC isolation using the hydrodynamic properties of the fluids. (a) Particle separation via “pinched flow fractionation” method.⁵ (b) CTC isolation using the spiral-shaped microchannel.¹⁴

channel, smaller particles can reach streamlines closer to the wall whereas larger particles remain traveling along the center of the channel. Another well-known geometry that can be used to separate CTCs by hydrodynamic cell sorting method is proposed by Hou *et al* (Figure 8b).¹⁴ Their proposed device, a spiral shaped microfluidic channel that consists of double inlets and double outlets, can continuously separate tumor and blood cells by the size difference between CTCs and leukocytes. Using this system, the obtained the recovery rate of 85 %, and clinical testing was performed as well.

1.3.2 Direct Filtration

It is reported that the size of the CTCs are, on average, larger than ambient blood cells, including erythrocytes and leukocytes, in whole blood. Average sizes of CTCs ranges from 12~25 μm while those of red blood cells and white blood cells are around 1-3 μm and 8-12 μm , respectively.⁹ The most intuitive approach for separating cells based on size exclusion method is perhaps by mechanically filtering target cells using a microsieve structure, which is designed to restrict passages to cells smaller than the “critical size.” The microsieve structure can be fabricated through conventional microfabrication process including typical photolithography⁵² or laser ablation⁵³ methods. Advantage of using the fabricated membranes, instead of using commercially available track-etch membrane is that it is possible to obtain a membrane with a uniform array of well-defined pores.

Lin *et al.* developed a parylene membrane micro-filter device with circular holes, with a center-to-center distance between adjacent pores of 20 μm (Figure 9a). The capture efficiency using this parylene membrane filter was 93 %.⁹ The size difference between CTCs and human blood cells was used to test 57 blood samples from patients with metastatic prostate, breast, colon, or bladder cancer. The result demonstrated CTC capture and identification in 51 of 57 patients compared with only 26 patients in 57 patients using the conventional CellSearchTM method. However, this process resulted in low capture cell viability due to the large stresses that developed in the cell membrane during the cell capture process.⁵⁴ Zheng *et al.* from the same group developed an upgraded version of parylene membrane (Figure 9b). The filtration device consisted of two layers of parylene with uniformly arrayed pores. The position of the bottom membrane layer was shifted in order to decrease stress experienced by the cell during the filtration process. Using this filter, they performed a cell isolation experiment and obtain the capture efficiency of approximately 86 %, and this was comparable to their previous filtration system. The captured cells were viable and even after 14 days of cell culture directly on the device.

Hosokawa *et al.* introduced a nickel filter with a rectangular micropore array using a conventional

photolithography technique (Figure 9c). They compared the recovery rates between the membrane circular and rectangular micropores. The recovery rate of captured cells using the membranes with rectangular pores was approximately 80 %, whereas the recovery rate using those with circular pore only 67 %. In addition, they were able to recover the CTC with higher purity. For the clinical tests, it was discovered that the percentage of CTCs in total captured cells was significantly higher on the using the membranes with rectangular pores (0.33 %). Table 1 summarizes the recent research in size selective filtration-based CTC separation methods.

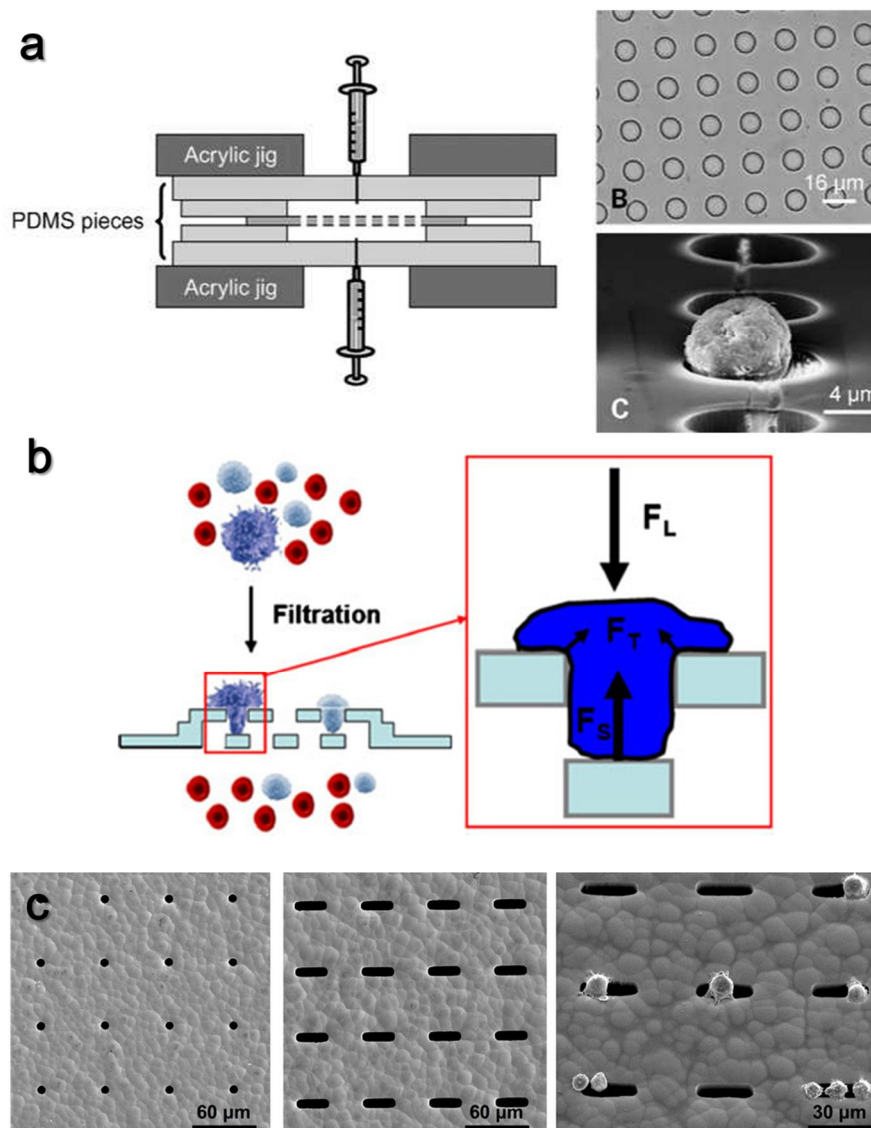


Figure 9 Examples of size-based CTC isolation using the direct filtration method. (a) A parylene membrane micro-filter device with circular holes. (b) A double-layered parylene membrane. (c) A nickel filter with a circular and rectangular micropore array.

Table 1 Recent research in size selective filtration-based CTC separation methods.

Reference	Device Performance			Sample Treatment			Cancer Type		Filter Profile		
	Yield* (%)	Purity (%)	Flow rate (mL/min)	RBC removal	Dilution	Pre-Fixation	Cell line	Clinical Test	Material	Pore size (μm)	Pore density (pores/ mm^2)
Zheng <i>et al.</i> ⁵⁵	86.5	-	0.1	Lysis	1:10	None	LNCaP	-	Parylene	7	4.4×10^2
Lin <i>et al.</i> ⁹	> 90	-	3.8	None	1:1	1 % NBF	RT3, T4, MCF7	Prostate, Colorectal, Breast	Parylene	8	-
Zheng <i>et al.</i> ⁵⁴	~90	-	2	None	1:10	None	LNCaP	-	Parylene	10	2.9×10^3
Desitter <i>et al.</i> ²⁶	88.0	-	15	Lysis	3:4	FC2 buffer**	NCI-H2030, H1975	-	Polycarbonate (PC)	7.5 6.5	1×10^2
Lim <i>et al.</i> ⁵²	> 80	~5.0	1	None	1:2	None	HepG2/GFP, MCF7, BT474	Breast, Colorectal, Prostate	Silicon	10	5×10^3
Coumans <i>et al.</i> ⁵⁶	> 80	~7.1	1.7	None	1:4	0.8 % PFA	PC3-9, SKBR3	-	Polycarbonate (PC)	5 8	3.4×10^3 9.0×10^2
Hosokawa <i>et al.</i> ⁵⁷	~ 80	0.1	200	-	-	-	SCLC, NSCLC	Lung	Nickel	9.0×30 (Rectangular)	3.0×10^1
Kim <i>et al.</i> ⁵⁸	68.7	11.8	-	Density gradient centrifugation	None	None	H358	-	Parylene	8.5×8.5 (Rectangular)	-
Hosokawa <i>et al.</i> ⁵⁹	68~100	-	0.2	-	-	-	A549, HCC 827, PC14	Lung	Poly(ethylene terephthalate) (PET)	8.0 ~ 9.0	-

*The yield refers to the capture efficiency of target cancer cell lines spiked into whole blood.

**FC2 buffer is an optimized proprietary dilution buffer used for RBC lysis and cell fixation in the ScreenCell™ system.

1.3.3 Size Amplification

Kim *et al.* proposed a CTC isolation platform which takes advantage of the size amplification technique along with multi-obstacle filter architecture.⁶ Unlike other size-based CTC isolation methods, antigen-antibody interaction was applied in size amplification. Specifically, the method consisted of two sequential processes (Figure 10). First step is the selective size amplification of CTCs, which was achieved by conjugating EpCAM coated solid melamine microbeads with cancer cells. This permitted avoidance of a size overlap between the CTC and leukocytes. Second step was the passing of microbead-conjugated CTCs through a multi-obstacle architecture (MOA) microfluidic filter. Their unique platform with multiple obstacles allowed more stable cell capture by reducing the shear stress exerted on cells while passing through the device. The recovery rate using this device turned out to be 89.7 % (N=7) when 10 cells per 1mL was infused in the system. In addition, white blood cells remained in the chip, however, the number ranged from 272~405 cells in each filter chip. The major reason for enhanced performance of CTC is distinct size discrimination between the target cells and leukocytes.

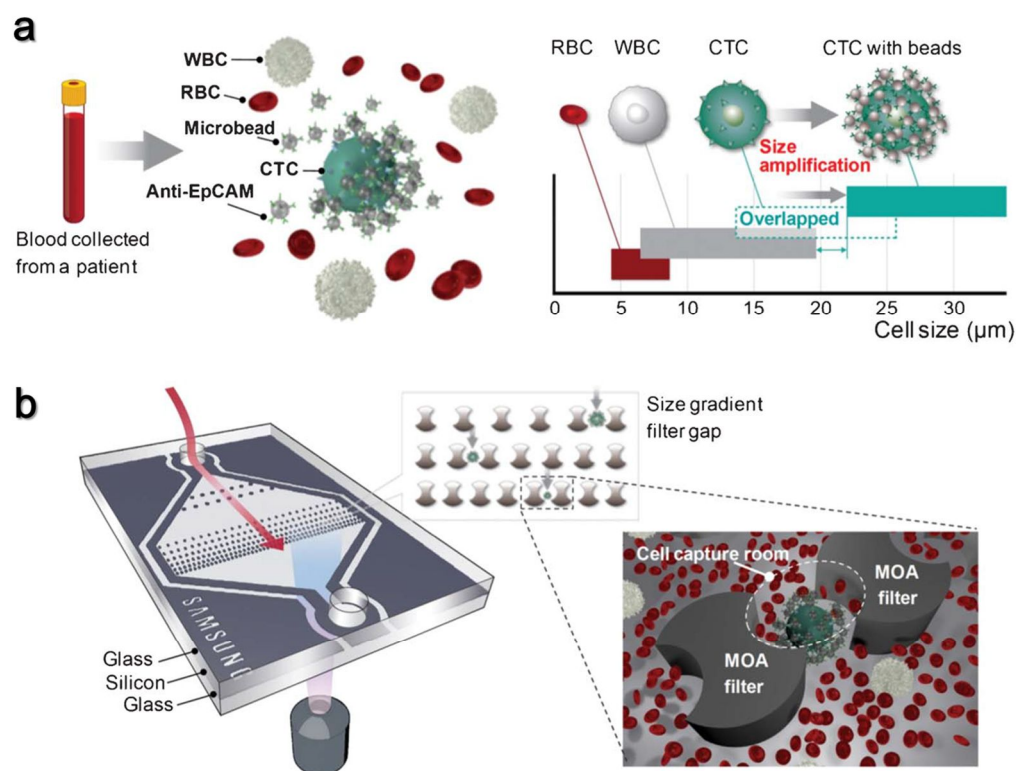


Figure 10 Schematic illustration of size amplification method using multi-obstacle architecture (MOA) filtration device.⁶ (a) Selective size amplification of CTCs was achieved by conjugating EpCAM coated solid melamine microbeads with cancer cells. (b) EpCAM coated solid melamine microbeads with cancer cells.

1.4 Research Outline

1.4.1 Objectives of the Thesis

One major drawback of CTC detection using a conventional microfluidic approach is that it generally requires a long processing time. In the case of isolation methods based on immunoaffinity, for example, the system is limited by the number of sufficient interactions between surface-bound antibodies and target cancer cells. Although various capture structures such as microposts¹⁰ and patterned herringbones¹⁶ have been shown to increase these interactions, throughputs of such platforms still remain within milliliters per hour. In this regard, size-based isolation methods are more efficient because these methods have a higher throughput as they are compatible with relatively higher flow rates (Table 2). Another advantage of CTC isolation approach based on size differences is that it has a potential to capture any type of CTCs regardless of their EpCAM expression level.

The throughput of the CTC isolation system can be further enhanced by exploiting a centrifugal microfluidics, or lab-on-a-disc. Compared to the conventional microfluidic system, lab-on-a-disc system offers a more efficient fluid control because it does not require external interconnects. Furthermore, only a simple rotary motor is necessary to propagate the fluid flow, whereas a complex instrumentation is needed in the laminar flow-based microfluidic system.³ In addition, the device can be fabricated in inexpensive materials such as polycarbonate, offering the cost-effective

Table 2 Comparison of different types of CTC isolation system.

Type of System (Approach)	Throughput		Profitability	Convenience	Reference
	Sample Processing Time	Sample Volume	Material	Automation & Integration	
CTC-iChip (Immunoaffinity)	>3 hours	10 mL	Silicon	×	Ozhumer <i>et al.</i> ¹²
CellSearch TM System ¹ (Immunomagnetism)	>1 hours	7.5 mL	Ferrofluid	Δ	Cristofanili <i>et al.</i> ¹⁵
MOFF-DEP separator (Dielectrophoresis)	~ 30 min	2 mL	PDMS	×	Moon <i>et al.</i> ¹⁹
Spiral Biochip (Hydrodynamic force)	~1 hour	3 mL	PDMS	×	Hou <i>et al.</i> ¹⁴
ScreenCell TM System ¹¹ (Direct filtration)	>3 min	3 mL	Polycarbonate	×	Desitter <i>et al.</i> ²⁶

manufacturing process for the mass production. Thus, centrifugal microfluidic system can serve as an excellent candidate for the CTC separation platform which requires a rapid and efficient sample processing.

The goal of this thesis is to **develop a size-selective centrifugal microfluidic system for the rapid and efficient isolation and characterization of the circulating tumor cells.** The detailed objectives for this research project include:

- (i) Fabrication of a biocompatible through-hole membrane for size-selective cancer cell separation.
- (ii) Design and fabrication of a membrane-installed high throughput lab-on-a-disc system, the CTC-capture disc for capture and detection of cancer cells.
- (iii) Evaluation of the device performance by processing buffer samples and whole blood samples at different cell concentration.
- (iv) Performance evaluation of CTC isolation using the cells spiked in whole blood samples and patients samples.

1.4.2 Outline of the Thesis

The thesis begins with the introduction of the research in Chapter 1. First of all, basic concepts of the circulating tumor cell (CTC) and its clinical significance are explained. Next, multiple CTC detection methods and commercialized CTC detection systems are briefly discussed, followed by an in-depth literature review of the size-based CTC isolation technologies. The concept of a lab-on-a-disc platform is also discussed in the end of Chapter 1. In Chapter 2, the process of sample preparation, device fabrication, experimental set-ups for cell capture experiments are explained in detail. System setup for imaging apparatus is explained as well. In Chapter 3, results and discussion related to the device fabrication process and cell separation experiments are discussed in detail. Specifically, size distribution of different cancer cell lines and the staining process are discussed first. Next, the fabrication of track-etch membrane installed CTC-capture device is explained in detail. Then, the performance of the device is evaluated through experimental results of cancer cell-spiked samples and patients samples. Chapter 4 proposes future directions of this research, specifically focusing on improving the capture efficiency and purity by exploiting the negative depletion method, and using the microfabricated through-hole membrane as an alternative for the polycarbonate track-etch membrane. Finally, conclusions and future prospects are summarized in Chapter 5.

CHAPTER 2 Experimental Methods & Materials

2.1 Sample Preparation

2.1.1 Chemicals and Reagents

For cell culture and passage experiments, following reagents were used: RPMI-1640 and fetal bovine serum (FBS) purchased from Hyclone™ (Logan, UT, USA); Antibiotic/antimycotic solution, 0.25 % Trypsin-EDTA, and 0.4 % Trypan Blue purchased from Gibco® (Grand Island, NY, USA); Cell stripper™ purchased from Cellgro® (Manassas, VA, USA); and Dimethyl sulfoxide (DMSO) purchased at from Sigma-Aldrich (St. Louis, MO, USA)

For through-hole membrane and CTC-capture disc fabrications, following chemicals and reagents were used: SU-8 2025 photoresist and SU-8 developer purchased from MicroChem Corp. (Newton, MA, USA); PDMS prepolymer (Sylgard 194) and a curing agent were from Dow Corning (Midland, MI, USA); (Tridecafluoro-1,1,2,2-terahydrooctyl)-1-trichlorosilane purchased from (UCT Bristol, PA, USA); Methoxypolyethylene glycol amine purchased from Sigma-Aldrich (St. Louis, MO, USA); and n-(triethoxysilylpropyl)-o-polyethylene oxide urethane (TPU) purchased from Gelest (Morrisville, PA, USA)

For cell staining procedure, following reagents were used: Phosphate Buffered Saline (PBS) tablets purchased from Ameresco (Framingham, MA, USA); Bovine Serum Albumin (BSA) purchased from Bio Basic Canada Inc. (Markham, Canada); Human IgG purchased from (R&D Systems, Minneapolis, MN, USA); 4',6-diamidino-2-phenylindole (DAPI) purchased from Sigma-Aldrich (St. Louis, MO, USA); Anti-Pan-Cytokeratin- (AE1/AE3) eFluor® 615 and Anti-Human CD45-FITC purchased from eBioscience (San Diego, CA, USA); Anti-Cytokeratin- PE* purchased from BD Bioscience (San Jose, CA, USA); 35 % Formaldehyde solution purchased from Samchun Chemical (Kyunggi, Korea); and Triton X-100 purchased from Biossesang Inc. (Kyunggi, Korea).

2.1.2 Blood Specimen Collection and Processing

All blood samples, including healthy donor blood samples and patient blood samples were collected after an Institutional Review Board (IRB) approval. For patient blood samples, blood was drawn from 10 lung cancer patients and 13 gastric cancer patients from Pusan National University Hospital. All Blood samples were stored in EDTA tubes (BD Vacutainer, Becton, Dickinson and Company, USA) at

4°C to avoid blood coagulation. Samples were processed within 12 hours after collection to ensure white blood cells are still viable.

2.1.3 Cancer Cell Lines

Cell culture and passage

MCF7 breast cancer cell lines, AGS gastric cancer cell line, and PC3 prostate cancer cell lines were used in this research. All the cell lines were purchased from American Type Culture Collection (Manassas, VA, USA) were cultured in RPMI Medium with 5% FBS and 1% antibiotics/antimycotics. Cell lines were grown in humid environment at 37°C and 5 % CO₂. The cells were sub-cultured at regular intervals. They were exposed to 1 mL of Cell stripper™ for 3 minutes and suspended in 1xPBS buffer to harvest the cells. Centrifugation conditions for live cells and fixed cells were 2500 rpm (600 g) for 3 min and 13200 rpm (16100 g) for 1 min, respectively. The condition was determined to keep from possible cell rupture or cell losses. Only passage cells from passages 2 to 20 were spike into 1xPBS buffer or whole blood samples for spike-in experiments.

Cell staining

MCF7 cells were stained using a predefined criteria for CTC characterization: DAPI for nucleus staining, Cytokeratin for a CTC identification and CD45 for leukocyte identification. Specifically, concentrations of staining solution used per test was as following: 100 ng/mL of DAPI, 8 µg/mL of Anti-Pan-Cytokeratin- eFluor® 615, 240 ng/mL of Anti-Cytokeratin- PE*, and 4 µg/mL of Human CD45- FITC. For the staining process, the cells were first blocked with 500 µg/mL of Fc blocker (Human IgG) for 15 minutes to at RT, followed by washing step with 0.5 % BSA in 1xPBS buffer solution. Then, the cells were fixed with 4 % paraformaldehyde for 15 minutes at RT, followed by a 5 minutes of permeabilization with 0.1 % Triton X-100 in 0.25 % BSA in 1xPBS solution. Then, the cells were incubated with a staining cocktail of DAPI, CK and CD45 for 20 minutes at RT. Lastly, washing step with 0.5 % BSA was performed in order to remove any excess of stain solutions.

Rare cell counting

CTC studies deal with a rare number of cells, as few as 1~10 cells per given volume of sample. Therefore, for spike-in experiments, it is critical to be able to obtain low numbers of cells with high accuracy. Schematic illustration of a rare cell counting process is shown in Figure 11. For the counting of 1~10 cells, 1µL with approximately 20 cells were loaded on a cell culture dish. After most of the cells sediment, the pipette tip was carefully positioned at the loaded cell solution. Individual cells were carefully suctioned while looking under the microscope. For the counting of 50 ~ 200 cells, 1µL

with approximately 50~200 cells were loaded on a cell culture dish and counted under a microscope. Then, 9 μL of 0.25 % Trypsin-EDTA solution was loading directly on the loaded cell. After 30 seconds of incubation, the entire solution (10 μL) was repeatedly pipetted several times to ensure all the cells inside the solution are detached. Then, 10 μL of cell solution was suctioned carefully. After the retrieval of the cells, the surface of the dish was scanned under a microscope to locate any possible non-specifically adsorbed cells. For the counting of 1000~10000 cells, cell solutions of desired numbers of cells were acquired via serial dilution process. Using a hemocytometer, equal volumes of the cells from the same stock solution was counted three times, to confirm the cell concentrations. Pipette tips were always blocked with 0.5 % BSA in 1xPBS buffer solution prior to suctioning of cells to avoid cell adherence to the surface of the tips.

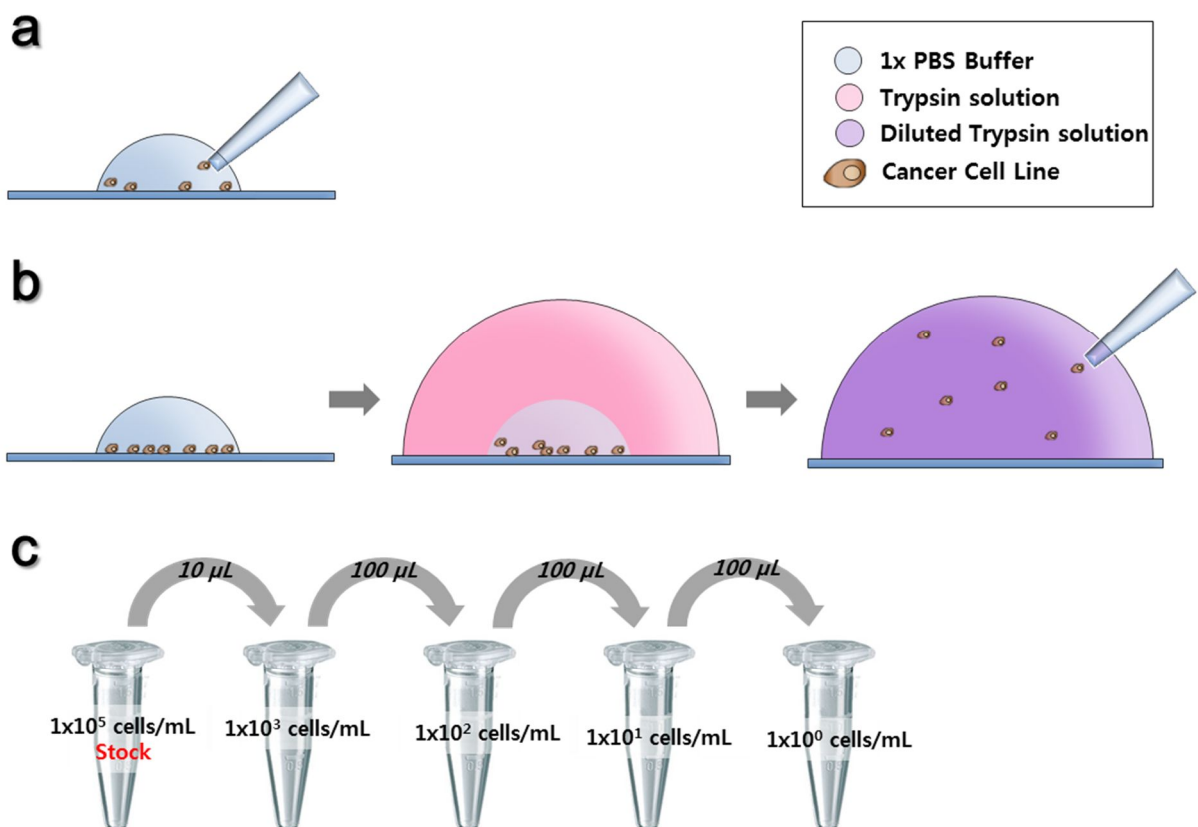


Figure 11 Schematic illustration of a rare cell counting process. (a) Cell counting protocols for 1~10 cells. (b) Cell counting protocols for 1~10 cells. (c) Cell counting protocols for 1000~10000 cells.

2.2 Device Fabrication

In this section, fabrication methods for the polycarbonate CTC-capture disc, disc operation process, and imaging process are briefly explained. Detailed disc fabrication results and evaluations will be elaborated in chapter 3.

2.2.1 Fabrication of the CTC-capture Disc

Disc Fabrication

The CTC-capture disc was designed with Solidworks 3D CAD design software (Waltham, MA, USA). Designed feature was fabricated using a CNC milling machine (M&I CNC Lab, Osan, Korea). Polycarbonate plates and sheets (PC: I-Components Co. Ltd, Korea) were used to create four individual device layers (1 top layer, 2 middle layers, and 1 bottom layer) of the CTC-capture disc (Figure 20). The thickness of the PC plates for each layers were 0.5 mm, 1 mm, 5 mm, and 1 mm, from top to bottom. Adhesive layers were separately designed and were incised using a cutting plotter (CE3000-60; Graphtec Corp., Japan). Fabricated PC device layers and adhesive layers were then appropriately bonded together using a pressure sensitive adhesive layer (DFM 200 clear 150 POLY H-9V-95, FLEXcon, USA). More detailed descriptions of the fabrication process the CTC-capture device are discussed in Chapter 3.

Polycarbonate Track-etch (PCTE) Membrane Installation

Commercially available hydrophilic polycarbonate track-etched membrane (PCTE) membranes (Whatman™, Florham Park, NJ, USA) were utilized in spike-in experiments. Track-etched membranes with the diameter of 13 mm, and the pore sizes of 5 μm and 8 μm were used in this research. Membrane was chemically bonded to the PC substrate by applying acetone to a bonding area.

2.2.2 Surface Passivation

The surface passivation was investigated by using three different types of reagents and chemicals: 1 % BSA, 1% Poly(ethylene glycol)bis(amine) (PEG-amine), and 1 % thermoplastic polyurethane (TPU). All the surfaces were cleaned with isopropyl alcohol (IPA) and sonicated in deionized water for 5 minutes prior to the experiments. The PEGylation of the PC surfaces, including the CTC-capture device and the track-etched membrane, the substrates were first treated with the oxygen plasma under the condition of 70%, 50 sccm, for 1 minutes (Cute plasma system; Femto Science, Korea), Then, the plasma treated substrates were incubated in 1% PEG-amine and diisopropylethyl amine for 2 hours at

RT, followed by a washing step with ethanol a final drying step. For the reaction with TPU, PC surfaces were treated under the same oxygen plasma condition (70 %, 50 sccm, 1 min). The substrates were treated with 1 % v/v TPU solution in ethanol for 2 hours at RT. After the incubation step, the substrates were washed with ethanol, baked at 80°C, and subsequently sonicated in ethanol for 3 min and dried. For analysis, contact angles for each surface were measured (goniometer; ramé-hart instrument co., Succasunna, NJ, USA).

2.3 System Settings

2.3.1 Disc-based Microfluidic System

The visualization system was used for the disc-based CTC capture experiments (Visualization System; HanRa Precision Eng Co., Korea). The disc operation system used in this experiment is composed of four individual modules: imaging module, motion control module, laser control module, and finally, a PC (Figure 13a). The imaging device is used to monitor and record the fluidic movements of the rotating disc, and is comprised of four individual components, which are CCD camera, lens, strobe light and manual stage. The camera installed in the imaging device is a CCD digital camera (IK-TF5C, Toshiba America, Inc., USA) in which video signal can save the 60 frame per 1 sec. For the motion control module, the device consists of a rotor, laser stage, magnet stage and controller. The rotor (SGMJV-02A 200W servomotor, Yaskawa Electric Co., Japan) offers a maximum rotational speed of 6000 rpm. Control PC contains software which is able to execute operations based on the pre-designed operating program. Using this software, it is possible to design the operating program of disc by manipulating variables including rotating speed, mixing frequency, laser irradiation, and position along with as saving conditions of image files. Laser irradiation and mixing tools were not utilized in this project. The operation program for the disc-based CTC isolation was created as shown Table 3.

Table 3 The operation program for the disc-based CTC isolation.

<i>No.</i>	<i>Staining Process</i>	<i>Fluidic State</i>	<i>Volume</i>	<i>Flow condition</i>	<i>Time</i>	
1	Sample Filtration	Flow	1 mL	2400 rpm*	15 sec	30 sec
2	Washing	Flow	1 mL	1200 rpm	15 sec	
4	Fc Blocking	Incubation	300 μ L	-	15 min	
5	Washing	Flow	500 μ L	1200 rpm	15 sec	
6	Fixation	Incubation	300 μ L	-	15 min	
7	Permeabilization	Incubation	300 μ L	-	5 min	50.8 min
8	Washing	Flow	500 μ L	1200 rpm	15 sec	
9	Staining	Incubation	300 μ L	-	15 min	
10	Washing	Flow	500 μ L	1200 rpm	15 sec	
Total Processing Time						51.3 min

* 2400 rpm is the maximum spin speed used for blood samples. Lower spin speed was applied for less viscous blood samples.

2.3.2 ScreenCell™ System

Figure 13b shows the experimental setup for ScreenCell™ filtration system. For the sample preparation process, four parts of ScreenCell™ FC2 buffer solution was added to three parts of blood samples, and the mixed sample was homogenized by inverting the tubes at least 5 times. ScreenCell™ FC2 buffer is a buffer solution made from ScreenCell™ which is known to fix and lyse the cells simultaneously. The volume of the blood samples used was the experiment was fixed to 1 mL. The diluted blood sample was then incubated for 8 minutes at RT. After the sample preparation step, the blood sample was loaded on module (i) of the ScreenCell™ Cyto Filtration Unit (Figure 14c). Then, Vacutainer™ tube was inserted to module (ii) in order to induce the sample filtration by vacuum. When the liquid reached the bottom of module (i), 1xPBS buffer solution was added to module (i) for a washing step. At the end of the filtration process, the filtration unit was disassembled to release the membrane. For staining procedure, the sequence of events and the concentrations of the reagents as well as the incubation times were identical as described in previous sections.

2.4 Imaging

Scanning Electron Microscopy (SNE 4500M; SEC E-Beam Pioneer, Korea) was used for the inspections of fabricated PDMS through-hole membrane. The samples were coated with gold prior to the inspection (SEC E-Beam Pioneer, Korea). For the characterization of captured cells, fluorescent inverted microscope (IX71; Olympus Corp., Japan) was utilized. The images of captured cells were analysed by using image analysis software (Metamorph, Molecular Devices, USA).

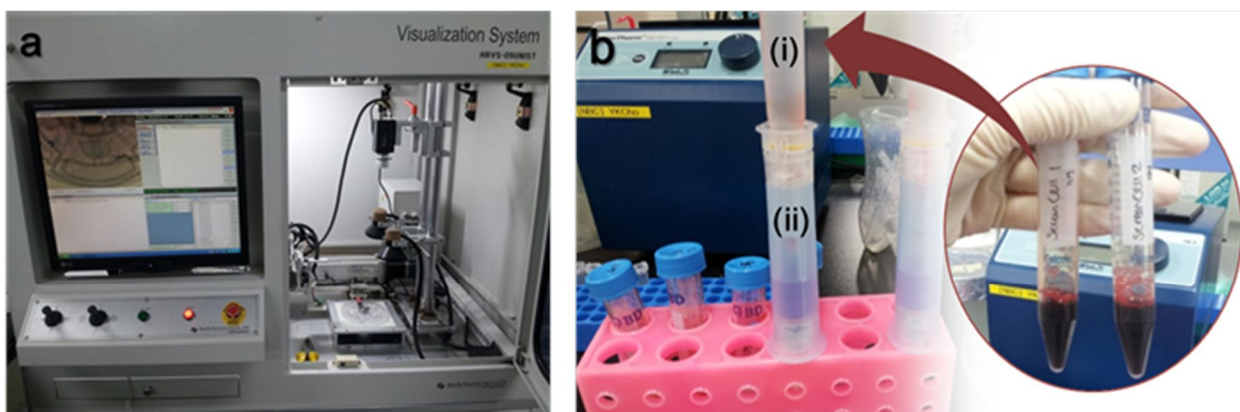


Figure 12 The system settings for (a) disc-based microfluidic system and (c) ScreenCell™ filtration system.

2.5 Fabrication of the PDMS Through-hole Membrane

Commercially available polycarbonate track-etch membranes consist of randomly distributed cylindrical pores. Random distribution of pores may result in the fusion of pores, and this would negatively affect cell isolation results by providing target cells with more chances of escape through the fused pores. For an alternative approach, it is possible to fabricate the membranes which have uniformly arrayed through-holes. The polydimethylsiloxane (PDMS)-based through-hole membrane fabrication method introduced in this section is the reproduction of the fabrication technique described in Choi *et al.*⁵³ Results of PDMS membrane fabrications are discussed in more in depth detail in chapter 4.

Patterns of the through-hole membrane were designed using a AutoCAD® software (Autodesk, San Rafael, CA, USA) which were then translated onto commercially fabricated chrome mask (MicroImage; Choongchung, South Korea). SU-8 Master for the membrane was fabricated by utilizing a standard photolithography technique. The fabrication process started with the spincoating of SU-8 negative photoresist on a bare silicon substrate (Etech, South Korea). SU-8 2025 photoresist was spincoated at 1800 rpm for 30 seconds on a 6" <100> P- type silicon wafer to obtain approximately 45 μm thickness of photoresist. Spincoated wafer was then soft baked at 65°C for 4 minutes and at 95°C for 6 minutes, sequentially, followed by UV exposure through the photomask (SUSS MicroTec, Garching, Germany). The photomask and the PR-coated silicon wafer were extensively cleaned with nitrogen gas prior to exposure step. Patterned wafer was then baked at 65°C for 4 minutes and at 95°C for 4 minutes. Finally, the patterned wafer was developed by submerging the wafer in SU-8 developer for 15 minutes.

Prior to a PDMS casting process, the surface of the fabricated SU-8 master was silanized with (Tridecafluoro-1,1,2,2-tetrahydrooctyl)-1-trichlorosilane. SU-8 master and the silanizing agent was placed inside the vacuum desiccator for 4 hours, forming the silane monolayer on the surface of the master. The casting of PDMS was performed by a conventional soft lithography process. A 1:10 mixture of a curing agent and PDMS prepolymer was poured onto a SU-8 master. Poured PDMS was then degassed in a vacuum desiccator for 6 hours in order to remove possible air bubbles trapped inside the pre-cured PDMS. Subsequently, degassed PDMS was baked in 65°C overnight and carefully demolded from the SU-8 master.

The next step was the surface passivation of the PDMS replica and the slide glass using a RIE apparatus (TTL, Korea). The surface of the PDMS mold was treated with CF₃ plasma under 50 sccm,

300 W treatment conditions for 100 seconds, and the surface of the slide glass was treated with the same gas plasma under 50 sccm, 15 W treatment conditions. Afterwards, the protruded patterns of the PDMS mold were faced with the slide glass in conformal contact. A pair of permanent magnets was then placed on both sides to hold molding block. Then, the empty space between the PDMS mold and the slide glass was gently filled with a 1:5 mixture of a curing agent and PDMS prepolymer. The molding block was put in a vacuum desiccator to remove air bubbles trapped in the PDMS gel, and was baked at 80°C for 4 hours. Lastly, the cured PDMS membrane was gently detached from the PDMS mold and the glass slide.

The final step of the membrane fabrication was the removal of the PDMS residual layer using the same RIE apparatus (TTL, Korea) used in the surface passivation of the PDMS mold and the slide glass. The surface of the PDMS membrane slightly etched with SF₆ (90 sccm)/ O₂ (6sccm) gas combination under the RF power of 500 W for 100 seconds. The etch rate was 0.47 ± 0.02 um/ min. RIE apparatus. The schematic illustration of the PDMS through-hole fabrication process is summarized in Figure 12.

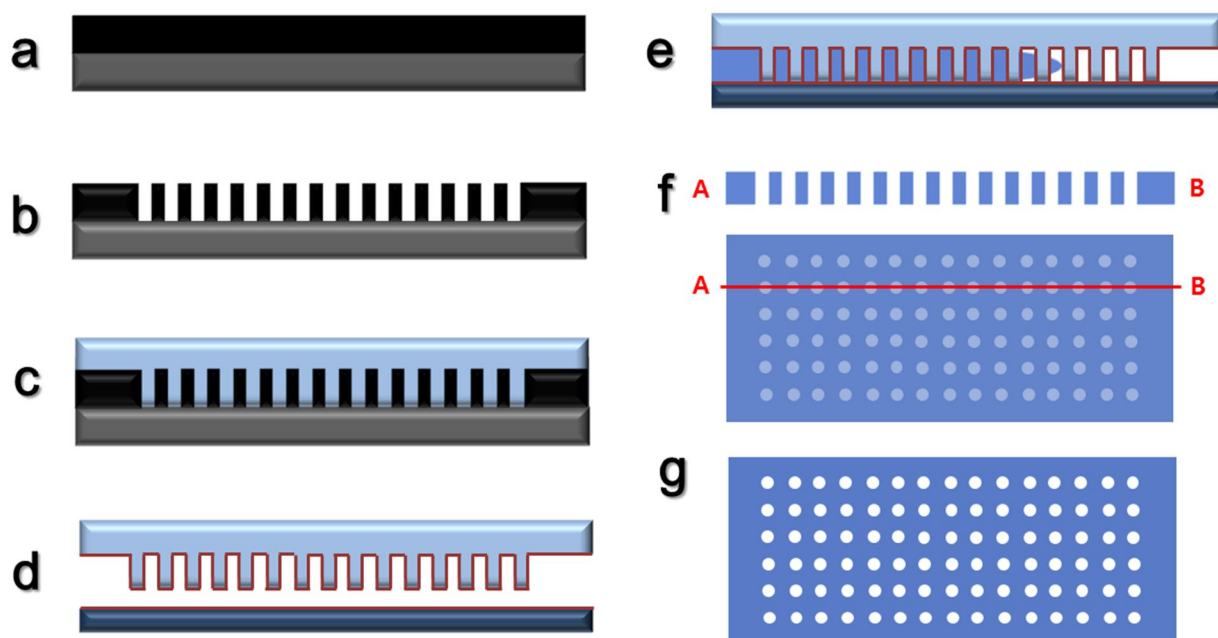


Figure 13 Schematic illustration of PDMS through-hole membrane fabrication process. The fabrication process consists of 6 individual steps: (a) SU-8 negative PR spincoating; (b) Soft bake, UV-exposure, and development; (c) Pouring of PDMS gel onto a SU-8 master; (d) Surface passivation; (e) Filling of PDMS gel; (f) Detachment of the PDMS membrane; (g) removal of the PDMS residual layer.

CHAPTER 3 CTC Isolation on a Centrifugal Microfluidic Device

3.1 Performance Metrics

The key objective of the CTC isolation technology is to efficiently capture rare cancer cells from blood sample, where the contaminant cells constitute the majority of the total cell population. In this research, two performance metrics- capture efficiency and purity- were applied to evaluate the performance of the devised CTC isolation platform. First of all, it is important to be able to isolate CTCs with high and consistent capture efficiency because the accurate enumeration of CTCs in patient blood samples is critical especially in clinical studies. As described in equation 1, the capture efficiency, which is also known as the recovery rate or capture yield, is defined as the percentage of the number of *captured* target cancer cells in the initial number of *input* target cells:

$$\text{Capture Efficiency} = \frac{\text{Target Cells}_{\text{final}}}{\text{Target Cells}_{\text{initial}}} \times 100 \quad \text{Eq. 2}$$

In this study, the number of input target cells is defined as the verified number of target cells infused in the syringe or the loading chamber of the capture device. The number of the input cell was proven to be accurate by optimizing the rare cell counting protocol proposed in chapter 2.

Secondly, the purity of captured cells is another important factor for the rare cell separation technology. As summarized in equation 2, purity is the percentage of the number of target cancer cells in *total number of captured cells* including any hematologic cells:

$$\text{Purity} = \left(\frac{\text{Target Cells}}{\text{Total Cells}} \right)_{\text{final}} \times 100 \quad \text{Eq. 3}$$

Purity of the output samples may vary among different blood samples even when the performance of the device is consistent because the numbers of leukocytes vary significantly among individuals. In the CTC studies, purity usually refers to the fraction of the captured cancer cells relative to the sum of the target cancer cells and *white blood cells, or leukocytes*. This is due to the fact the majority of the red blood cells are eliminated prior to processing the sample by lysing the RBCs or selectively excluding them via density gradient-based separation method. However, RBC elimination step is sometimes not required if the CTC isolation device is capable of efficiently sorting out RBC contaminants without any clogging issues.

Overall, capture of CTCs at high efficiency and high purity is considered critical in CTC isolation technology in order to proceed with downstream molecular analyses including mutational or genomic analyses with captured target cells.

3.2 Preliminary Studies

3.2.1 Size Distribution of Different Cancer Cell Lines

The sizes of the cancer cells can vary even within a particular cell line. Prior to performing the cancer cell isolation experiments using the devised CTC capture devices, the sizes of the cancer cell lines were measured in order to determine the average sizes as well as the size variation of different types of cell lines, including MCF7 breast cancer cell line, AGS gastric cancer cell line, and PC3 prostate cancer cell line. Figure 14a summarizes the average sizes and variations of three different types of cancer cell line and leukocytes. The average sizes of MCF7, PC3, and AGS cell lines ranged from 12 μm to 15 μm (N=20), whereas, the average size of the WBC was smaller than 8 μm . Figure 14b shows the bright field image and immunofluorescence images of MCF7 cells filtered on the PCTE membrane. The size of the MCF7 cells were directly compared with the 8 μm pores of the PCTE membrane to determine the size difference between the cells and the pores.

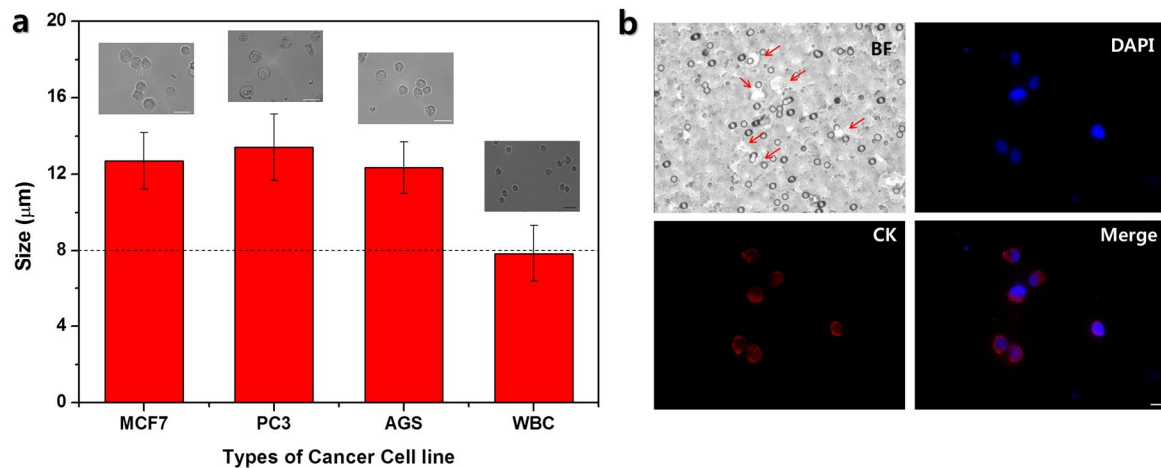


Figure 14 The cell size analysis of cancer cell lines. (a) The average sizes and variations of three different types of cancer cell line, MCF7, AGS, and PC3, and leukocytes. The dashed line represents the pore size of the PCTE membrane. The scale bare represents 20 μm . (b) Fluorescence image of isolated MCF7 breast cancer cells on a PCTE membrane. The size of the MCF7 cells compared to 8 μm pore of the PCTE membrane. The scale bare represents 10 μm .

3.2.2 Optimization of the Staining Protocol

Target cancer cells can be stained with fluorescent antibodies prior to the enumeration step to identify and distinguish them from other contaminant blood cells. In this study, breast cancer cell-line MCF7 was stained using a predefined criteria for CTC characterization: DAPI for nucleus staining, Cytokeratin for a CTC, and CD45 for leukocyte identification. The optimal staining condition was determined by varying the concentration of each staining solution and altering the order of the steps of the staining procedure. Optimized concentrations of each staining solutions was as following: 100 ng/mL of DAPI, 8 μ g/mL of Anti-Pan-Cytokeratin- eFluor® 615, 240 ng/mL of Anti-Cytokerain- PE, and 4 μ g/mL of Human CD45- FITC. Two different staining methods were performed to determine the more favorable order of sequence for the staining procedure. In method 1, the cells were first blocked with Fc blocker in order to block non-specific staining, followed by a washing step with 0.5 % BSA in 1xPBS buffer solution. The cells were fixed with 4 % paraformaldehyde followed by the permeabilization step with 0.1 % Triton X-100. Finally, the cells were incubated with a staining cocktail of DAPI and CK. and CD45. In method 2, the sequence of the event was identical except for the CD45 incubation step, where CD45 was stained prior to fixation and permeabilization steps. The purpose of switching the order of CD 45 incubation step in method 2 to was to further prevent non-specific staining of target cancer cells with CD45. Figure 15 summarizes the result of the staining process using both method 1 and method 2. It can be concluded that cancer cells and leukocytes are clearly distinguished using the first method. However, it was difficult to identify leukocyte using method 2, when the CD45 incubation step was performed before the fixation step.

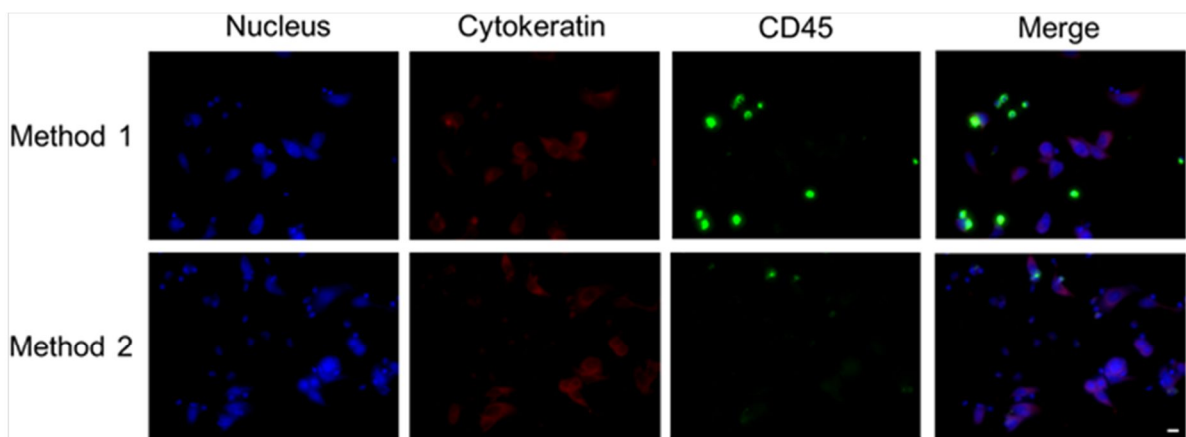


Figure 15 Fluorescence images of fluorescently labeled MCF7 breast cancer cells. The sequence of staining method 1 is Fc blocking – fixation – permeabilization – DAPI, CK, and CD45 staining. The sequence of staining method 2 is Fc blocking – CD45 staining – fixation – permeabilization – DAPI and CK staining. The scale bare represents 10 μ m.

3.3 Optimization of Device Fabrications

3.3.1 Disc Design

For the CTC-capture disc, the device consisted of the loading chamber, inlet channel, filtration zone, outlet channel, and the waste chamber (Figure 16). The size of the device was 60 mm in diameter, and the thickness of the device was approximately 7.5 mm. The volume capacity of the loading chamber and waste chamber were approximately 1200 μL and 2100 μL . The inlet channel, which had a depth of 1 mm, started from the loading chamber and it was directly connected to the filtration zone. The width of the inlet channel was as wide 10 mm, and this minimized the fluidic resistance which could adversely affect the cells, which are contained within the fluid sample. Filtration zone consists of the upper space, polycarbonate track-etch membrane, and lower upper space. As the disc rotates, fluids contained in the loading chamber would be transferred to the filtration zone, initially filling up the upper space of the filtration zone. Then the fluid would be filtered via inserted track-etch membrane. Similar to CTC-capture disc, the layers consisted of 0.25 mm top PC layer, 0.1 mm pressure sensitive adhesive layer, 1 mm middle PC layer, 0.1 mm pressure sensitive adhesive layer, mm body PC layer, and 0.1 mm pressure sensitive adhesive layer. Polycarbonate track-etch membrane was inserted in the groove from the back side of 5 mm body PC layer.

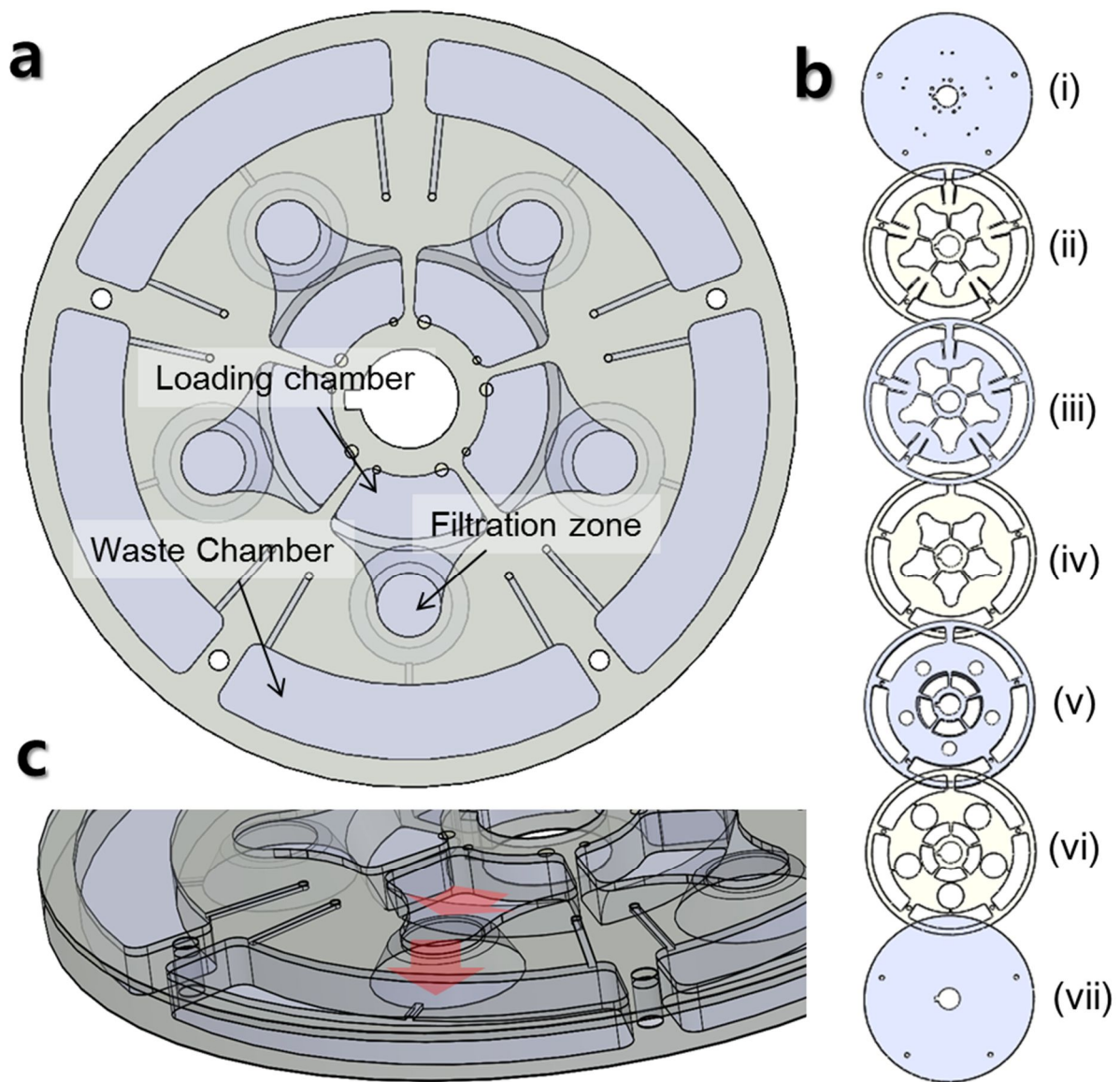


Figure 16 Illustration of the centrifugal microfluidic device for CTC isolation. PC track-etched membrane is bonded underneath the body layer. (a) Front-view of the disc design (b) The layer composition is as follows: (i) 0.25 mm top PC layer, (ii) 0.1 mm pressure sensitive adhesive layer, (iii) 1 mm middle PC layer, (iv) 0.1 mm pressure sensitive adhesive layer, (v) 5 mm body PC layer, and (vi) 0.1 mm pressure sensitive adhesive layer. (c) Side-view of the disc design showing the fluid flow pattern

3.3.2 Membrane Installation

As mentioned in the previous section, carbonate track-etch membrane, which has the thickness of 10 μm , was inserted in the groove from the back side of the 5 mm body PC layer (Figure 17a). The membrane was chemically bonded using acetone by partially dissolving the bonding area of the membrane. Specifically, a drop of acetone was loaded onto the edges of the bonding area, and it spread through the edges of the membrane by the capillary action. In order to determine the integrity of the membrane-bonded disc under hydrodynamic flow conditions, an aqueous solution of red dye was infused in the loading chamber of the membrane installed disc (Figure 17b). As a result, it was confirmed that the membrane bonding was successful and leakage was not observed even when the device was operated at 4200 rpm with the maximum loading volume, 1200 μL . In the case of the CTC-capture chip, the leakages did not occur with a flow rate as high as 1 mL/min. In addition, the delamination of the device rarely occurred even at maximum loading volume and the spinning condition. The reproducibility of the chemical bonding method was 97.3 % (N=110).

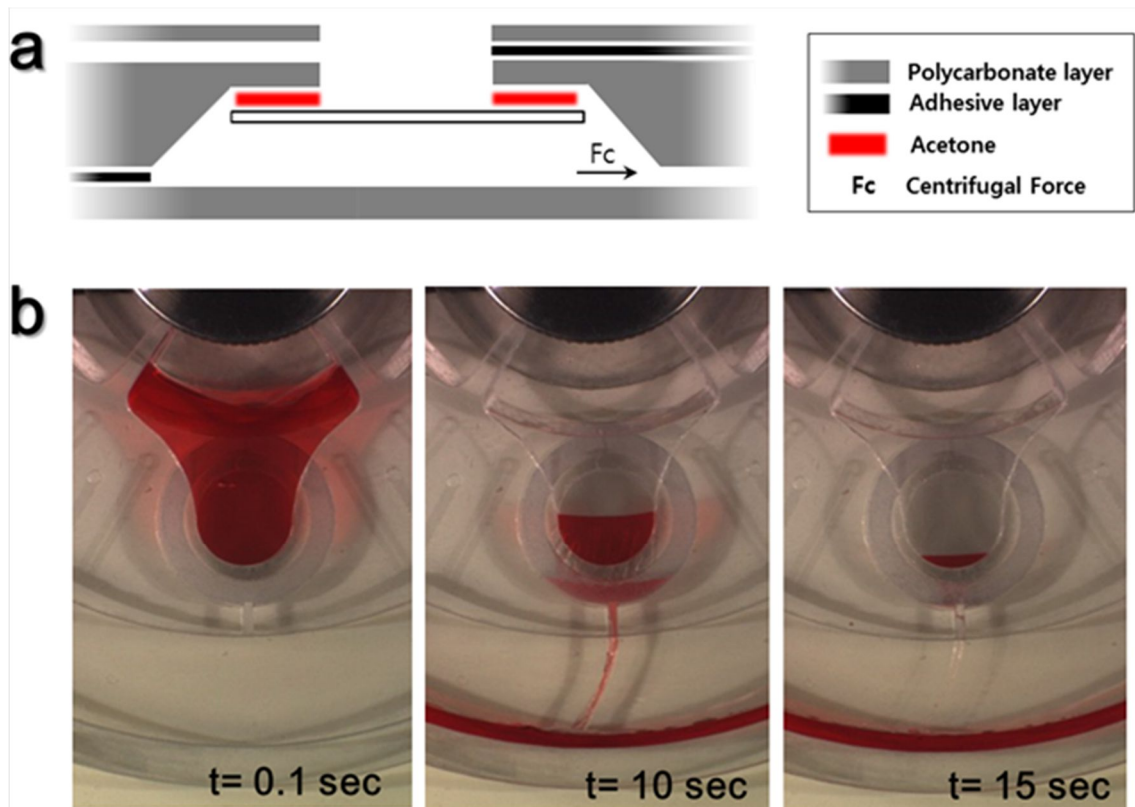
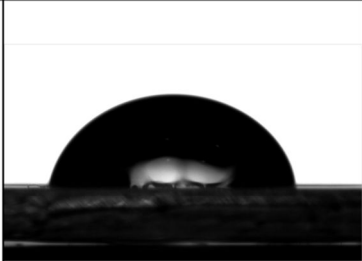
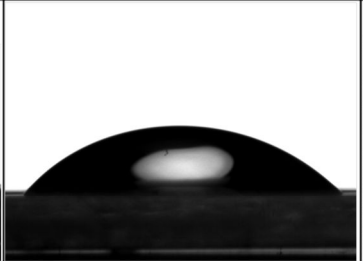
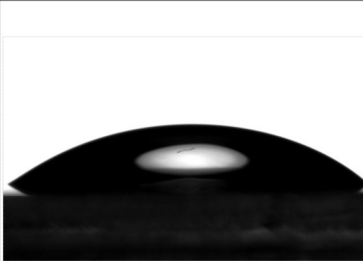
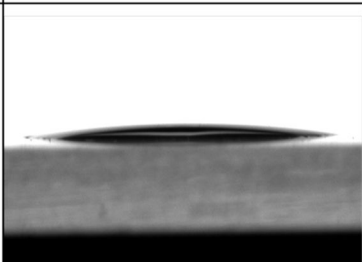
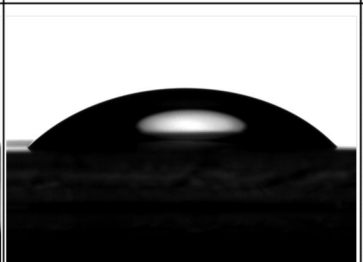
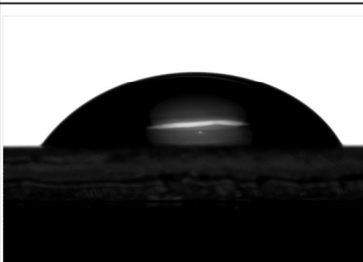


Figure 17 Result of the leakages test on a CTC-capture disc. (A) Cross-section images of the filtration zone. (B) Operation images of the CTC-disc. The chamber was filled with 1 mL of aqueous dye solution and the device was operated at 4200 rpm.

3.3.3 Surface Passivation

Surface passivation of the polycarbonate (PC) substrate was a mandatory step in order to prevent a non-specific adsorption of the biomolecules including target cancer cells. In order to select the surface treatment condition with maximum surface passivation efficiency, six different surfaces were used, including controls, pristine PC substrate. Five different surface treatment methods included 1 % BSA treatment on both pristine PC surface and plasma treated PC surface, TPU modified PC surface, and lastly, PEG treated PC surface. The result of the surface treatment was confirmed with measuring the contact angles of each surface. It was determined that pristine PC had the average contact angle of 85.3 degrees while other modified surfaces had smaller contact angles ranging from 7.62 degrees (plasma treated PC surface) to 58.5 degrees (PEG treated surface). Table 4 summarizes the contact angle analysis of substrates with six different surfaces.

Table 4 Summary of the contact angle analysis of six different surfaces using various surface passivation methods.

Sample	Pristine	Pristine, BSA	Plasma, BSA
Figure			
Contact angles (°)	85.3 ± 7.34	46.9 ± 3.80	38.0 ± 3.51
Sample	Plasma	TPU	PEG
Figure			
Contact angles (°)	7.62 ± 3.88	44.8 ± 6.77	58.5 ± 3.39

Performance of surface passivation was confirmed by loading the MCF-7 cancer cell lines on each surface modified substrate. Initially, approximately 100 cells were loaded on each surface. After 5 minutes of incubation, loaded 1xPBS buffer solution with cells was retrieved followed by an intensive washing step. Afterwards, remaining numbers of cells on the surface of the substrates were counted. As a result, over 70 % of the cells remained on the surface in the case of pristine and plasma treated PC substrates. The substrate that had the lowest number of remaining cells was 1 % BSA treated substrate, which had approximately 15 % of the cells remained on the surface. Considering that cells are not incubated for over 5 minutes during cell capture experiments, it was concluded that it was efficient enough to treat 1 % BSA on a pristine PC surface in order to effectively prevent the non-specific cell adsorption on the surface of the CTC capture device. Figure 18 summarizes the effectiveness of the different types of passivation methods.

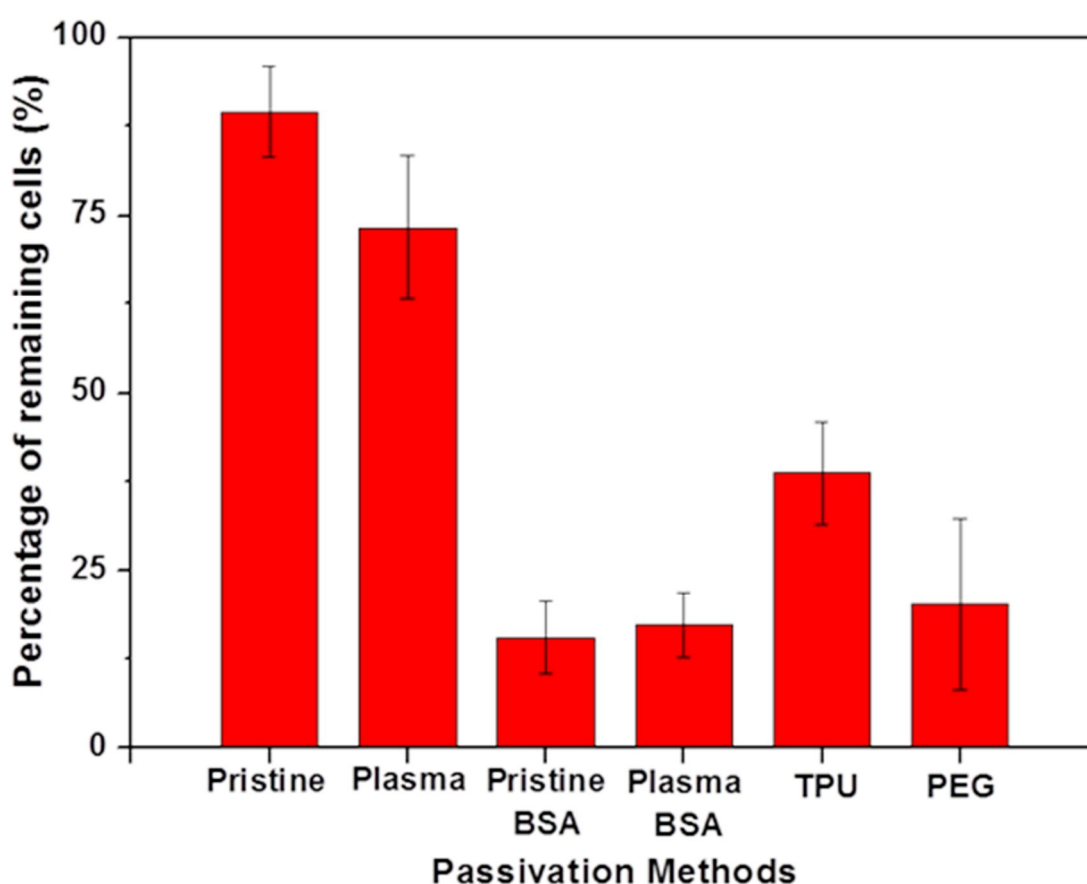


Figure 18 The result showing the effectiveness of the different types of passivation methods. Over 70 % of the cells remained on the surface in the case of pristine and plasma treated PC substrates. The substrate that had the lowest number of remaining cells was 1% BSA treated substrate. which had approximately 15 % of the cells remained on the surface.

3.4 Cell-line Experiments

3.4.1 Determination of the Spin Condition

When dealing with the fluid that contains fragile cells, it is important that the pressure difference across the porous membrane is kept below a threshold value where cells will be damaged. When the fluid flows through an orifice, or a pore, in a laminar condition, the relationship between the flow rate (Q) and the pressure drop (ΔP) across the orifice can be summarized as following⁶⁰:

$$Q = \frac{r^3 \Delta P}{3\mu} \left[1 + \frac{8L}{3\pi r} \right]^{-1} \quad \text{Eq. 4}$$

where r is the radius of the orifice, μ is the coefficient of dynamic viscosity, which is 3-4 cP in case of blood⁶¹, and L is the depth of the orifice, or the channel height of the “flow channel.” The relationship between the flow rate and the pressure drop can be modified as in equation 4, when multiple circular pores are present in the membrane with the thickness L ⁶²⁻⁶³:

$$\Delta P = \mu R Q = \left[\frac{128L\mu}{\pi d^4} + \frac{24\mu}{d^3} \right] \frac{Q}{N} f(k) \quad \text{Eq. 5}$$

where R is the membrane resistance per unit area, N is the number of pores, k is the fraction of open area of the pores, d is the pore diameter, L is the pore depth (i.e. thickness of the membrane). The function $f(k)$ in equation 4 is defined as the following⁶⁴:

$$f(k) = 1 - \sum_{i=1}^{\infty} a_i k^{(i+1)/2} \quad \text{Eq. 6}$$

Above equation is an infinite series solution with the first three coefficients (i.e. a_1 , a_2 , a_3) equal to 0.334, 0.111, and 0.066, respectively. The relationship between the pressure drop across the porous membrane and the flow rate can be further simplified if the viscous losses in the porous membrane are neglected, and the open area, k , of the membrane is less than 10 % since the function $f(k)$ converges to unity. Thus, the final equation simplifies to⁶⁵:

$$\Delta P = \left(\frac{24\mu}{d^3} \right) \cdot \frac{Q}{N} \quad \text{Eq. 7}$$

In this section, the pressure difference across the membrane in the CTC-capture disc system was calculated by my measuring the flow rate of the blood sample at different spinning conditions, 1200 rpm, 2400 rpm, and 3600 rpm. Determined pressure drop for each condition was compared with the pressure drop across the membrane in the ScreenCellTM system. Figure 19 summarizes the result of variation of pressure drop across the membrane at different filtration settings. The line (a) represents the theoretical relationship between the pressure drop and the flow rate in the ScreenCellTM system, where the red square indicates the resulting pressure drop at the flow rate of 15.31 mL/min, which is

the flow rate generated during the filtration process. The line (b) represents the theoretical relationship between the pressure drop and the flow rate in the CTC-capture disc system. Blue square indicates the resulting pressure drop at the flow rate of 19.05 mL/min, 40.54 mL/min, and 72.29 mL/min. It was concluded that the pressure drop across the porous membrane in ScreenCell™ was 872.1 Pa, which falls in the range of the pressure drops generated in 1200 rpm, 2400 rpm, and 3600 rpm condition in the CTC-capture disc system, which were 480.0 Pa, 1036.2 Pa, and 1839.6 Pa, respectively.

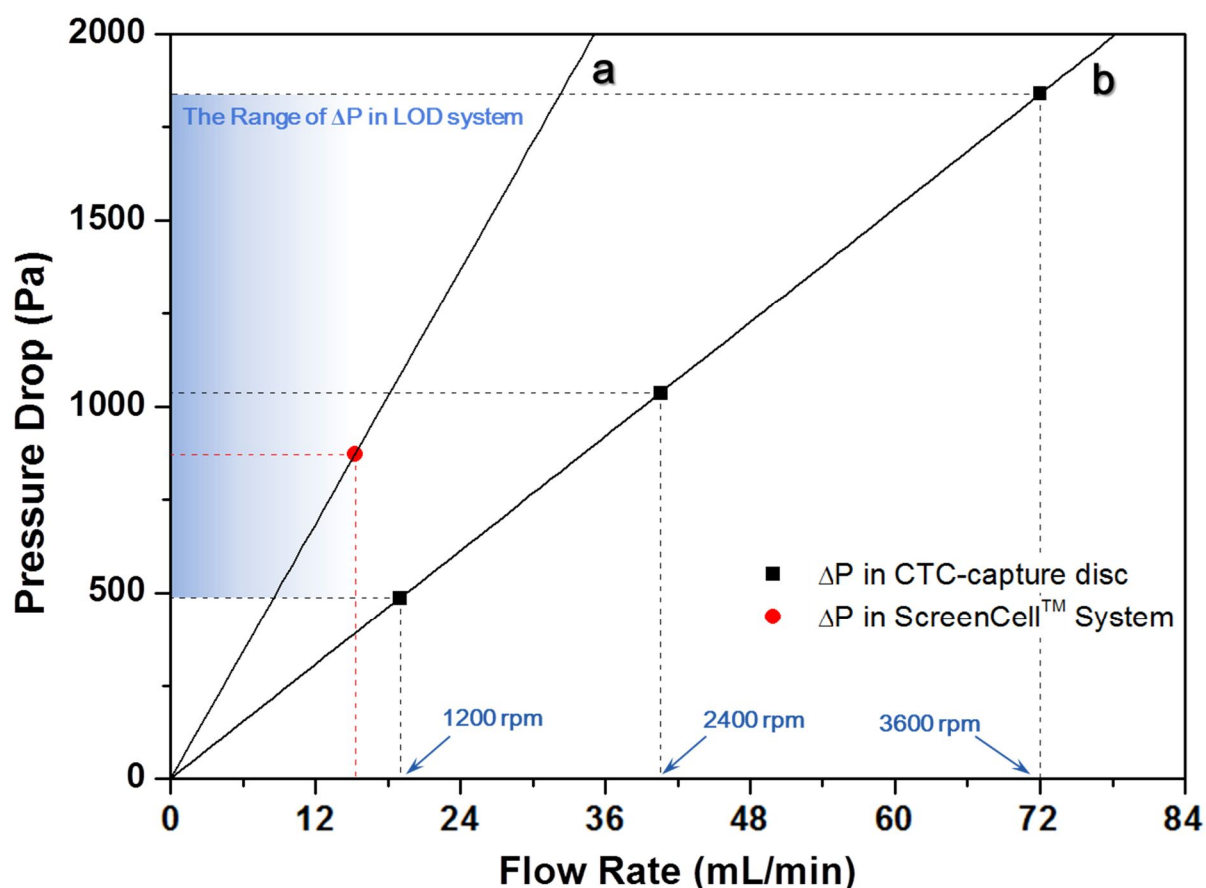


Figure 19 Variation of pressure drop across the membrane at different filtration settings. (a) Theoretical relationship between the pressure drop and the flow rate in the ScreenCell™ system. The red data point represents the resulting pressure drop at the flow rate of $2.55 \times 10^{-7} \text{ m}^3/\text{s}$. (b) Theoretical relationship between the pressure drop and the flow rate in the CTC-capture disc system. Black data points represent the resulting pressure drop at the flow rate of 19.05 mL/min, 40.54 mL/min, and 72.29 mL/min.

3.4.2 Capture Efficiencies at Various Flow Conditions

The cell capture experiment was performed in order to confirm the validity of the operation conditions of the CTC-capture disc system. The samples were processed using CTC-capture disc at the spinning condition of 1200 rpm, 2400 rpm, and 3600 rpm. For each trial, approximately 100 MCF7 breast cancer cells were spiked into healthy donor blood sample. For the comparison of capture efficiencies with the ScreenCell™ systems, approximately 100 MCF7 breast cancer cells were spiked into the identical donor blood.

Figure 20 summarizes the result of the capture efficiencies at various conditions. As it can be seen in the case of the disc system, the capture efficiencies ranged from 43.3 %~ 55.2 % regardless of different spinning conditions. It was concluded that, within the range of 1200 rpm to 3600 rpm, the differences in the angular velocity of the spinning disc do not significantly affect the cell capture efficiency.

The cell capture experiment was repeated using the fixed spin condition of 2400 rpm in order to compare the performance of the device with the ScreenCell™ systems. For the sample preparation process, 1.3 mL of ScreenCell™ FC2 buffer solution was added to 1 mL of MCF7 cell spiked blood samples for both samples. Mixed samples were homogenized by inverting the tubes multiple times followed by the 8 minutes of incubated step. Diluted blood samples were processed afterwards. As summarized in Figure 21, in the case of the CTC-capture disc system, the capture efficiency was approximately 61.4 %, whereas the capture efficiency using the ScreenCell™ systems was approximately 71.6 %. Although the capture efficiency of cells using the CTC-capture disc is slightly lower than that in ScreenCell™ systems, it can be concluded that the separation performance of the CTC-capture disc is comparable to the ScreenCell™ systems considering the fact that sample handling in the ScreenCell™ systems is more straightforward compared to the handling in the CTC-capture disc system.

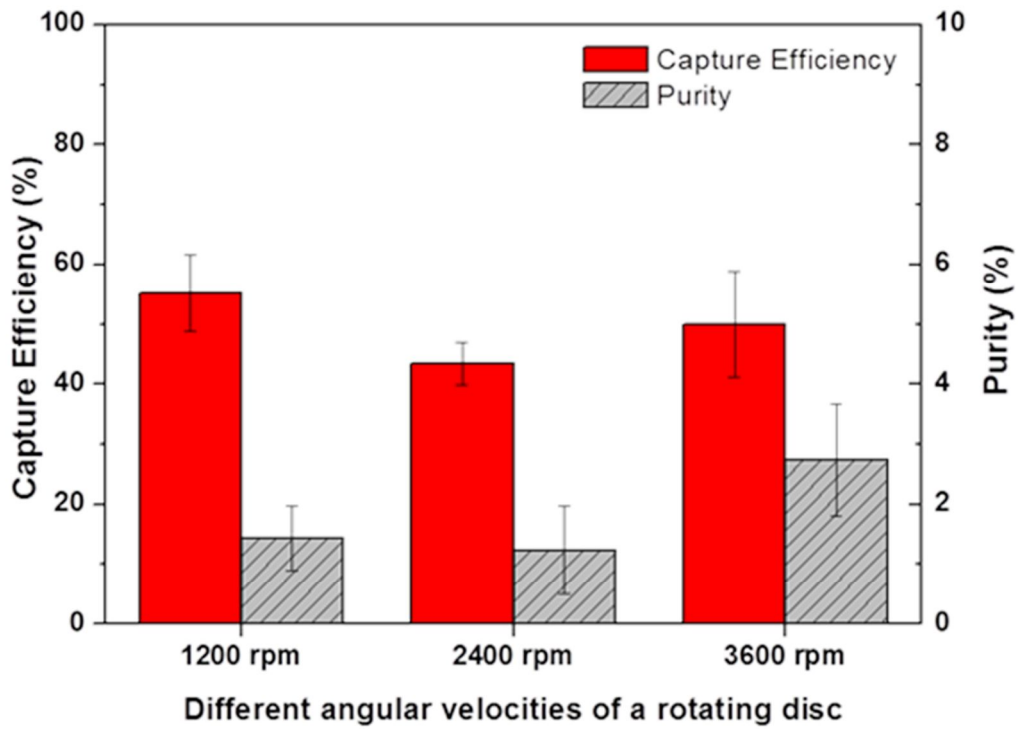


Figure 20 The effect of the angular velocity of a rotating disc on the cancer cell capture efficiency and purity.

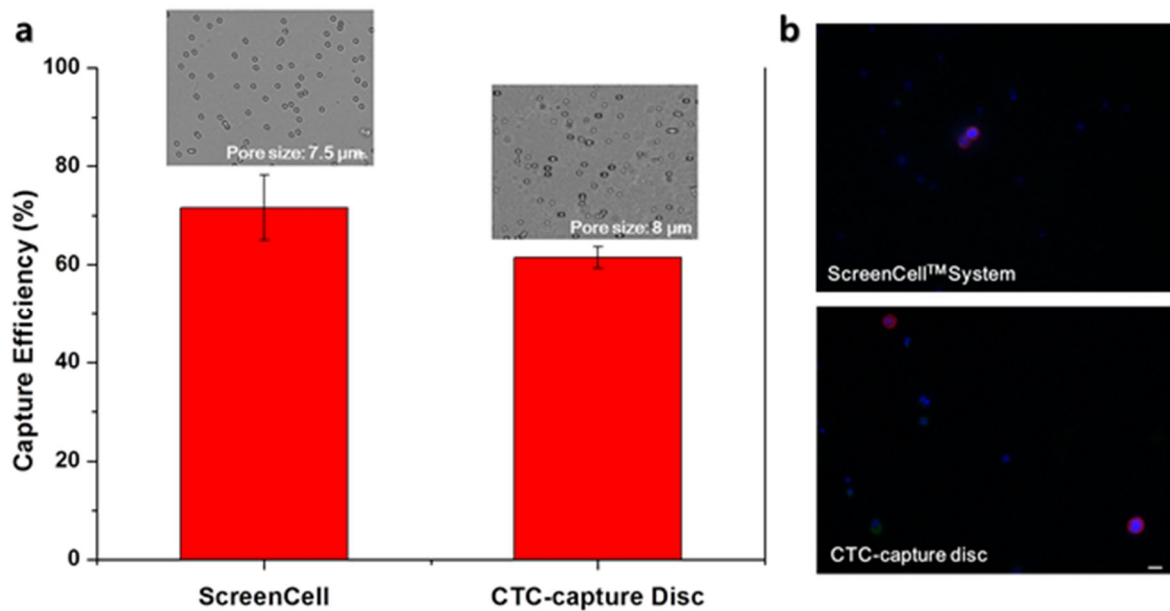


Figure 21 Comparison between different filter devices. (a) Capture efficiencies of cancer cells using ScreenCell™ System and CTC-capture disc (2400 rpm). Bright-field images above the bar graphs are the representative images of the PCTE membrane inserted in each device. (b) Fluorescence images of the cells captured from ScreenCell™ System (top) and CTC-capture disc (bottom). The scale bar represents 10 μm.

3.4.3 Capture Efficiencies at Different Cell Concentrations

In CTC studies, the efficient isolation of the cancer cells is critical especially when the cell concentration of the input sample is considerably low. In this section, the capture efficiency was evaluated at various input cell concentrations ranging from 1 cell to 150 cells in 1 mL of sample in order to evaluate the consistency of the capture efficiency at different cell concentrations. The experiment was performed with the MCF7-spiked 1xPBS buffer solution as well as MCF7-spiked whole blood sample. The spin rate of the disc was 2400 rpm.

Figure 22a shows the recovery of MCF7 cells spiked into 1 mL of 1xPBS buffer solution and healthy whole blood sample at cell concentrations ranging from 1 cell to 1000 cells. The overall capture efficiency of the MCF7 cells in 1xPBS buffer solution was slightly above approximately 50.5 %, which was similar to the capture efficiencies obtained when the cell line was spiked into whole blood samples (53.3 %). In addition, the r^2 value which was close to unity indicated that capture efficiency result at each cell concentration was fairly consistent.

Figure 22b shows the capture efficiency and the purity of MCF7 cells spiked into whole blood samples at cell concentrations ranging from 1 cell to 150 cells. In this experiment, the purity of the captured cells was evaluated along with the capture efficiency of the input cancer cell. The result of the capture efficiency using the whole blood sample was 53.3 %, which was similar to the capture efficiency obtained when the cells were spiked into 1xPBS buffer solution. Isolated number of leukocytes varied, ranging from 200 cells to 800 cells. Theoretically, the number of the leukocytes should remain consistent because the experiment was performed with the blood samples from the identical donor. Variations in the number of leukocyte may have resulted from the damages of cells during the disc operation. Another possibility can be that the staining of the CD45 was not efficiency performed.

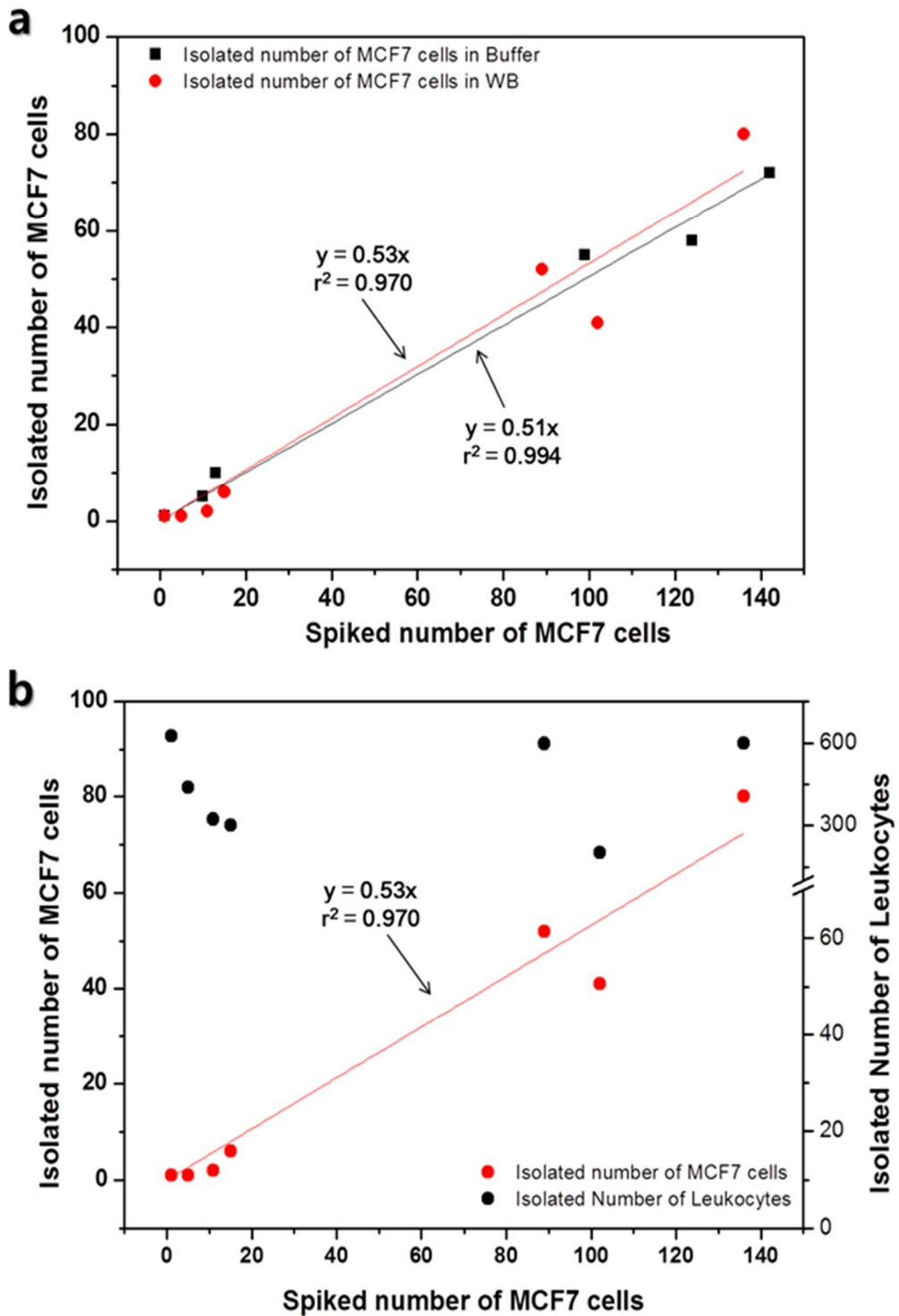


Figure 22 (a) The capture efficiency of MCF7 cells spiked into 1X PBS buffer solution (black) and whole blood sample (red) at cell concentrations ranging from 1 cell to 150 cells. (b) The capture efficiency (red) and the purity (black) of MCF7 cells spiked into whole blood samples at cell concentrations ranging from 1 cell to 150 cells.

3.4.4 Dilution Factor

In most of the proposed CTC isolation platforms, the dilution of whole blood samples is sometimes necessary in order to avoid the leakage or the clogging of the red blood cells. Processing the undiluted whole blood sample, which is indeed an unfavorable condition, may result in a lower capture yield of the target cells. In this section, the effect of the dilution factor on the capture efficiency was studied. As shown in Figure 23, three different blood sample conditions were used. For the diluted blood samples, 1 mL of whole blood was diluted with 250 μ L and 500 μ L of 1xPBS buffer solutions, respectively. As a result, it was concluded that the dilution factor is not the critical component which affects the capture efficiency of the target cancer cells. Furthermore, the purity of the captured cells did not vary significantly at different ratio of dilution factors.

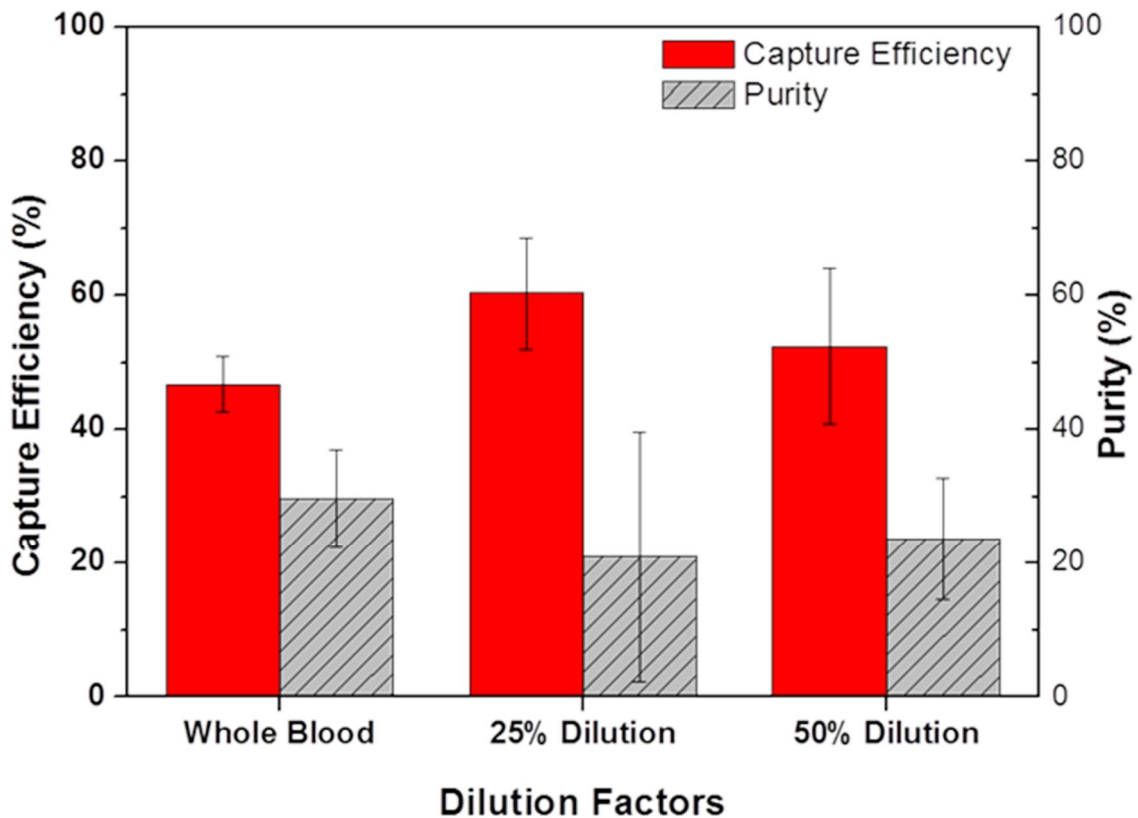


Figure 23 The effect of the dilution factors on the cancer cell capture efficiency and purity.

3.5 CTC Isolation from Patient Blood

3.5.1 Clinical Tests

For the clinical evaluation, 10 lung cancer patients and 13 gastric cancer patients in Pusan National Hospital were enrolled in the study. Patient blood samples were processed within 6 hours, and different volumes of whole blood samples ranging from 2.2 mL to 4.4 mL were directly loaded onto the device for the CTC isolation experiment. Experiment for the sample L64 was not successful because the RBCs from the sample caused the clogging of the membrane during the filtration process. All other samples were processed without any technical difficulties. Figure 24 is the summarized result showing the performance of CTC-capture disc using clinical samples. The number of isolated CTCs from lung cancer patients ranged from 5 CTCs to 21 CTCs, and those from gastric cancer ranged from 5 CTCs to 29 CTCs. All counts were normalized to 7.5 mL, the input volume used in CellSearch™ System⁹, in order to directly compare the number of captured CTC in a fixed volume of blood sample.

Table 5 is the list of lung cancer patient samples and gastric cancer patient samples with the individual CTC counts. The CTC detection rate for the lung cancer patient was 50 %, and the detection rate for the gastric cancer patients was approximately 38.4 %. Considering the fact that the capture efficiencies from the spike-in experiments were approximately 60 % in most cases, the 50 % of the CTC detection rate in the patient sample experiments offers the indication of a considerably high detection rate. In order to increase the detection rate, it is essential to increase the input sample volume to generate a statistically meaningful enumeration data. As it can be inferred from Table 6, the detection rate of the CTC-capture disc is comparable to the FDA-cleared CellSearch™ system. The CTC detection rate of other microfluidic system ranged from 60 % to 100 %. However, it is not valid to draw any firm conclusions from the enumeration results of patient samples. In other words, the effectiveness of each platform cannot be determined by simply comparing the CTC counts due to heterogeneity of patient samples.

Figure 25 shows representative immunofluorescence images of CTCs and WBCs obtained from lung cancer patients and gastric cancer patients. It can be inferred from the images that the size of the CTCs varies in a wide range. The size distribution of the isolated CTCs from gastric cancer patients was compared with that of AGS gastric cancer cell line by measuring the diameter of each cell via Metamorph image analysis software (Figure 26). The size of the cells ranged from 6 μm to 22 μm, and the average size of the CTCs from gastric cancer patients was larger than the average size of the AGS gastric cancer cell line.

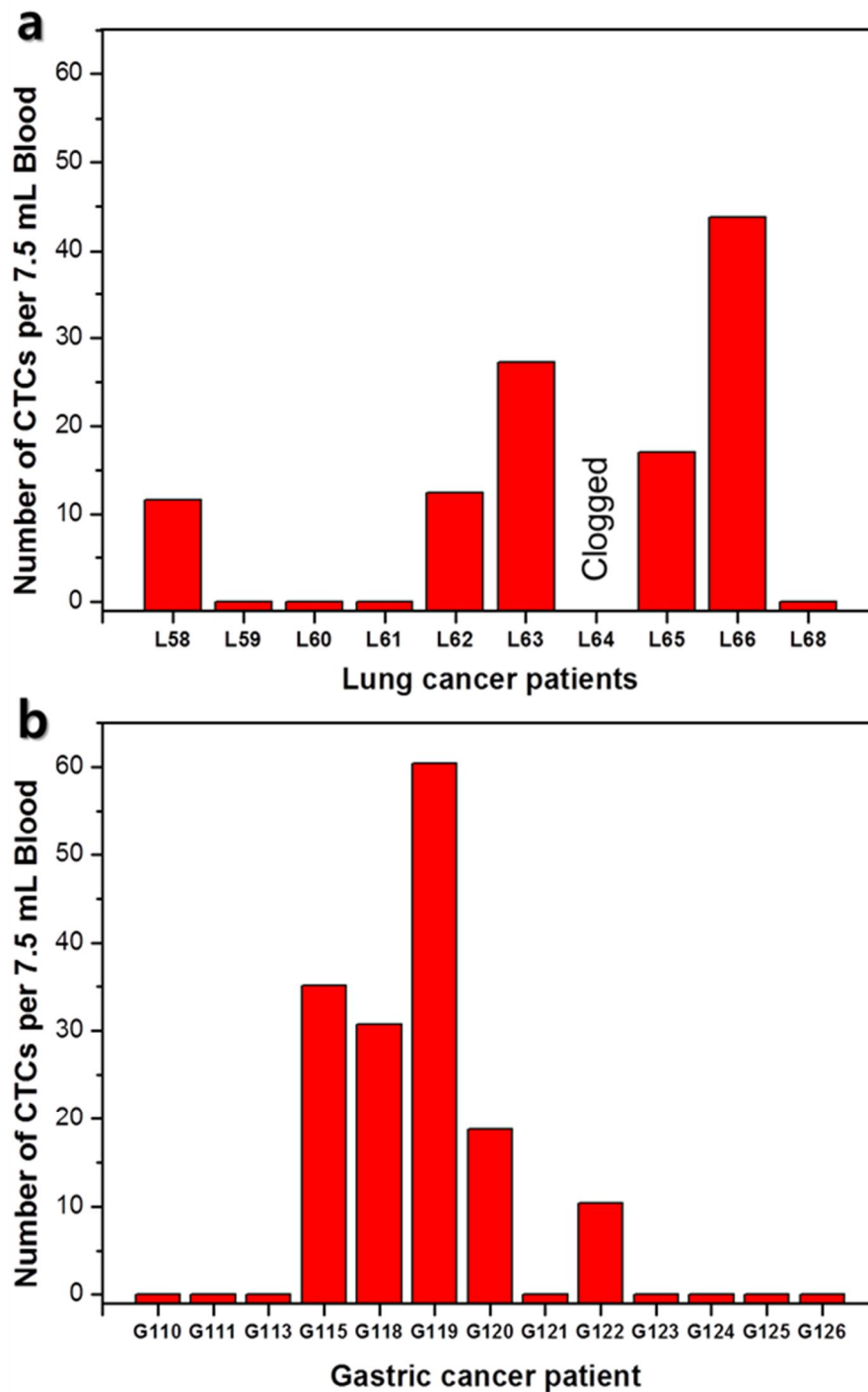


Figure 24 Results showing the performance of CTC-capture disc in clinical samples. Various volumes of blood samples were used in the experiment, and the result was normalized to directly compare the number of captured CTC in 7.5 mL of blood sample, which is the fixed input volume used in Cellsearch System.⁹ (a) The CTC isolation result of 10 lung cancer patients (b) The CTC isolation result of 13 gastric cancer patients.

Table 5 List of lung cancer patient samples and gastric cancer patient samples showing the number of captured CTCs with the stage information.

Sample No.	Cancer Type	Stage Number	Number of Captured CTCs	Sample Volume (mL)	CTCs/ 7.5 mL of Blood
L58	Lung	IIA	5	3.2	11.7
L59**	Lung	-	0	2.4	0
L60	Lung	IIIB	0	3.6	0
L61	Lung	IV	0	4	0
L62	Lung	IV	4	2.4	12.5
L63	Lung	IIIA	16	4.4	27.3
L64*	Lung	IB	-	4.4	-
L65	Lung	IB	5	2.2	17.0
L66	Lung	IV	21	3.6	43.8
L68	Lung	IV	0	3	0
G110	Gastric	IIIB	0	3.2	0
G111	Gastric	IIIC	0	4.2	0
G113	Gastric	IIIC	0	4.2	0
G115	Gastric	IA	15	3.2	35.2
G118	Gastric	IIIC	18	4.4	30.7
G119	Gastric	IV	29	3.6	60.4
G120	Gastric	IIIC	9	3.6	18.8
G121	Gastric	IIA	0	3.6	0
G122	Gastric	IIIB	5	3.6	10.4
G123	Gastric	IA	0	3.6	0
G124	Gastric	IIIB	0	4	0
G125**	Gastric	-	0	3.4	0
G126	Gastric	IA	0	4.2	0

* Immunofluorescence detection was not possible due to an RBC clogging of the membrane.

** Stage information was unidentified.

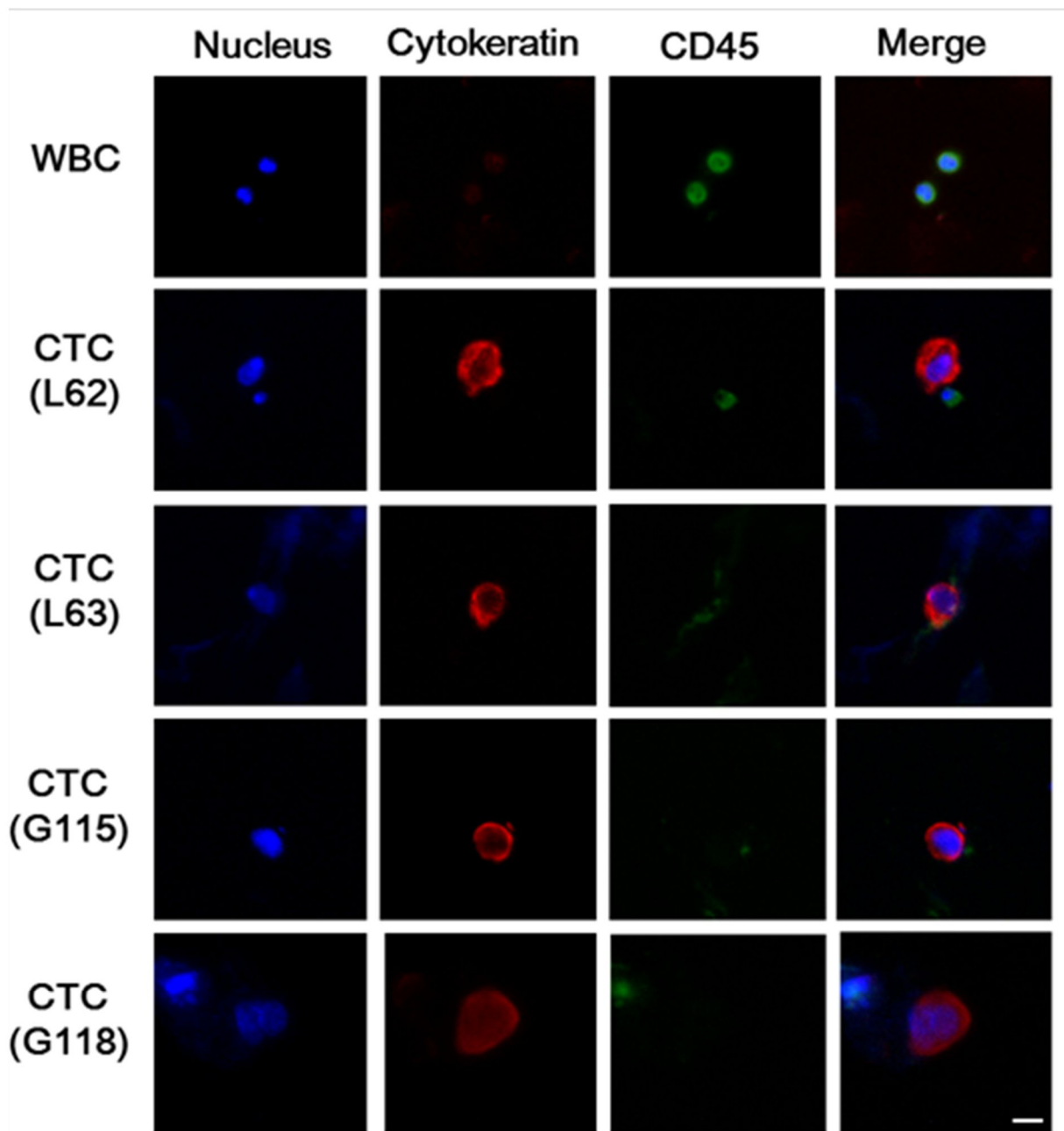


Figure 25 Gallery of CTCs and leukocytes captured using the size-selective CTC-capture disc from lung cancer patients (L62 and L63) and gastric cancer patients (G115 and G118). Cells were stained with DAPI (nucleus), PE-labeled anti-cytokeratin (CTC), and FITC-labeled anti-CD45 (leukocyte). The scale bare represents 10 μ m.

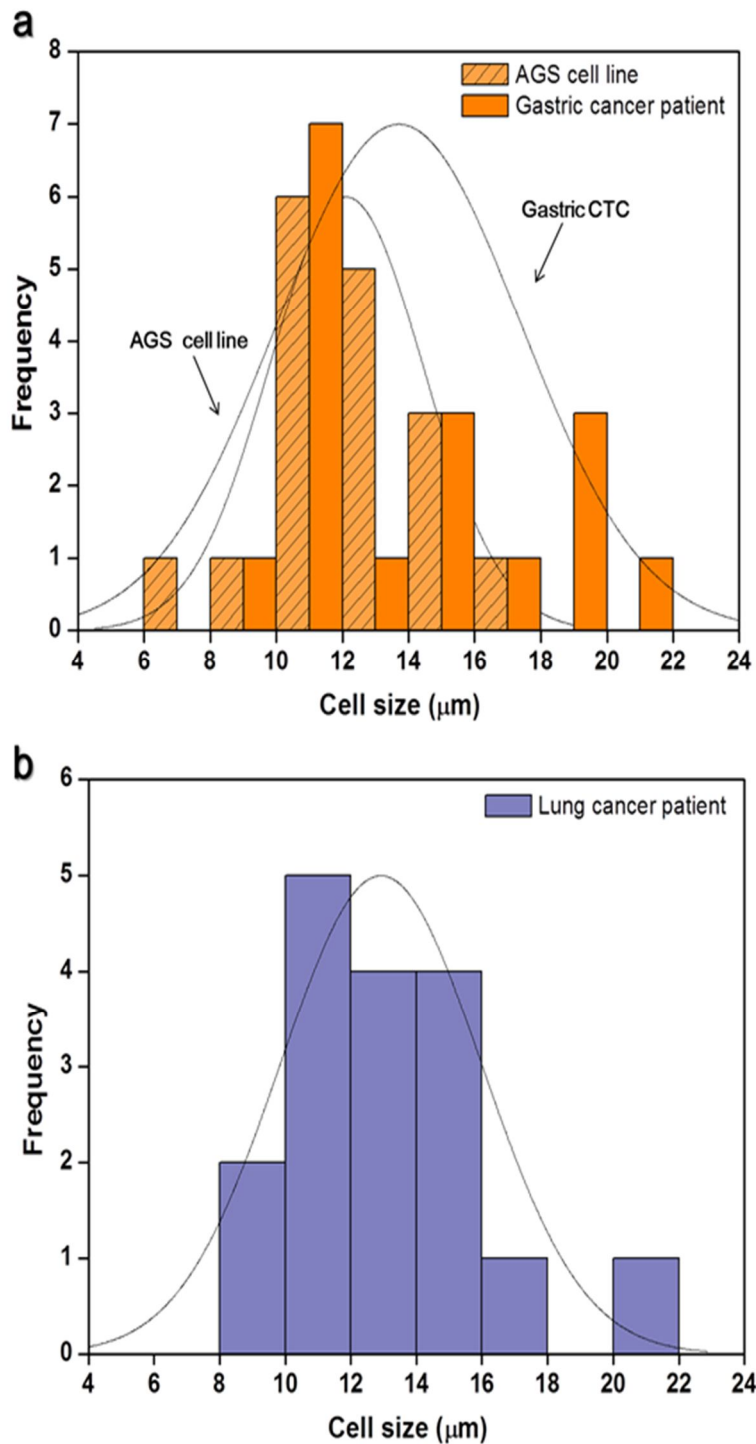


Figure 26 Histogram plots showing the size distribution of the CTCs isolated from (a) gastric patient blood samples (orange), and cancer cells from AGS gastric cancer cell line (slashed light orange), and (b) lung patient blood samples (purple). The size of the cancer cells ranges from 6 μm to 22 μm .

Table 6 Summary of the clinical evaluation results using different types of CTC isolation systems.

CTC Isolation System (Approach)	Capture Efficiency(%)	Cancer Type	Total Number of Patients	Detection Rate* (%)	No. of CTCs	Processed Sample Volume (mL)	Processing Time	Reference
CellSearch™ System (Immunomagnetism)	42	Colorectal Breast	12 11	33.3 54.5	1-22 1-114 (per processed volume)	7.5	> 3 hours	Lin <i>et al.</i> ⁹
Micropost Chip (Immunoaffinity)	65	Prostate	36	63.8	16-292 (per processed volume)	0.9- 5.1	> 3 hours	Nagrath <i>et al.</i> ¹⁰
Herringbone Chip (Immunoaffinity)	> 90	Prostate	15	93.0	12~3,167 (per mL)	-	~30 min	Stott <i>et al.</i> ¹⁶
CTC-iChip (Immunoaffinity)	> 90	Prostate	41	90.2	0.5-610 (per mL)	6- 12	~3 hours	Ozkumur <i>et al.</i> ¹²
Micro-Velcro Chip (Immunoaffinity)	80-95	Prostate	40	-	1-99 (per mL)	-	2 hours	Lu <i>et al.</i> ⁶⁶
Slanted Spiral Chip (Hydrodynamics)	~80	Lung Breast	5 5	100 100	3-125 (per mL)	7.5	4.4 min	Warkiani <i>et al.</i> ⁶⁷
ScreenCell™ System (Direct filtration)	~80	Cutaneous Melanoma	23	70	0-11 (per processed volume)	2	> 3 min	Schuur <i>et al.</i> ¹¹
Filter-based Chip (Direct filtration)	> 90	Colorectal Breast	12 11	83.3 100	2-26 1-60 (per processed volume)	7.5	-	Lin <i>et al.</i> ⁹
Filter-based CTC-capture Disc	50-65	Lung gastric	10 13	50 38.4	5-21 5-29 (per processed volume)	2.2-4.4	> 3 min	Lee <i>et al.</i>

* Detection rate refers to the fraction of the number CTC detected cancer patients compared to the total number of tested cancer patients.

3.6 Conclusion

Size-based isolation methods are more efficient because these methods have a higher throughput as they are compatible with relatively higher flow rates. In this chapter, a label-free lab-on-a-disc platform was introduced for a rapid and efficient detection of CTCs from whole blood samples as well as clinical samples. Polycarbonate track-etch membrane was used to isolate CTCs based on the size difference between the target cell and other blood cells. The device was tested with MCF-7 cancer cell spiked in both 1xPBS buffer solution as well as whole blood sample. The capture efficiency of the target cancer cell using the devised system ranged from 50 % to 60 %, and the purity of the captured cells varied widely, ranging from 15 % to 30 %. In addition, blood samples from gastric cancer and breast cancer patients were tested. The number of CTCs ranging from 5 to 29 CTCs was captured. Overall, the CTC detection rate for the lung cancer patient was 50 %, and the detection rate for the gastric cancer patients was 38.4 %.

CHAPTER 4 Future Directions

4.1 Negative Depletion

The capture efficiency and the purity of cancer cells using the proposed CTC-capture disc ranges from 50~65 % and 15~30 %, respectively. In this chapter, two ideas are proposed in order to further enhance the performance of the device. First of all, negative depletion strategy can be applied for a sample pre-treatment step prior to the size selective cell separation step. Negative enrichment method is a cell enrichment technique where non-target cells are captured and removed, instead of selectively capturing target cancer cells. The negative enrichment technique may not be efficient if it is used as a main detection method. However, it can be beneficial if it is applied prior to the main detection step, since it is possible to remove unwanted background cells, such as leukocytes, beforehand, consequently leading to an enhanced purity of the final product.

4.2 PDMS Through-hole Membrane Fabrication

Another way to enhance the sensitivity of the device is to use a microfabricated through-hole membrane. As discussed previously, random distribution of pores in PCTE membrane may result in the fusion of pores, which would result in lower cell capture efficiency results by allowing target cells to escape through the fused pores more easily. In this section, a biocompatible membrane which uniformly arrayed through-holes was fabricated by taking advantage of micromachining technologies. The polydimethylsiloxane (PDMS)-based through-hole membrane fabrication method introduced in this section is the reproduction of the fabrication technique described in Choi *et al.*⁵³

4.1.1 Mask Design

The desired dimension of the PDMS through-hole membrane is 13 mm in diameter with an effective filter area of 10 mm, with the thickness of 45~50 μm , and the pore size of 8 μm was selected for the final product. In addition the patterns with pore size larger than 8 μm were designed for the purpose of confirming the validity of the fabrication process. Throughout the experiment, pore sizes of 8 μm , 10 μm , 12 μm , and 20 μm were used. In term of the spacing between each pores, center-to-center distance between adjacent pores was 36 μm for the designs with pore sizes of 8 μm , 10 μm , and 12 μm , For the design with a pore size of 20 μm , the center-to-center distance between adjacent pores was 30 μm . The open areas or the membrane design with pore sizes of 8 μm , 10 μm , 12 μm , and 20

μm were 4.5 %, 7.0 %, 10.0 %, and 22.7 %, respectively. Circular patterns around the membrane were added to the final design in order to avoid the collapsing of the membrane during the PDMS-gel filling step (Figure 12e). As mentioned in Chapter 2, the patterns were designed by using a AutoCAD® software. Figure 27 is the example of one of the mask design that was used for the membrane fabrication experiments.

4.1.2 SU-8 Master Fabrication

The fabrication of SU-8 mold is the initial step of the PDMS through-hole membrane fabrication (Figure 12a). SU-8 master for the membrane was fabricated by utilizing a standard photolithography technique. The process starts with the spincoating of the SU-8 negative photoresist on a bare silicon substrate. The desired thickness of the final product is approximately 45~50 μm . Using the optimized spincoating condition (1800 rpm for 30 seconds), it was possible to obtain the uniform thickness of approximately 45 μm . Spincoated wafer was then soft baked at 65°C for 4 minutes and at 95°C for 4 minutes, sequentially.

It is important to have clear-cut and accurate profile characteristics of microstructures especially when the fabricated product is used as a master for a subsequent PDMS mold generation. Specifically, it is imperative that the sidewalls of the micro-trenches are vertical in order to obtain the PDMS replica

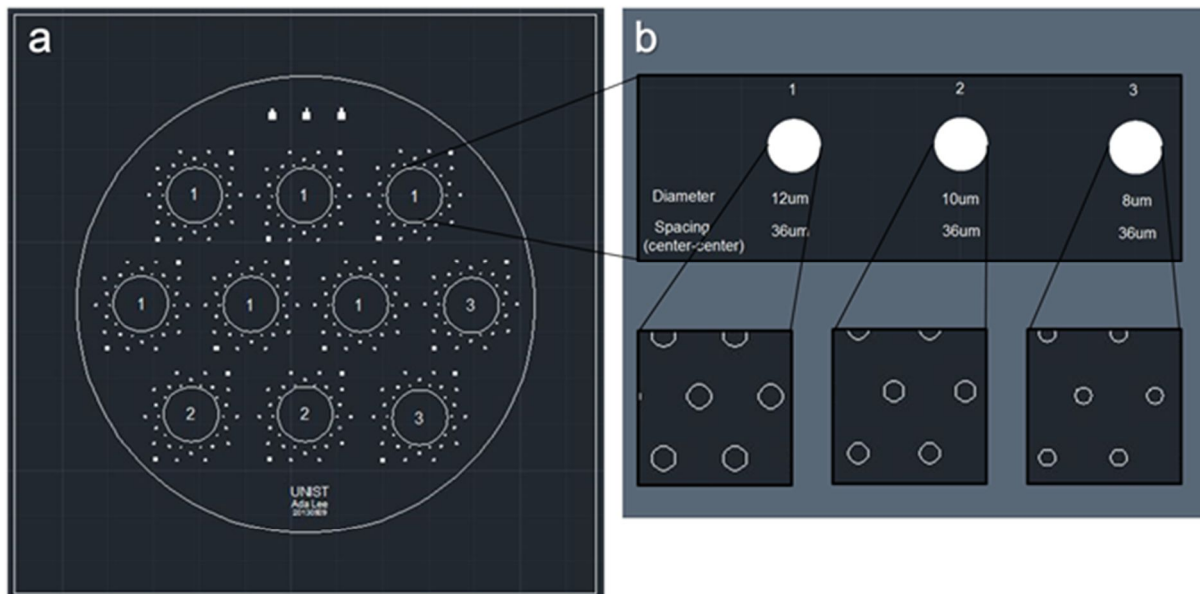


Figure 27 Example of the mask design used for through-hole membrane fabrication. Three of the four types of membrane features were designed in this mask. The center-to-center distance between adjacent pores was 36 μm .

with intact straight pillars. Patterns with a positive draft angle (i.e. $\gamma > 90$) will have the diameter of the micro-trench wider at the top (W_t) than it is at the bottom (W_b) (Figure 28). In this case, frictional resistance between the SU-8 mold and replicated PDMS microstructure will increase during the demolding step, and this may cause a defect in both the SU-8 mold and PDMS replica. In other words, it is likely that PDMS replica will be torn apart, leaving the remnant PDMS remain trapped inside the trench. If the walls of the trenches are perfectly vertical with draft angle of zero degree ($\gamma = 90$ in Figure 28a), demolding process will become relatively easier since the removal process of the PDMS replica from the SU-8 mold will only involve the initial detachment and possibly the frictional sliding along the interface between molded PDMS and the SU-8 cavity wall.⁶⁸ Consequently, it is critical to reduce undercuts by precisely controlling the draft angles of the micro-trenches in order to use such a high aspect ratio (HAR)-arrayed structure for a subsequent PDMS mold generation.

As mentioned previously, the target pore size and membrane thickness is 8 μm and 45~ 50 μm , respectively, resulting with the aspect ratio ranging from 5.6:1~ 6.6:1. Fabricating such a high aspect ratio of SU-8 patterns requires an appropriate UV exposure dosage, which is a critical factor that determines the verticality as well as the dimensional accuracy of the microstructure. The optimal UV condition for the patterning of SU-8 photoresist was 180 mJ/cm. Furthermore, minimal and uniform proximity gap between the mask and wafer was maintained throughout the UV exposure step in order to minimize the diffraction error.⁶⁹

Development was the final step of the SU-8 mold fabrication procedure. Development of narrow and deep trenches of patterned SU-8 mold required a submergence of the wafer in the SU-8 developer for at least 15 minutes. As a result, it was possible to obtain a SU-8 mold with micro-arrayed trench patterns with the size as small as 8 μm . Figure 29 is the results of the fabricated SU-8 master.

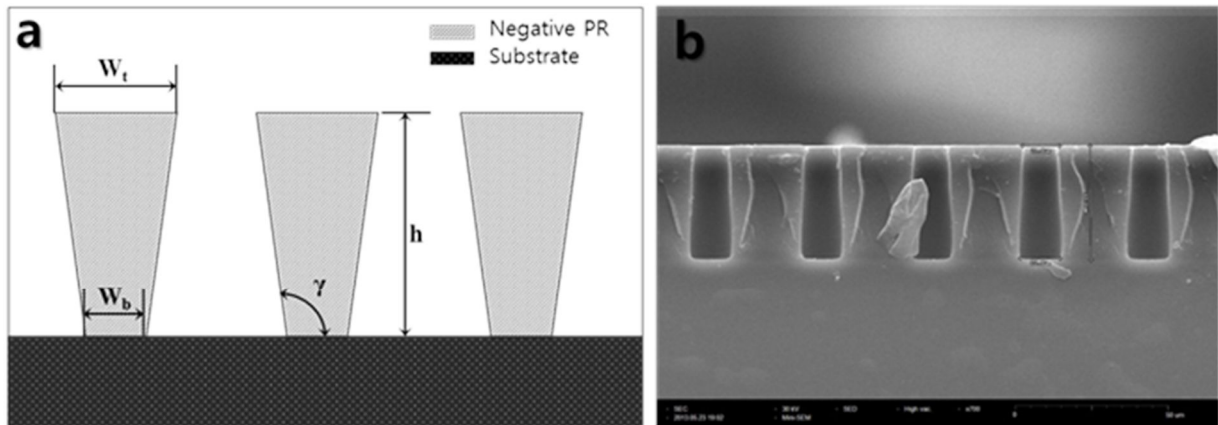


Figure 28 (a) Schematic illustration of the microstructures with undercuts. W_t , W_b , γ , and h represents: top widths, bottom widths, and height, respectively. (b) Representative cross-sectional SEM image showing the microstructures with undercuts (700x). The diameter of the micro-trench at the top is 11.9 μm while it is 12.9 μm at bottom.

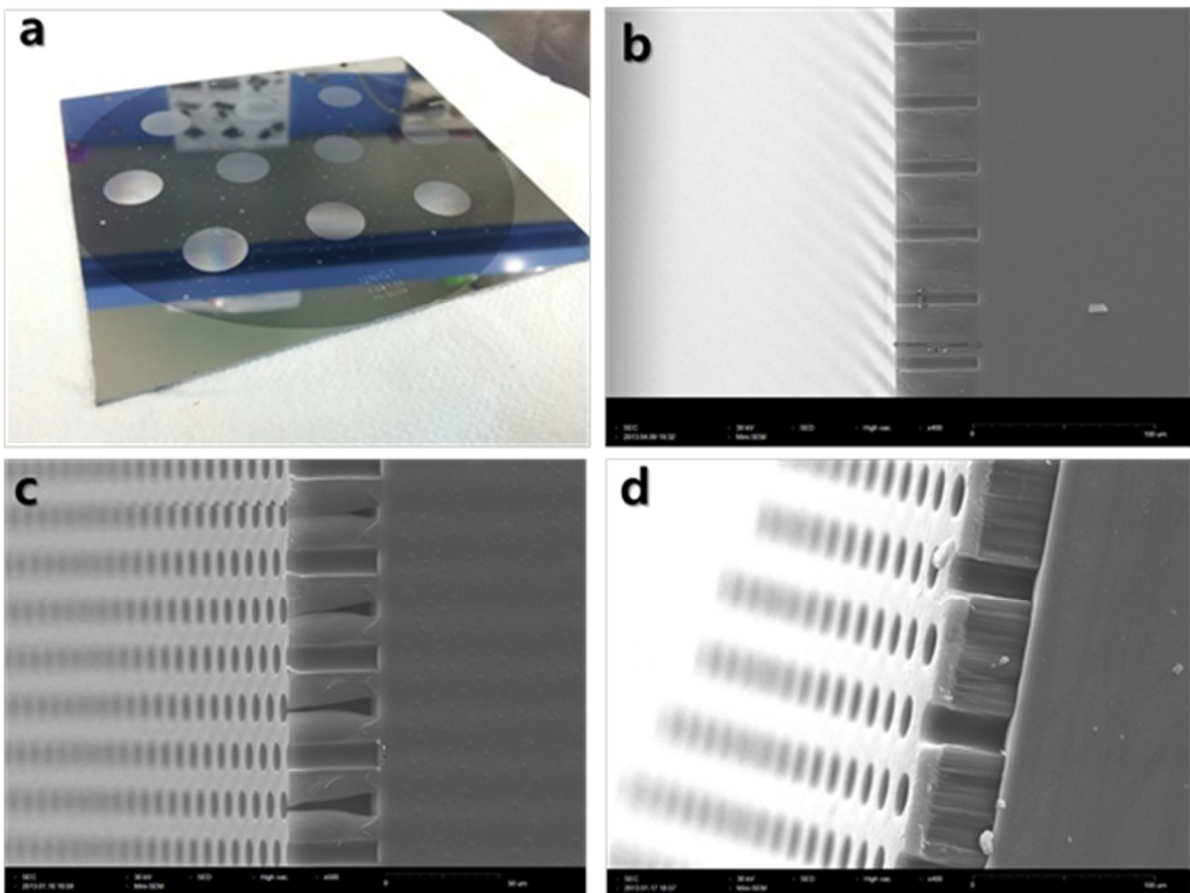


Figure 29 Results of SU-8 master fabrication. (a) A photograph image of a fabricated SU-8 master. (b-d) Representative cross-sectional SEM images showing images showing the cross-sections of the SU-8 molds with trench diameters of (b) 8 μm , (c) 12 μm , and (d) 20 μm in diameter. Magnifications are 400x, 500x, and 400x, respectively.

4.1.3 PDMS Master Fabrication

PDMS is one of the most commonly used silicon-based organic polymer in a variety of microfluidics and bioMEMS applications because it is cheap, transparent, biocompatible, and easy to handle.⁷⁰ Among various different candidates including silicon or thermoplastics, PDMS was selected as the mold for the through-hole membrane, particularly because it is a highly flexible material with the shear modulus (G) of approximately 250 kPa at a room temperature.

Prior to a PDMS casting process, the surface of the fabricated SU-8 master was passivated with (tridecafluoro-1,1,2,2-tetrahydrooctyl)-1-trichlorosilane in order to minimize the force of friction that will be exerted by each surface (i.e. the sidewall of the trenches in SU-8 mold and the surface of the PDMS pillar) on the other. The casting of PDMS was performed by a conventional soft lithography process. As a result, it was possible to acquire vertical and straight PDMS pillars for those that had diameters of 20 μm and 12 μm . However, the PDMS pillar with the diameter of 10 μm and 8 μm resulted with significant deformations in most cases (Figure 30b).

PDMS mold can deform during the demolding process, and deformed PDMS structures have a tendency to return to its original shape owing to its high elasticity. However, in the case of protruding structures with high aspect ratio, it is likely that, in some cases, the structures will experience a buckling or a collapse.⁷¹ One reason that can explain this phenomenon is that the protruding structures experience high frictional force when they are being detached from the mold, even after the surface of the PDMS mold is carefully passivated. Specifically, the stress caused by the frictional force can exceed the maximum mechanical strength of the microposts if the diameter of the microposts is too small. This will eventually cause the protruding microstructures to either break off or collapse.⁷²

The stability of the PDMS microposts can be dependent upon their own weight.⁷² According to Roca-Cusachs *et al.*, for the micropost that has a height of h a diameter of b , the critical aspect ratio (the maximum aspect ratio of the micropost free from the risk of collapsing) is dependent on $b^{-1/3}$.⁷¹ This indicates that as the diameter of the post decreases, it become more difficult to attain higher aspect ratio microstructure. In a nutshell, stability of the demolded PDMS microstructure is dependent upon two factors: frictional force exerted during the detachment and the weight of the microposts. These factors may have caused the microstructures structures with pillar diameter less than 10 μm to collapse, as shown in Figure 30b.

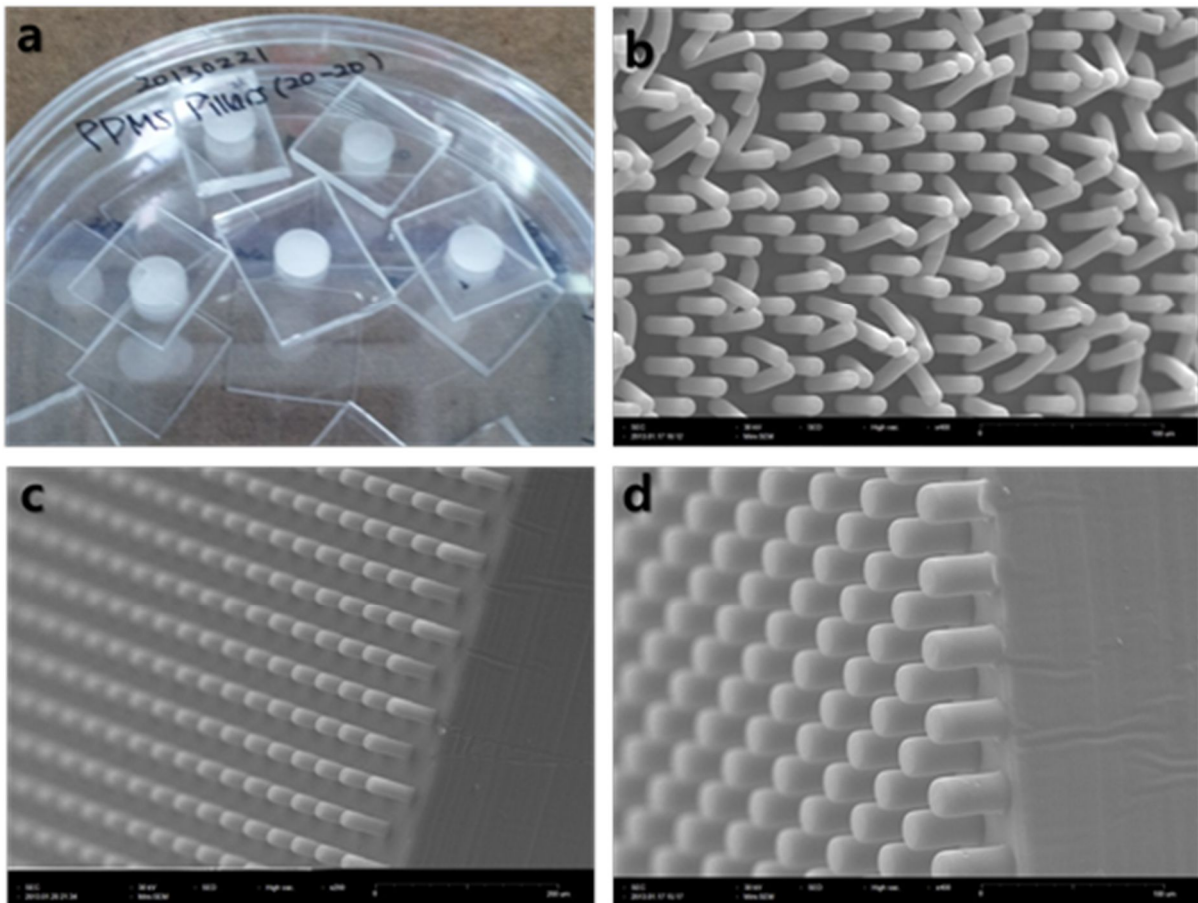


Figure 30 Results of PDMS master fabrication. (a) A photograph of a demolded PDMS masters. (b) Representative side-view SEM image showing the failure-mode of PDMS mold with a pillar diameter of $8\ \mu\text{m}$. Representative cross-sectional SEM images of PDMS masters with pillar diameters of (c) $12\ \mu\text{m}$, and (d) $20\ \mu\text{m}$ in diameter. For Figures (b), (c), and (d), magnifications are 400x, 200x, and 400x, respectively.

4.1.4 Surface Passivation and Demolding of PDMS Membrane

The critical step prior to using the demolded PDMS microposts as a second master for the PDMS through-hole membrane fabrication was the surface treatment of the PDMS molds and the slide glass which would be facing the pillar-side of the PDMS mold in conformal contact (Figure 12d). Since the PDMS mold had an extremely high surface area with densely packed micropost array, it was likely that the resulting membrane will remain attached to the PDMS mold after a detachment. Peeling off the membrane from a thickly packed micropost array may cause a breakage of the micropost structures. Thus, the surface condition was manipulated so that the demolded PDMS through-hole membrane will remain on the slide glass.

Instead of (tridecafluoro-1,1,2,2-tetrahydrooctyl)-1-trichlorosilane which was used for SU-8 mold passivation, the surface was treated with CF_3 plasma for the fine controls of the treatment conditions. The treatment condition was optimized using two different variables, with the fixed gas pressure of 50 sccm: RF power and the duration of the plasma treatment. The effect of the surface treatment was analyzed by measuring the contact angles of each substrate. Table 6 summarizes the result for the PDMS surface passivation, and Table 7 summarizes the surface passivation result for the slide glass with nine different conditions. In the case of the surface treatment of the PDMS mold, contact angles ranged from $87.71 \pm 2.64^\circ$ to $92.73 \pm 3.29^\circ$; the results were not significantly different from one another. In the case of the surface treatment of the slide glass, however, the contact angles varied from $12.9 \pm 1.21^\circ$ to $100.7 \pm 2.21^\circ$. For the final condition, RF power of 300W for 100 seconds was selected for the surface treatment of the PDMS molds. For the condition for the slide glass, RF power of 15 W for 10 seconds was selected.

In order to fill the PDMS gel in a space between the membrane and the slide glass, passivated PDMS mold was first faced with the slide glass in conformal contact. Then, a pair of permanent magnets was then placed on both sides to hold the molding block. Then, the empty space between the PDMS mold and the slide glass was gently filled with a 1:5 mixture of a curing agent and PDMS prepolymer. A 1:5 mixture of the curing agent and PDMS was used because it was less viscous compared to a 1:10 mixture, allowing a more effective filling of the PDMS gel. The molding block was then baked at $80^\circ C$ for 4 hours. Lastly, the cured PDMS membrane was gently detached from the PDMS mold and the glass slide. The optimized surface treatment condition mentioned above allowed a smooth detachment of the membrane from the PDMS mold, keeping it slightly attached on the slide glass surface. Figure 31 is the result showing the detached PDMS membrane from the PDMS mold.

Table 7 The surface passivation results for the PDMS mold with different conditions.

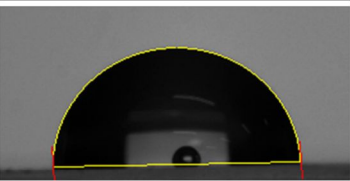
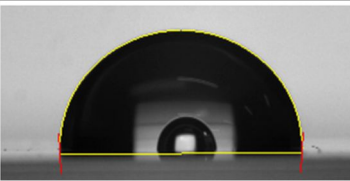
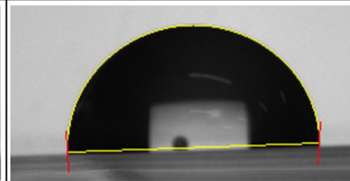
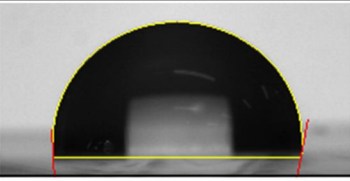
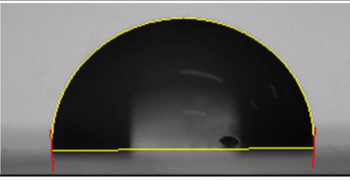
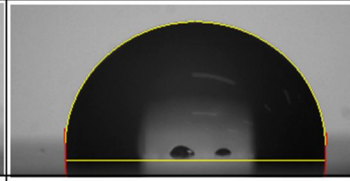
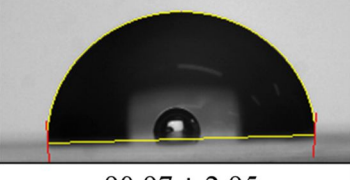
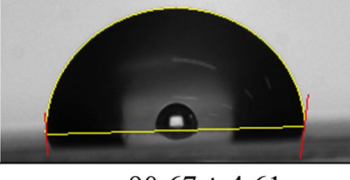
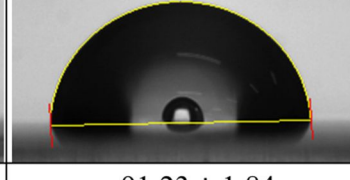
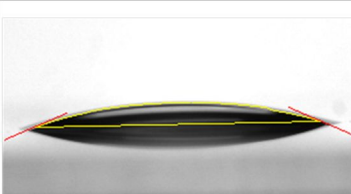
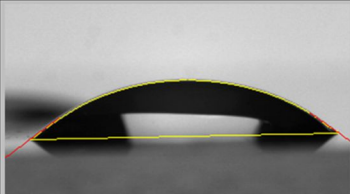
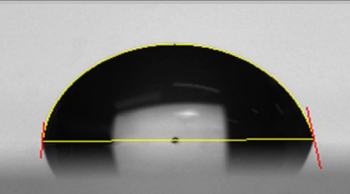
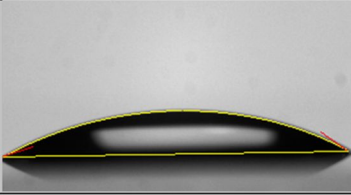
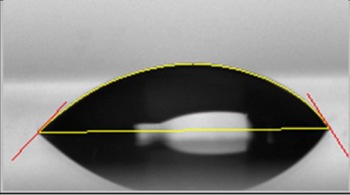
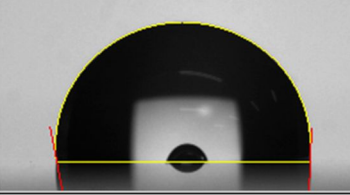
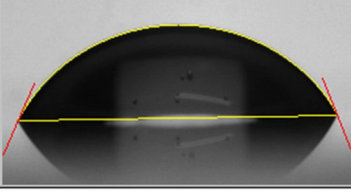
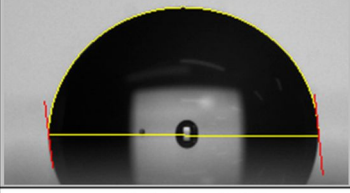
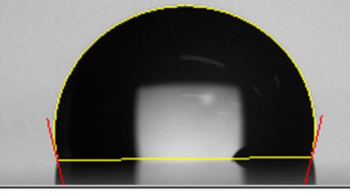
Power Time	100 W	200 W	300 W
100 sec			
	87.71 ± 2.64	92.46 ± 1.93	92.34 ± 1.85
300 sec			
	91.83 ± 2.59	93.63 ± 1.17	92.73 ± 3.29
900 sec			
	90.97 ± 2.95	90.67 ± 4.61	91.23 ± 1.84

Table 8 The surface passivation results for the slide glass with different conditions.

Power Time	10 W	20 W	30 W
5 sec			
	12.9 ± 1.21	54.8 ± 10.43	82.04 ± 11.06
10 sec			
	21.3 ± 3.31	63.1 ± 8.55	95.8 ± 4.12
20 sec			
	59.0 ± 11.45	96.8 ± 4.87	100.7 ± 2.21

4.1.5 Back-side Etching

Above membrane casting process often resulted in a thin residual PDMS layer left behind on the membrane because it is difficult to obtain PDMS microposts with perfectly vertical edges. The final step of the membrane fabrication was, therefore, the removal of the PDMS residual layer. The surface of the PDMS membrane was slightly etched with SF₆ (90 sccm)/ O₂ (6sccm) gas combination under the RF power of 500 W for 100 seconds. The etch rate was determined to be $0.47 \pm 0.02 \mu\text{m}/\text{min}$. As a result, it was possible to remove residual PDMS layers. Figure 32 summarizes the final result of the PDMS through-hole membrane with uniformly arrayed through-holes.

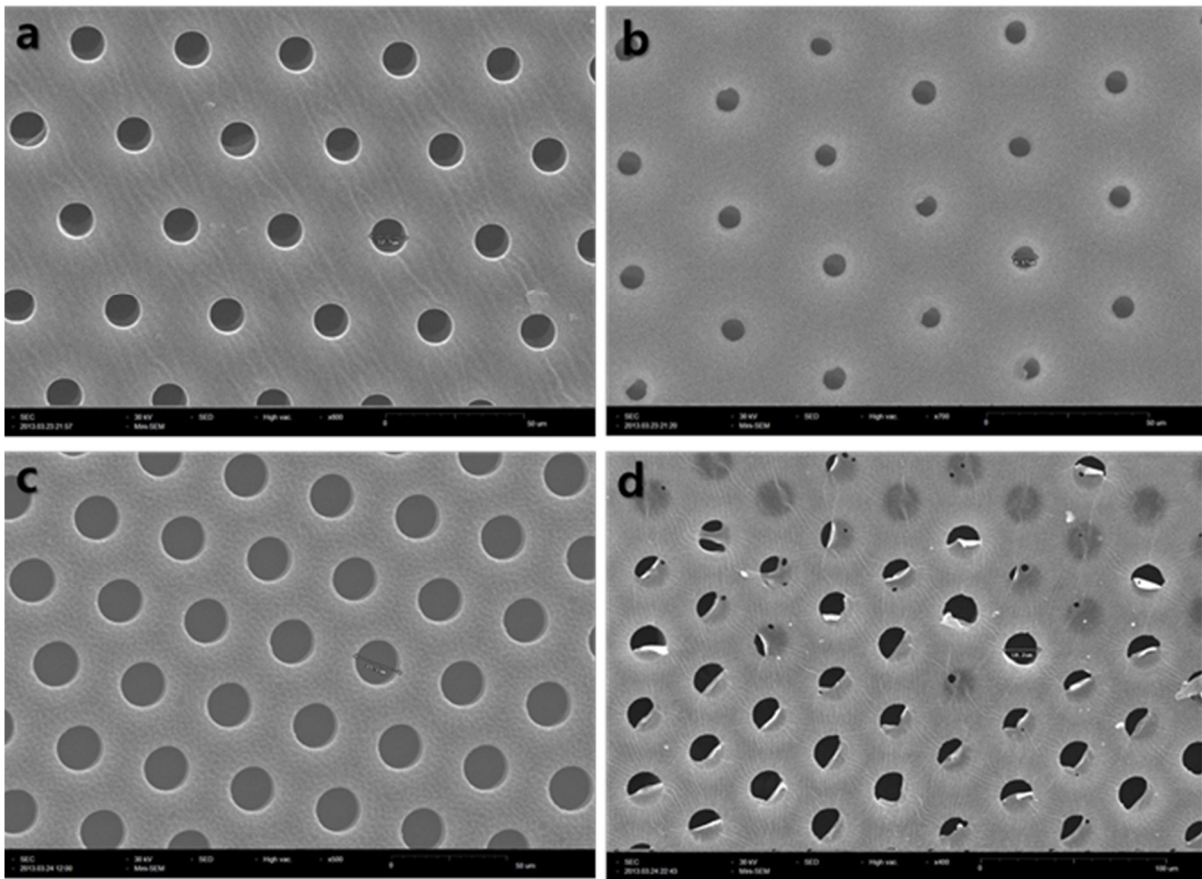


Figure 30 Results of PDMS through-hole membrane fabrication. Representative SEM images showing images showing front side (a) and back side (b) of the PDMS through-hole membrane with the hole size of 12 μm . Representative SEM images showing images showing front side (c) and back side (d) of the PDMS through-hole membrane with the hole size of 20 μm . Magnifications are 600x, 700x, 500x, and 400x respectively.

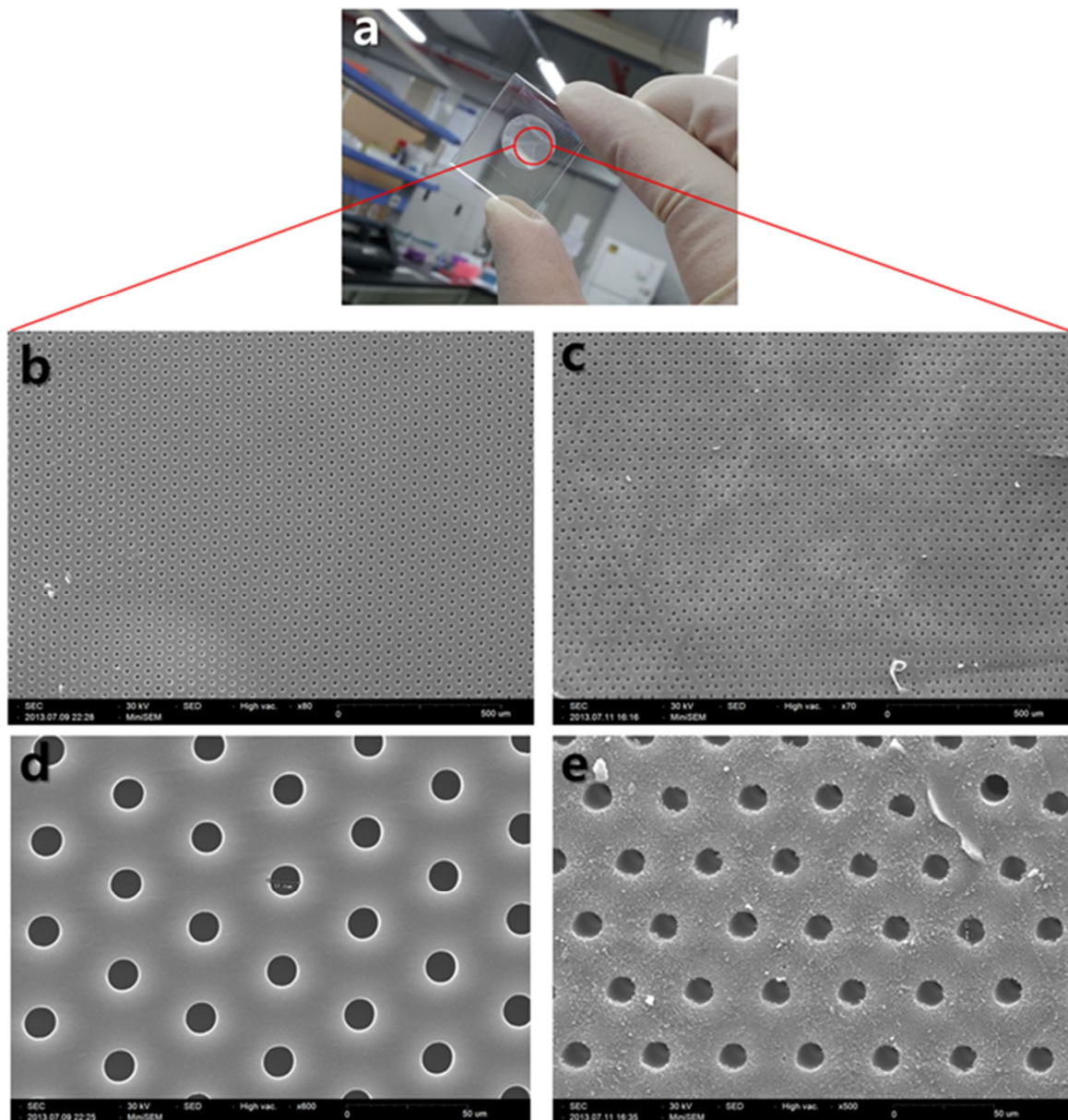


Figure 31 Results of PDMS through-hole membrane fabrication after the completion of back-side etching. (a) A photograph of the final product. Representative SEM images showing images showing front side (b, d) and back side (c, e) of the same PDMS through-hole membrane with hole sizes of 12 μm . Magnifications for Figures (b), (c), (d), and (e) are 80x, 70x, 600x, and 500x, respectively.

4.1.6 Performance Evaluation

For the proposed membrane fabrication method, two critical aspects remained unsolved. First of all, the membrane fabrication using proposed fabrication method was not as efficiency reproducible as expected. Multiple steps of the fabrication process, including SU-8 mold fabrication, PDMS casting, surface passivation of the PDMS mold and a slide glass, PDMS gel filling, and the detachment, resulted with a long turn-around time. Furthermore, fabrication of the membranes using a high aspect ratio feature was a very challenging process. Specifically, it was difficult to obtain the PDMS mold with the micropost diameter of 8 μm . The possible reason for this may be due to the fact that the diameter of the micropost compared to its height was too small to withstand the frictional force exerted on the thin and flexible microposts, leading to serious structural deformations of the microposts. In order to overcome difficulties mentioned above, it is possible to take advantage of alternating membrane fabrication methods including laser ablation method⁷³ or dry-etching methods⁷⁴.

CHAPTER 5 Concluding Remarks

5.1 Summary of the Work

In this chapter, a label-free lab-on-a-disc platform was introduced for a rapid and efficient detection of CTCs from whole blood samples as well as clinical samples. Polycarbonate track-etch membrane was used to isolate CTCs based on the size difference between the target cell and other blood cells. The device was tested with MCF-7 cancer cell spiked in both PBS buffer solution as well as whole blood sample. The capture efficiency of the target cancer cell using the devised system ranged from 50 % to 60 %, and the purity of the captured cells varied widely, ranging from 15 % to 30 %. In addition, blood samples from gastric cancer and breast cancer patients were tested. The number of CTCs ranging from 5 to 29 CTCs was captured. Overall, the CTC detection rate for the lung cancer patient was 50 %, and the detection rate for the gastric cancer patients was 38.4 %. The negative depletion method prior to the filtration is proposed in order to increase the purity of the product for a downstream molecular analysis. In addition, PDMS through-hole membrane with regular size and alignment was fabricated to use it as an alternative for the filter, and it is expected to enhance the sensitivity of the device.

5.2 Strength and Limitation

The strength of the proposed CTC-capture disc is that it requires less than 3 minutes to process whole blood samples. Considering that most of the immunoaffinity-based CTC isolation platforms require at least a few hours to complete the sample processing procedure, our system, which exploits size-based filtration method on a lab-on-a-disc system, significantly reduces the process time. Another advantage of our work is that the CTC isolation processes do not require sample pre-treatment step. In other words, the whole blood sample can be directly loaded onto the disc. Owing to these advantages, the CTC-capture disc platform can be highly competitive candidate for a point-of-care testing (POCT) device in the field of cancer diagnosis. However, the system still has a room for improvement. Since our CTC-capture disc platform is not yet an automated system, it requires a trained expert to run the samples in order to avoid experimental errors pertaining to technical discrepancies.

5.3 Future Prospect

For the future work, the automation of the system is essential to minimize the turnaround time of the entire process, starting from the sample infusion step to the detection step. This is possible by applying automated unit operations, i.e. active valving, mixing, and metering, onto the lab-on-a-disc platform. By taking advantage of the unit operations, it is also possible to integrate additional detection modules directly onto our CTC-capture disc. This will provide us with a more rapid and efficient way of performing downstream molecular analysis, including quantitative PCR and Next Generation Sequencing.

References

1. Cell Search: Circulating Tumor Cell Test. (accessed Jan.).
2. Kaiser, J., Cancer's Circulation Problem. *Science* **2010**, 327 (5969), 1072-1074.
3. Madou, M.; Zoval, J.; Jia, G.; Kido, H.; Kim, J.; Kim, N., LAB ON A CD. *Annual Review of Biomedical Engineering* **2006**, 8 (1), 601-628.
4. Fluxion Bioscience: Innovated tools for cellular analysis. (accessed Jan).
5. Yamada, M.; Nakashima, M.; Seki, M., Pinched Flow Fractionation: Continuous Size Separation of Particles Utilizing a Laminar Flow Profile in a Pinched Microchannel. *Analytical Chemistry* **2004**, 76 (18), 5465-5471.
6. Kim, M. S.; Sim, T. S.; Kim, Y. J.; Kim, S. S.; Jeong, H.; Park, J.-M.; Moon, H.-S.; Kim, S. I.; Gurel, O.; Lee, S. S.; Lee, J.-G.; Park, J. C., SSA-MOA: a novel CTC isolation platform using selective size amplification (SSA) and a multi-obstacle architecture (MOA) filter. *Lab on a chip* **2012**, 12 (16), 2874-2880.
7. Allard, W. J.; Matera, J.; Miller, M. C.; Repollet, M.; Connelly, M. C.; Rao, C.; Tibbe, A. G. J.; Uhr, J. W.; Terstappen, L. W. M. M., Tumor Cells Circulate in the Peripheral Blood of All Major Carcinomas but not in Healthy Subjects or Patients With Nonmalignant Diseases. *Clinical Cancer Research* **2004**, 10 (20), 6897-6904.
8. Schroeder, A.; Heller, D. A.; Winslow, M. M.; Dahlman, J. E.; Pratt, G. W.; Langer, R.; Jacks, T.; Anderson, D. G., Treating metastatic cancer with nanotechnology. *Nat Rev Cancer* **2012**, 12 (1), 39-50.
9. Lin, H. K.; Zheng, S.; Williams, A. J.; Balic, M.; Groshen, S.; Scher, H. I.; Fleisher, M.; Stadler, W.; Datar, R. H.; Tai, Y.-C.; Cote, R. J., Portable Filter-Based Microdevice for Detection and Characterization of Circulating Tumor Cells. *Clinical Cancer Research* **2010**, 16 (20), 5011-5018.
10. Nagrath, S.; Sequist, L. V.; Maheswaran, S.; Bell, D. W.; Irimia, D.; Ulkus, L.; Smith, M. R.; Kwak, E. L.; Digumarthy, S.; Muzikansky, A.; Ryan, P.; Balis, U. J.; Tompkins, R. G.; Haber, D. A.; Toner, M., Isolation of rare circulating tumour cells in cancer patients by microchip technology. *Nature* **2007**, 450 (7173), 1235-1239.
11. ScreenCell: Non-invasive technology for isolating Rare Circulating Cells. (accessed Jan.).
12. Ozkumur, E.; Shah, A. M.; Ciciliano, J. C.; Emmink, B. L.; Miyamoto, D. T.; Brachtel, E.; Yu, M.; Chen, P.-i.; Morgan, B.; Trautwein, J.; Kimura, A.; Sengupta, S.; Stott, S. L.; Karabacak, N. M.; Barber, T. A.; Walsh, J. R.; Smith, K.; Spuhler, P. S.; Sullivan, J. P.; Lee, R. J.; Ting, D. T.; Luo, X.; Shaw, A. T.; Bardia, A.; Sequist, L. V.; Louis, D. N.; Maheswaran, S.; Kapur, R.; Haber, D. A.; Toner, M., Inertial Focusing for Tumor Antigen-Dependent and -Independent Sorting of Rare Circulating Tumor Cells. *Science Translational Medicine* **2013**, 5 (179), 179ra47.

13. CytoTrack. (accessed Jan.).
14. Hou, H. W.; Warkiani, M. E.; Khoo, B. L.; Li, Z. R.; Soo, R. A.; Tan, D. S.-W.; Lim, W.-T.; Han, J.; Bhagat, A. A. S.; Lim, C. T., Isolation and retrieval of circulating tumor cells using centrifugal forces. *Sci. Rep.* **2013**, *3*.
15. Cristofanilli, M.; Budd, G. T.; Ellis, M. J.; Stopeck, A.; Matera, J.; Miller, M. C.; Reuben, J. M.; Doyle, G. V.; Allard, W. J.; Terstappen, L. W. M. M.; Hayes, D. F., Circulating Tumor Cells, Disease Progression, and Survival in Metastatic Breast Cancer. *New England Journal of Medicine* **2004**, *351* (8), 781-791.
16. Stott, S. L.; Hsu, C.-H.; Tsukrov, D. I.; Yu, M.; Miyamoto, D. T.; Waltman, B. A.; Rothenberg, S. M.; Shah, A. M.; Smas, M. E.; Korir, G. K.; Floyd, F. P.; Gilman, A. J.; Lord, J. B.; Winokur, D.; Springer, S.; Irimia, D.; Nagrath, S.; Sequist, L. V.; Lee, R. J.; Isselbacher, K. J.; Maheswaran, S.; Haber, D. A.; Toner, M., Isolation of circulating tumor cells using a microvortex-generating herringbone-chip. *Proceedings of the National Academy of Sciences* **2010**, *107* (43), 18392-18397.
17. Haerberle, S.; Brenner, T.; Zengerle, R.; Ducree, J., Centrifugal extraction of plasma from whole blood on a rotating disk. *Lab on a chip* **2006**, *6* (6), 776-781.
18. Lee, B. S.; Lee, J.-N.; Park, J.-M.; Lee, J.-G.; Kim, S.; Cho, Y.-K.; Ko, C., A fully automated immunoassay from whole blood on a disc. *Lab on a chip* **2009**, *9* (11), 1548-1555.
19. Moon, H.-S.; Kwon, K.; Kim, S.-I.; Han, H.; Sohn, J.; Lee, S.; Jung, H.-I., Continuous separation of breast cancer cells from blood samples using multi-orifice flow fractionation (MOFF) and dielectrophoresis (DEP). *Lab on a chip* **2011**, *11* (6), 1118-1125.
20. Adams, A. A.; Okagbare, P. I.; Feng, J.; Hupert, M. L.; Patterson, D.; Gottert, J.; McCarley, R. L.; Nikitopoulos, D.; Murphy, M. C.; Soper, S. A., Highly Efficient Circulating Tumor Cell Isolation from Whole Blood and Label-Free Enumeration Using Polymer-Based Microfluidics with an Integrated Conductivity Sensor. *Journal of the American Chemical Society* **2008**, *130* (27), 8633-8641.
21. Kamande, J. W.; Hupert, M. L.; Witek, M. A.; Wang, H.; Torphy, R. J.; Dharmasiri, U.; Njoroge, S. K.; Jackson, J. M.; Aufforth, R. D.; Snively, A.; Yeh, J. J.; Soper, S. A., Modular Microsystem for the Isolation, Enumeration, and Phenotyping of Circulating Tumor Cells in Patients with Pancreatic Cancer. *Analytical Chemistry* **2013**, *85* (19), 9092-9100.
22. Chen, H.; Wang, L.; Li, P. C. H., Nucleic acid microarrays created in the double-spiral format on a circular microfluidic disk. *Lab on a chip* **2008**, *8* (5), 826-829.
23. Zhang, N.; Deng, Y.; Tai, Q.; Cheng, B.; Zhao, L.; Shen, Q.; He, R.; Hong, L.; Liu, W.; Guo, S.; Liu, K.; Tseng, H.-R.; Xiong, B.; Zhao, X.-Z., Electrospun TiO₂ Nanofiber-Based Cell Capture Assay for Detecting Circulating Tumor Cells from Colorectal and Gastric Cancer Patients. *Advanced Materials* **2012**, *24* (20), 2756-2760.

24. Martinez-Duarte, R.; Gorkin Iii, R. A.; Abi-Samra, K.; Madou, M. J., The integration of 3D carbon-electrode dielectrophoresis on a CD-like centrifugal microfluidic platform. *Lab on a chip* **2010**, *10* (8), 1030-1043.
25. Hoshino, K.; Huang, Y.-Y.; Lane, N.; Huebschman, M.; Uhr, J. W.; Frenkel, E. P.; Zhang, X., Microchip-based immunomagnetic detection of circulating tumor cells. *Lab on a chip* **2011**, *11* (20), 3449-3457.
26. DESITTER, I.; GUERROUAHEN, B. S.; BENALI-FURET, N.; WECHSLER, J.; JÄNNE, P. A.; KUANG, Y.; YANAGITA, M.; WANG, L.; BERKOWITZ, J. A.; DISTEL, R. J.; CAYRE, Y. E., A New Device for Rapid Isolation by Size and Characterization of Rare Circulating Tumor Cells. *Anticancer Research* **2011**, *31* (2), 427-441.
27. Kang, J. H.; Krause, S.; Tobin, H.; Mammoto, A.; Kanapathipillai, M.; Ingber, D. E., A combined micromagnetic-microfluidic device for rapid capture and culture of rare circulating tumor cells. *Lab on a chip* **2012**, *12* (12), 2175-2181.
28. Ferlay J, S. H., Bray F, et al. Cancer Incidence and Mortality Worldwide: IARC Cancer Base No. 10. (accessed Jan.).
29. Mocellin, S.; Keilholz, U.; Rossi, C. R.; Nitti, D., Circulating tumor cells: the 'leukemic phase' of solid cancers. *Trends in Molecular Medicine* **2006**, *12* (3), 130-139.
30. Allan, A. L.; Vantyghem, S. A.; Tuck, A. B.; Chambers, A. F.; Chin-Yee, I. H.; Keeney, M., Detection and quantification of circulating tumor cells in mouse models of human breast cancer using immunomagnetic enrichment and multiparameter flow cytometry. *Cytometry Part A* **2005**, *65A* (1), 4-14.
31. Iakovlev, V.; Goswami, R.; Vecchiarelli, J.; Arneson, N. R.; Done, S., Quantitative detection of circulating epithelial cells by Q-RT-PCR. *Breast Cancer Res Treat* **2008**, *107* (1), 145-154.
32. Xenidis, N.; Perraki, M.; Kafousi, M.; Apostolaki, S.; Bolonaki, I.; Stathopoulou, A.; Kalbakis, K.; Androulakis, N.; Kouroussis, C.; Pallis, T.; Christophylakis, C.; Argyraki, K.; Lianidou, E. S.; Stathopoulos, S.; Georgoulas, V.; Mavroudis, D., Predictive and Prognostic Value of Peripheral Blood Cytokeratin-19 mRNA-Positive Cells Detected by Real-Time Polymerase Chain Reaction in Node-Negative Breast Cancer Patients. *Journal of Clinical Oncology* **2006**, *24* (23), 3756-3762.
33. Braun, S.; Vogl, F. D.; Naume, B.; Janni, W.; Osborne, M. P.; Coombes, R. C.; Schlimok, G.; Diel, I. J.; Gerber, B.; Gebauer, G.; Pierga, J.-Y.; Marth, C.; Oruzio, D.; Wiedswang, G.; Solomayer, E.-F.; Kundt, G.; Strobl, B.; Fehm, T.; Wong, G. Y. C.; Bliss, J.; Vincent-Salomon, A.; Pantel, K., A Pooled Analysis of Bone Marrow Micrometastasis in Breast Cancer. *New England Journal of Medicine* **2005**, *353* (8), 793-802.
34. Pachmann, K.; Camara, O.; Kavallaris, A.; Krauspe, S.; Malarski, N.; Gajda, M.; Kroll, T.; Jörke, C.; Hammer, U.; Altendorf-Hofmann, A.; Rabenstein, C.; Pachmann, U.; Runnebaum, I.; Höffken, K., Monitoring the Response of Circulating Epithelial Tumor Cells to Adjuvant Chemotherapy in Breast

Cancer Allows Detection of Patients at Risk of Early Relapse. *Journal of Clinical Oncology* **2008**, *26* (8), 1208-1215.

35. Ring, A. E.; Zabaglo, L.; Ormerod, M. G.; Smith, I. E.; Dowsett, M., Detection of circulating epithelial cells in the blood of patients with breast cancer: comparison of three techniques. *Br J Cancer* **2005**, *92* (5), 906-912.

36. Zabaglo, L.; Ormerod, M. G.; Parton, M.; Ring, A.; Smith, I. E.; Dowsett, M., Cell filtration-laser scanning cytometry for the characterisation of circulating breast cancer cells. *Cytometry Part A* **2003**, *55A* (2), 102-108.

37. Cabioglu, N.; Igci, A.; Yildirim, E. O.; Aktas, E.; Bilgic, S.; Yavuz, E.; Muslumanoglu, M.; Bozfakioglu, Y.; Kecer, M.; Ozmen, V.; Deniz, G., An ultrasensitive tumor enriched flow-cytometric assay for detection of isolated tumor cells in bone marrow of patients with breast cancer. *The American Journal of Surgery* **2002**, *184* (5), 414-417.

38. Cruz, I.; Ciudad, J.; Cruz, J. J.; Ramos, M.; Gómez-Alonso, A.; Adansa, J. C.; Rodríguez, C.; Orfao, A., Evaluation of Multiparameter Flow Cytometry for the Detection of Breast Cancer Tumor Cells in Blood Samples. *American Journal of Clinical Pathology* **2005**, *123* (1), 66-74.

39. Chen, J.; Li, J.; Sun, Y., Microfluidic approaches for cancer cell detection, characterization, and separation. *Lab on a chip* **2012**, *12* (10), 1753-67.

40. Esmaeilsabzali, H.; Beischlag, T. V.; Cox, M. E.; Parameswaran, A. M.; Park, E. J., Detection and isolation of circulating tumor cells: Principles and methods. *Biotechnology advances* **2013**, *31* (7), 1063-84.

41. Mikolajczyk, S. D.; Millar, L. S.; Tsinberg, P.; Coutts, S. M.; Zomorodi, M.; Pham, T.; Bischoff, F. Z.; Pircher, T. J., Detection of EpCAM-Negative and Cytokeratin-Negative Circulating Tumor Cells in Peripheral Blood. *Journal of Oncology* **2011**, *2011*.

42. Paterlini-Brechot, P.; Benali, N. L., Circulating tumor cells (CTC) detection: Clinical impact and future directions. *Cancer Letters* **2007**, *253* (2), 180-204.

43. Morgan TM, L. P., Vessella RL, Detection and characterization of circulating and disseminated prostate cancer cells. *Frontiers in Bioscience* **2007**, *12* (1), 3000-3009.

44. Vahey, M. D.; Voldman, J., High-Throughput Cell and Particle Characterization Using Isodielectric Separation. *Analytical Chemistry* **2009**, *81* (7), 2446-2455.

45. Hong B, Z. Y., Detecting Circulating Tumor Cells: Current Challenges and New Trends. *Theranostics* **2013**, *3* (6), 377-394.

46. Lalmahomed, Z. S.; Kraan, J.; Gratama, J. W.; Mostert, B.; Sleijfer, S.; Verhoef, C., Circulating Tumor Cells and Sample Size: The More, the Better. *Journal of Clinical Oncology* **2010**, *28* (17), e288-e289.

47. Gorkin, R.; Park, J.; Siegrist, J.; Amasia, M.; Lee, B. S.; Park, J.-M.; Kim, J.; Kim, H.; Madou, M.; Cho, Y.-K., Centrifugal microfluidics for biomedical applications. *Lab on a chip* **2010**, *10* (14), 1758-1773.
48. Park, J.; Sunkara, V.; Kim, T.-H.; Hwang, H.; Cho, Y.-K., Lab-on-a-Disc for Fully Integrated Multiplex Immunoassays. *Analytical Chemistry* **2012**, *84* (5), 2133-2140.
49. Schembri, C. T.; Ostoich, V.; Lingane, P. J.; Burd, T. L.; Buhl, S. N., Portable simultaneous multiple analyte whole-blood analyzer for point-of-care testing. *Clinical Chemistry* **1992**, *38* (9), 1665-70.
50. Mårtensson, G.; Skote, M.; Malmqvist, M.; Falk, M.; Asp, A.; Svanvik, N.; Johansson, A., Rapid PCR amplification of DNA utilizing Coriolis effects. *Eur Biophys J* **2006**, *35* (6), 453-458.
51. Peytavi, R.; Raymond, F. R.; Gagné, D.; Picard, F. J.; Jia, G.; Zoval, J.; Madou, M.; Boissinot, K.; Boissinot, M.; Bissonnette, L.; Ouellette, M.; Bergeron, M. G., Microfluidic Device for Rapid (<15 min) Automated Microarray Hybridization. *Clinical Chemistry* **2005**, *51* (10), 1836-1844.
52. Lim, L. S.; Hu, M.; Huang, M. C.; Cheong, W. C.; Gan, A. T. L.; Looi, X. L.; Leong, S. M.; Koay, E. S.-C.; Li, M.-H., Microsieve lab-chip device for rapid enumeration and fluorescence in situ hybridization of circulating tumor cells. *Lab on a chip* **2012**, *12* (21), 4388-4396.
53. Jongchan, C.; Kyeong-Hwan, L.; Sung, Y., Fabrication of PDMS through-holes using the MIMIC method and the surface treatment by atmospheric-pressure CH₄/He RF plasma. *Journal of Micromechanics and Microengineering* **2011**, *21* (9), 097001.
54. Zheng, S.; Lin, H.; Lu, B.; Williams, A.; Datar, R.; Cote, R.; Tai, Y.-C., 3D microfilter device for viable circulating tumor cell (CTC) enrichment from blood. *Biomedical microdevices* **2011**, *13* (1), 203-213.
55. Zheng, S.; Lin, H.; Liu, J.-Q.; Balic, M.; Datar, R.; Cote, R. J.; Tai, Y.-C., Membrane microfilter device for selective capture, electrolysis and genomic analysis of human circulating tumor cells. *Journal of Chromatography A* **2007**, *1162* (2), 154-161.
56. Coumans, F. A. W.; van Dalum, G.; Beck, M.; Terstappen, L. W. M. M., Filtration Parameters Influencing Circulating Tumor Cell Enrichment from Whole Blood. *PLoS ONE* **2013**, *8* (4), e61774
57. Hosokawa, M.; Yoshikawa, T.; Negishi, R.; Yoshino, T.; Koh, Y.; Kenmotsu, H.; Naito, T.; Takahashi, T.; Yamamoto, N.; Kikuhara, Y.; Kanbara, H.; Tanaka, T.; Yamaguchi, K.; Matsunaga, T., Microcavity Array System for Size-Based Enrichment of Circulating Tumor Cells from the Blood of Patients with Small-Cell Lung Cancer. *Analytical Chemistry* **2013**, *85* (12), 5692-5698.
58. Kim, E. H.; Lee, J. K.; Kim, B. C.; Rhim, S. H.; Kim, J. W.; Kim, K. H.; Jung, S. M.; Park, P. S.; Park, H. C.; Lee, J.; Jeon, B. H., Enrichment of cancer cells from whole blood using a microfabricated porous filter. *Analytical Biochemistry* **2013**, *440* (1), 114-116.

59. Hosokawa, M.; Kenmotsu, H.; Koh, Y.; Yoshino, T.; Yoshikawa, T.; Naito, T.; Takahashi, T.; Murakami, H.; Nakamura, Y.; Tsuya, A.; Shukuya, T.; Ono, A.; Akamatsu, H.; Watanabe, R.; Ono, S.; Mori, K.; Kanbara, H.; Yamaguchi, K.; Tanaka, T.; Matsunaga, T.; Yamamoto, N., Size-Based Isolation of Circulating Tumor Cells in Lung Cancer Patients Using a Microcavity Array System. *PLoS ONE* **2013**, *8* (6), e67466.
60. Dagan, Z.; Weinbaum, S.; Pfeffer, R., Theory and experiment on the three-dimensional motion of a freely suspended spherical particle at the entrance to a pore at low Reynolds number. *Chemical Engineering Science* **1983**, *38* (4), 583-596.
61. Viscosity. http://uqu.edu.sa/files2/tiny_mce/plugins/filemanager/files/4282164/Viscosity.pdf.
62. Kuiper, S.; van Rijn, C.; Nijdam, W.; Raspe, O.; van Wolferen, H.; Krijnen, G.; Elwenspoek, M., Filtration of lager beer with microsieves: flux, permeate haze and in-line microscope observations. *Journal of Membrane Science* **2002**, *196* (2), 159-170.
63. Kuiper, S.; Brink, R.; Nijdam, W.; Krijnen, G. J. M.; Elwenspoek, M. C., Ceramic microsieves: influence of perforation shape and distribution on flow resistance and membrane strength. *Journal of Membrane Science* **2002**, *196* (2), 149-157.
64. Dagan, Z.; Weinbaum, S.; Pfeffer, R., An infinite-series for the creeping motion through an orifice of finite length. *J. FLUID MECH.* **1982**, *115*, Feb. 1982, 505-523.
65. Holdich, R.; Kosvintsev, S.; Cumming, I.; Zhdanov, S., Pore design and engineering for filters and membranes. *Philosophical Transactions of the Royal Society A: Mathematical, Physical and Engineering Sciences* **2006**, *364* (1838), 161-174.
66. Lu, Y.-T.; Zhao, L.; Shen, Q.; Garcia, M. A.; Wu, D.; Hou, S.; Song, M.; Xu, X.; OuYang, W.-H.; OuYang, W. W. L.; Lichterman, J.; Luo, Z.; Xuan, X.; Huang, J.; Chung, L. W. K.; Rettig, M.; Tseng, H.-R.; Shao, C.; Posadas, E. M., NanoVelcro Chip for CTC enumeration in prostate cancer patients. *Methods* **2013**, *64* (2), 144-152.
67. Warkiani, M. E.; Guan, G.; Luan, K. B.; Lee, W. C.; Bhagat, A. A. S.; Kant Chaudhuri, P.; Tan, D. S.-W.; Lim, W. T.; Lee, S. C.; Chen, P. C. Y.; Lim, C. T.; Han, J., Slanted spiral microfluidics for the ultra-fast, label-free isolation of circulating tumor cells. *Lab on a chip* **2014**, *14* (1), 128-137.
68. Zhang, J.; Chan-Park, M. B.; Conner, S. R., Effect of exposure dose on the replication fidelity and profile of very high aspect ratio microchannels in SU-8. *Lab on a chip* **2004**, *4* (6), 646-653.
69. Yao, C.; Ching-Yo, L.; Wei, D.-H.; Loechel, B.; Gruetzner, G., Wall profile of thick photoresist generated via contact printing. *Microelectromechanical Systems, Journal of* **1999**, *8* (1), 18-26.
70. Bélanger, M. C.; Marois, Y., Hemocompatibility, biocompatibility, inflammatory and in vivo studies of primary reference materials low-density polyethylene and polydimethylsiloxane: A review. *Journal of Biomedical Materials Research* **2001**, *58* (5), 467-477.

71. Roca-Cusachs, P.; Rico, F.; Martínez, E.; Toset, J.; Farré, R.; Navajas, D., Stability of Microfabricated High Aspect Ratio Structures in Poly(dimethylsiloxane). *Langmuir* **2005**, *21* (12), 5542-5548.
72. Shao, G.; Wu, J.; Cai, Z.; Wang, W., Fabrication of elastomeric high-aspect-ratio microstructures using polydimethylsiloxane (PDMS) double casting technique. *Sensors and Actuators A: Physical* **2012**, *178* (0), 230-236.
73. Masters, T.; Engl, W.; Weng, Z. L.; Arasi, B.; Gauthier, N.; Viasnoff, V., Easy Fabrication of Thin Membranes with Through Holes. Application to Protein Patterning. *PLoS ONE* **2012**, *7* (8), e44261.
74. Chen, W.; Lam, R. H. W.; Fu, J., Photolithographic surface micromachining of polydimethylsiloxane (PDMS). *Lab on a chip* **2012**, *12* (2), 391-395.

Acknowledgements

I would like to thank my advisor, Professor Yoon-Kyoung Cho, for her ongoing encouragement, support, and instruction throughout my thesis research. I would also like to thank my dissertation committee members, Professor Sebyung Kang and Professor Steven Soper who provided me with valuable feedback and insightful comments.

I have been privileged to work with the FRUITS group members. I thank all past and current lab members. Special thanks to our lab chief, Tae-Hyeong Kim for leading the group, and our lab manager Juhee Park, for academic and personal advice throughout my master's studies. I also appreciate my lab colleague Ja-Ryoung Han for safely going through this tough time together. I would also like to thank our CTC team, Vijajya Sunkara, Juhee Park again, Chi-ju Kim, and Min-ji Lim. I wish you all the best of luck with your research.

I would also like to express my appreciation to the CTC team Pusan National Hospitals. It had been a great honor for me to work with Professor Shin-Young Kim and researchers, Jin-Hyun Lee and Hee-Jun Lee.

Last but not least, I would like to thank my family members: Mom, Dad, and my sister, Lynn, for the continuous support and encouragement they have given throughout my time in graduate school. I could not have made it without them. Thank you.

Curriculum Vitae

Ada Younglim Lee

Mobile : +82-10-4757-4109

E-mail : ada0713@gmail.com

EDUCATION

2012. 3 – present M.S. Candidate, Biomedical Engineering
Ulsan National Institute of Science and Technology, Ulsan, Republic of Korea
(Advisor: Professor Yoon-Kyoung Cho)
2007. 8 – 2011. 12 B.S., Biochemistry and Molecular Biophysics 2011 (*Cum Laude*, With Honors)
University of Arizona, Tucson, AZ, USA
-

RESEARCH INTERESTS

- Lab-on-a-chip, Lab-on-a-disc
 - Biomedical application in microfluidic system
 - Cancer Biology
-

RESEARCH PUBLICATIONS

1. **Lee, A.**; Park, J.; Sunkara, V.; S. Kim; Cho, Y. K., Size-selective Circulating Tumor Cell Isolation on a Centrifugal Microfluidic Device. In preparation.
 2. Alabaster, A.; Isoe, J.; Zhou, G.; **Lee, A.**; Murphy, A.; Day, W. A.; Miesfeld, R. L., Deficiencies in acetyl-CoA carboxylase and fatty acid synthase 1 differentially affect eggshell formation and blood meal digestion in *Aedes aegypti*. *Insect Biochemistry and Molecular Biology* **2011**, *41* (12), 946-955.
-

CONFERENCES

1. **Younglim Lee** and Yoon-Kyoung Cho, "Rapid and efficient label-free circulating tumor cell isolation on a centrifugal microfluidic device," Annual Fall Meeting of The Korean BioChip Society, November 13~14, 2013, Chuncheon, Korea
 2. **Ada Lee**, Dong-Kyu Park, and Yoon-Kyoung Cho*, "Rapid and efficient circulating tumor cell isolation using size-based filtration on a portable centrifugal microfluidic device," Nanobiotech-Montreux Conference, November 12 – 14, 2012 Montreux, Switzerland
-

HONORS & AWARDS

- 2014 Brain Korea 21 Plus (BK21 Plus) Scholarship – *UNIST*
- 2012-2014 Research Assistant Scholarship – *UNIST*
- 2010 Undergraduate Biology Research Program (UBRP) Scholarship – *University of Arizona*
- 2008 Dean's List with Distinction – Spring, *University of Arizona*
- 2007 Dean's List – Fall, *University of Arizona*
- 2007-2011 Arizona Excellence Award Scholarship – *University of Arizona*
-